# CAM–2017

## Conference on Accessory Minerals

**September 13 – 17, 2017**
**Vienna, Austria**

**Institut für Mineralogie und Kristallographie, Universität Wien**

in collaboration with

**Earth Science Institute, Slovak Academy of Sciences, Bratislava**
**Department of Geological Sciences, Masaryk University, Brno**
**and**
**Naturhistorisches Museum Wien**

# Book of abstracts

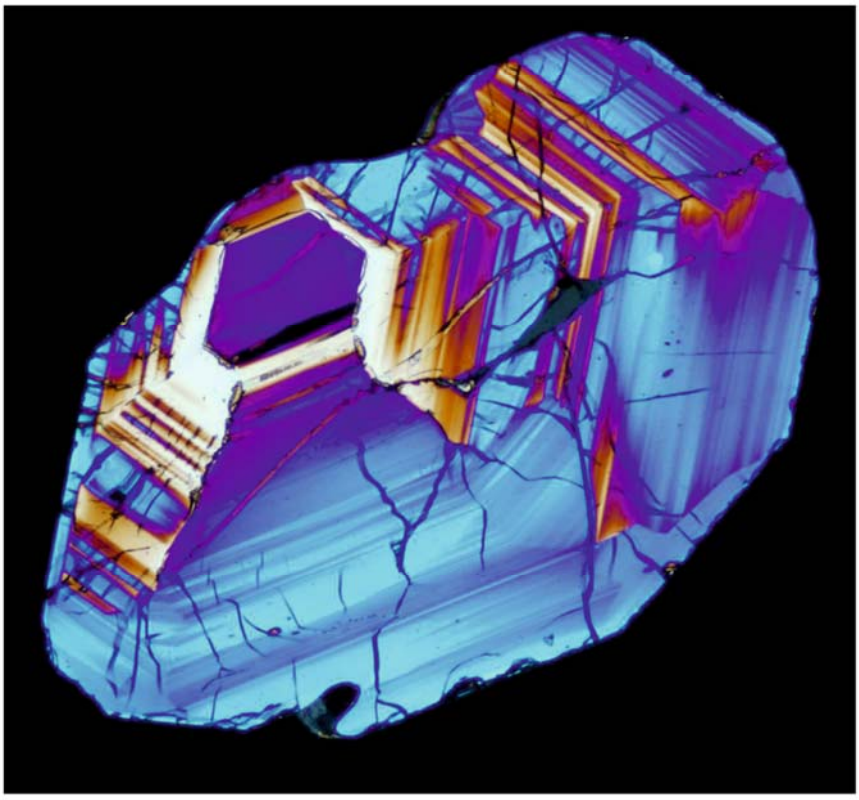


**ORGANISERS:**

**Lutz Nasdala**
Vienna, Austria
lutz.nasdala@univie.ac.at

**Igor Broska**
Bratislava, Slovakia
igor.broska@savba.sk

**Milan Novák**
Brno, Czech Republic
mnovak@sci.muni.cz


universität wien

EARTH SCIENCE INSTITUTE

UNIVERSITAS MASARYKIANA BRUNENSIS

nhm naturhistorisches museum wien

Cover image:

Cross-polarised transmitted-light photomicrograph of a zoned zircon crystal from a potassic granulite mined in the Plešovice quarry (ca. 15 km southwest of České Budějovice, Czech Republic). Low interference colours indicate elevated radiation damage that is associated with notable volume expansion; such growth zones are therefore surrounded by fractures in neigbouring, less radiation-damaged zones. Sample courtesy J. Sláma, sample preparation A. Wagner.

# Contents

# Plenary lectures

**Gregory Lumpkin**

Institute of Materials Engineering, Australian Nuclear Science and Technology Organisation, Lucas Heights, NSW, Australia

"The nuclear fuel cycle: Role of accessory minerals in problem solving"

September 13, 18:30–19:30:

Public evening lecture at the Natural History Museum

**Ray Macdonald**

Institute of Geochemistry, Mineralogy and Petrology, University of Warsaw, Poland

"The chevkinite group and its extra-ordinary range of compositions and occurrences"

September 14, 14:10-14:45

**Urs Schaltegger**

Earth and Environmental Sciences, Department of Earth Sciences, University of Geneva, Switzerland

"High-precision U-Pb dating of actinide-rich accessory minerals: Using petrochronology to unravel the timing of complex magmatic and meta-morphic processes"

September 15, 09:30-10:05

# Program

| | | |
|---|---|---|
| **Sept. 13** | before 13:30 | **Registration**, coffee |
| | 13:30–13:45 | Opening |
| | 13:45–15:25 | Oral presentations |
| | 17:00–18:30 | **Ice breaker** (Natural History Museum) |
| | 18:30–19:30 | **Public lecture** at the Natural History Museum: **Gregory Lumpkin** (Institute of Materials Engineering, Australian Nuclear Science and Technology Organisation, Lucas Heights, NSW, Australia): *"The nuclear fuel cycle: Role of accessory minerals in problem solving"* |
| **Sept. 14** | 09:15–10:35 | Oral presentations |
| | *Coffee break* | |
| | 11:10–12:10 | Oral presentations |
| | *Lunch break* | |
| | 14:10–14:45 | **Plenary Talk: Ray Macdonald** |
| | 14:45–16:05 | Oral presentations |
| | 16:05–17:30 | Poster viewing (snacks, coffee, wine) |
| | 18:15 till late | **Conference dinner** (Heuriger Kierlinger, Nußdorf) |
| **Sept. 15** | 09:30–10:05 | **Plenary talk: Urs Schaltegger** |
| | 10:05–10:45 | Oral presentations |
| | *Coffee break* | |
| | 11:10–12:10 | Oral presentations |
| | *Lunch break* | |
| | 14:15–16:15 | Oral presentations |
| | 16:15–16:30 | Closure |
| **Sept. 16** | 08:00 | **Post-conference field trip start** (Althanstr. 14, 1090 Wien) [Ends **Sept. 17, ~ 19:00**] |
| | 09:00 | **Guided tour at the NHM** (Burgring 7, 1010 Wien) |

# Abstracts

# Accessory Ba minerals as indicators of crystallization conditions in alkaline igneous rocks

**Andersen, T.[1,2]*, Elburg, M.A.[2]**

*[1] Department of Geosciences, University of Oslo, PO Box 1047 Blindern, N-0316 Oslo, Norway)*
*[2] Department of Geology, University of Johannesburg, South Africa*
** E-Mail: tom.andersen@geo.uio.no*

A number or rare Ba silicate and phosphate minerals occur as accessory minerals in peralkaline nephelinite at Nyiragongo, Democratic Republic of Congo, and in agpaitic nepheline syenite in the Pilanesberg Complex, South Africa. In both examples, the Ba-minerals formed as part of late magmatic to early post-magmatic / deuteric mineral assemblages. Although no thermodynamic data are available for these minerals, it is still possible to extract some indications about their relative stability in chemical potential space from chemographic analysis.

In the Nyiragongo nephelinite, andremeyerite ($BaFe_2^{2+}Si_2O_7$), fresnoite ($Ba_2TiOSi_2O_7$) and "unknown" Na-Ba phosphate ($Na_{0.7}K_{0.3}Ba_{0.7}Sr_{0.2}Ca_{0.1}PO_4$), Na-Ti-Fe-Ba silicate $[Na_{1.0}K_{0.1}Ca_{0.4}Ba_{1.8}Sr_{0.2}(Fe,Mg,Mn)_{3.3}(Ti,Nb)_{1.4}(Si_2O_7)_2(F_{1.6}(O,OH)_{2.4}]$ and Ba-Fe silicate ($Ba_2FeSi_2O_7$) minerals occur in different late magmatic to postmagmatic / deuteric mineral assemblages together with combeite, kirschteinite, götzenite, cuspidine, delhayelite and umbrianite (Andersen et al. 2012; 2014). Andremeyerite is associated with extremely peralkaline silicate glass, and is undoubtedly of magmatic origin (Fig. 1). Some of the other minerals (in particular the phosphate and Na-Ba-Ti silicate mineral) may be late magmatic, or have formed by autometasomatic processes induced by degassing magma. Andremeyerite, Na-Ba-Ti silicate and Na-Ba phosphate minerals reflect increasing levels of peralkalinity, and a transition from andremeyerite through the $Ba_2FeSi_2O_7$ mineral and fresnoite to baryte a trend of increasing oxygen fugacity (Fig. 2a).

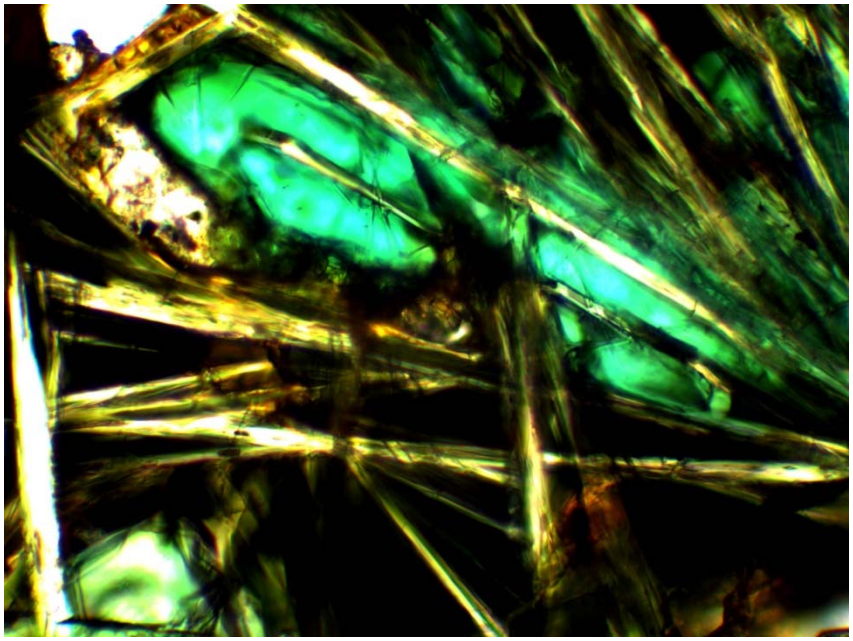

***Fig. 1.*** *Andremeyerite (bright green) with acicuar crystals of götzenite and silicate glass in nephelinite from Nyiragongo, DRC (Andersen et al. 2014). Width of frame: ca. 1mm*

In the Pilanesberg complex, bafertisite [$Ba_2Fe_4^{2+}Ti_2(Si_2O_7)_2O_2(OH)_2F_2$] and jinshajiangite [$BaNaFe_4^{2+}Ti_2(Si_2O_7)_2O_2(OH)_2F$], the latter forming epitaxial overgrowths on the former, occur as part of highly agpaitic interstitial mineral assemblages in white foyaite, together with astrophyllite, aenigmatite, lorenzenite and hilairite(Andersen et al. 2016).

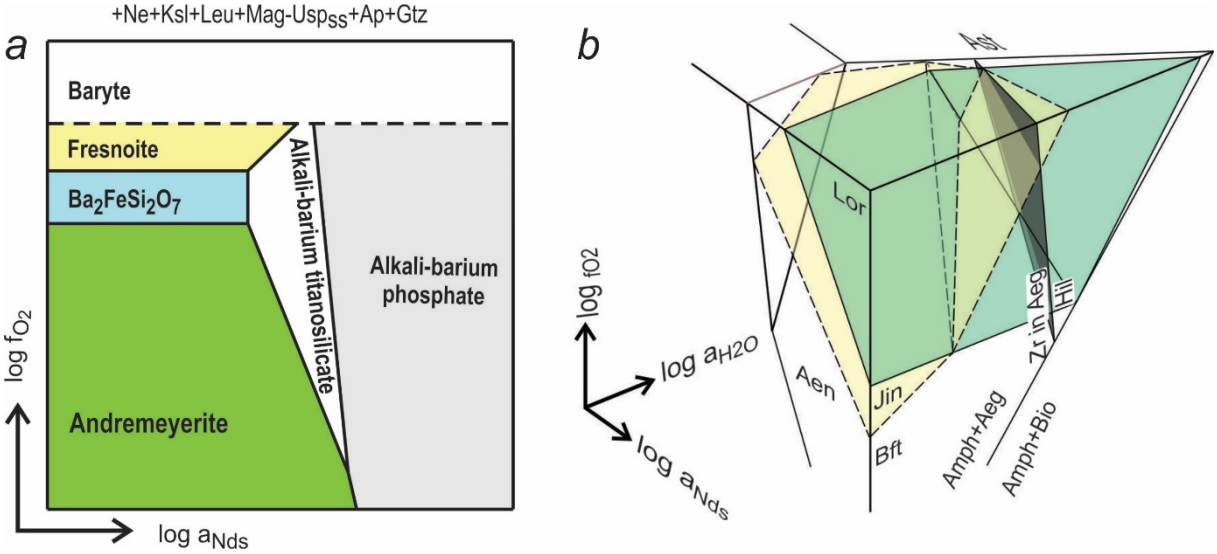


***Fig. 2.*** *Stability relationships in log $a_{Nds}$ – log $a_{H2O}$ –log $f_{O2}$ space (Nds: $Na_2Si_2O_5$ component) for accessory Ba minerals in a: Peralkaline nephelinite at Nyiragongo (Andersen et al. 2014) and b: Agpaitic nepheline syenite (white foyaite) in Pilanesberg (Andersen et al. 2016). Abbreviations: Ne: Nepheline, Ksl: Kalsilite, Leu: Leucite, Ap: Apatite, Gtz: Götzenite, Mag-Usp$_{SS}$. Magnetite-ulvöspinel solid solution, Aen: Aenigmatite, Ast: Astrophyllite, Lor: Lorenzenite, Amph: Amphibole (arfvedsonite-magnesium arfvedsonite), Aeg: Aegirine, Bio: Biotite, Hil: Hilairite, Bft: Bafertisite, Jin: Jinshajiangite*

Surkhobite [$KBa_3Ca_2Na_2Mn_{16}Ti_8(Si_2O_7)_8O_8(OH)_4(F,O,OH)_8$] has formed as a late member of eudialyte-bearing magmatic mineral assemblages in green foyaite. These minerals reflect highly alkaline conditions during latest magmatic to early deuteric stages of the crystallization history, and in the case of the bafertisite-jinshajiangite transition, possibly a trend approaching a hyperagpaitic fluid regime in the intrusion (Fig. 2b).

***Acknowledgments:*** *Thanks are due to Muriel Erambert (Department of Geosciences, University of Oslo) for skilful electron microprobe support, to the Royal Museum of Central Africa (Tervuren, Belgium) and Florias Mees for loan of material from Nyiragongo, and to R.E. Harmer for introducing T.A. to Pilanesberg.*

## References:

Andersen, T., Elburg, M.A., Erambert, M, (2012) Petrology of combeite- and götzenite-bearing nephelinite at Nyiragongo, Virunga Volcanic Province in the East African Rift. Lithos 152:105–121

Andersen, T., Elburg, M.A., Erambert, M, (2014) Extreme peralkalinity in delhayelite- and andremeyerite-bearing nephelinite from Nyiragongo volcano, East African Rift. Lithos 206–207:164–178

Andersen, T., Elburg, M.A., Erambert, M, (2016) The miaskitic-to-agpaitic transition in peralkaline nepheline syenite (white foyaite) from the Pilanesberg Complex, South Africa. Chemical Geology, http://dx.doi.org/10.1016/j.chemgeo.2016.08.020

# Carbothermal mobilisation of HFSE minerals

**Aßbichler, D.[1,*], Lenz, C.[2,3], Heuss-Aßbichler, S.[1], Kunzmann, T.[1]**

*[1] Ludwig-Maximilians-Universität München*
*[2] Institut für Mineralogie & Kristallographie, University of Vienna*
*[3] Nuclear Fuel Cycle Research, ANSTO, Sydney*
** E-Mail: d.assbichler@lmu.de*

Sanidinites are magmatic cumulates with trachytic to phonolitic composition. The sanidinites from Laacher See volcano, Eifel, Germany, are famous for their abundant crystallization of high field strength element (HFSE) minerals with individual idiomorphic crystals. Remarkable is the occurrence of two late magmatic generations of zircon (Fig. 1). Type I zircon is rich in REE and Th. It exposes an oscillatory zoning and is always strongly affected by resorption. It is mantled by a REE and Th depleted, type II zircon, but with abundant inclusions of thorite and pyrochlore as well as calcite, and fluid inclusions.

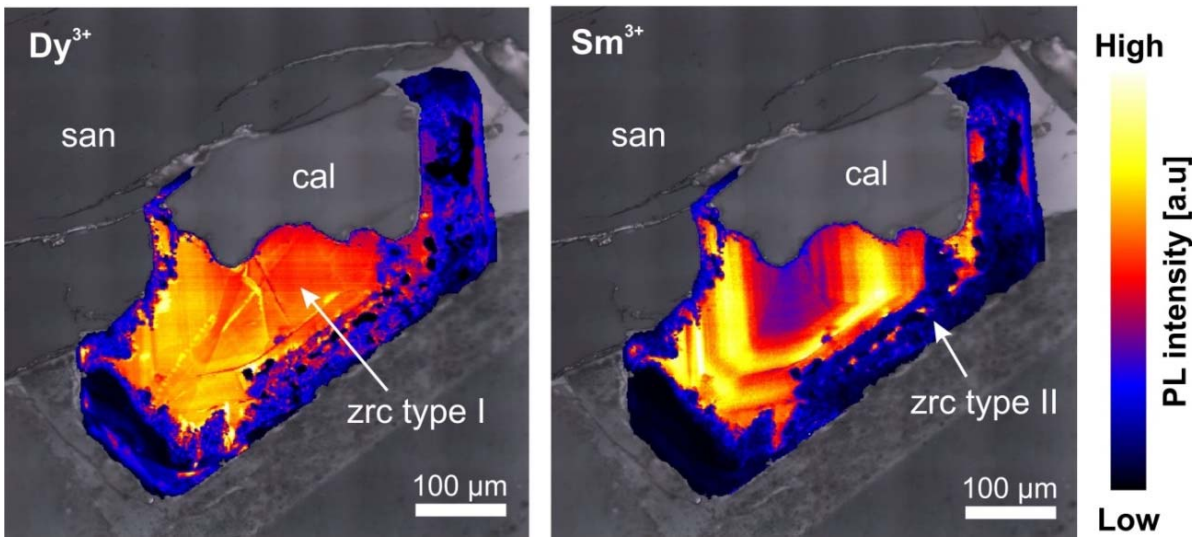


***Fig. 1.*** *Laser-induced photoluminescence maps overlay microscopic images of a strongly resorbed zircon (type I) within a miarolithic cavity of a nosean-bearing, calcite-rich sanidinite from Laacher See volcano, Eifel, Germany. The intensity of $Dy^{3+}$ and $Sm^{3+}$ emissions is colour-coded. It indicates high REE concentrations within the zircon core (type I). The type I zircon shows clear oscillatory zoning and strong resorption features. The euhedral overgrowth-rim of type II zircon is depleted in REE and rich in inclusions*

The geochemical investigation of the sanidinites reveals a high content of volatiles in these rocks, up to 5 wt% $SO_3$ and 0.5wt % Cl. There is a positive correlation of Zr and REE with $Na_2O$, $SO_3$, Cl, and LOI ($CO_2$).

Our investigations point to following crystallization sequence: Sanidine crystallized first, forming a framework of interlocking crystal laths with miarolithic cavities. Afterwards, different mineral assemblages crystallized within the miarolithic cavities. According to the composition and mineral assemblages within the cavities, two groups of sanidinites can be distinguished: (1) Haüyne sanidinites (HS) contain clear blue haüyne, plagioclase, clinopyroxene and biotite, as well as accessory apatite, magnetite and titanite. HFSE are mainly incorporated in titanite with concentrations up to 3.3 wt% $ZrO_2$ and 4

wt% $Nb_2O_5$, and apatite. Zircon was only rarely observed. (2) Nosean sanidinites (NS) contain high proportions of nosean and calcite and minor to accessory contents of clinopyroxene, biotite and apatite. A special feature is the occurrence of often euhedral HFSE minerals, including zircon ($ZrSiO_4$), baddeleyite ($ZrO_2$), thorite ($ThSiO_4$) and pyrochlore ($Ca_2Nb_2O_7$).

Detailed mineralogical and microchemical investigations give evidence for a further subdivision of the crystallization sequence within the cavities of the nosean sanidinites: Two different generations of nosean can be distinguished: N-I Nosean is characterized by abundant concentrically arranged silicate melt inclusions and high amount of $CO_2$ vapour inclusions, indicating crystallization from a residual, $CO_2$ vapour saturated melt. In contrast, N-II nosean is characterized by a mostly euhedral grain shape and the absence of melt- and fluid inclusions. Its occurrence together with calcite, pyrochlore, thorite and baddeleyite suggests its crystallization from a $CO_2$-rich (co-magmatic) fluid (vapour). The microchemistry of nosean indicates the presence of $SO_3$ and Cl in the fluid. The change from a silicate melt dominated condition to fluid dominated environment is evidence by etching and resorption structures, as well as carbonate filled fluid veins, observed only within sanidine and N-I nosean. Further indications for the formation of the mineral assemblage out of a gaseous phase are beside the high volatile content in the whole rock composition, the porous structure of the nosean sanidinites with abundant "empty" miarolithic cavities and abundant $CO_2$ vapour inclusions in the minerals. The euhedral grain shape of most crystals within the cavities, and the jagged grain boundaries of calcite are typical for the growth from a fluid.

These trends correlate with the changed growth features of zircon. The oscillatory zoned type I zircons (see Fig. 1), with typically high contents of Th and REE (up to 2.2 wt% $REE_2O_3$), indicate a late magmatic growth from a highly evolved melt. The strong resorption textures of type I zircon point to changed crystallization conditions thereafter. The newly grown type II zircon is characterized by low REE and Th concentrations and abundant inclusions of thorite, pyrochlore and fluids ($CO_2$) and minor calcite. These zircons occur not only as rims around type I zircon (see Fig. 1), but also as individual euhedral crystals within the miarolithic cavities. They also appear along grain boundaries or as fillings of etching holes within the sanidine laths. Notably, type II zircon appears always in conjunction with calcite.

Our results indicate a late stage co-magmatic, carbothermal formation of the calcite bearing nosean sanidinites. This process can explain the relative enrichment of HFSE minerals, carbonates and volatiles in nosean sanidinites. It leads to the formation of two different generations of nosean and zircon. According to our observations, we conclude that after the crystallization of type I zircon from a melt enriched in REE, it was partly dissolved and transported by a $CO_2$-rich fluid/vapour and re-precipitated as REE-poor type II zircon together with pyrochlore, forming individual euhedral crystals within the miarolithic cavities. The occurrence of baddeleyite in some samples is an indicator for changed crystallization conditions, marked by a fluid with lower Si activity.

***Acknowledgments:*** *We thank the Federal Ministry of Education and Research (BMBF) for the financial support within the Matressource research program TS-Protect (03X3569). The field trip to Laacher See volcano was financially supported by the LMU Excellence Mentoring program. Moreover, financial support was provided by the Austrian Science Fund (FWF) through project J3662-N19 to C.L.*

# Chemical composition and evolution of tourmaline-supergroup minerals from the hydrothermal veins in Gemeric Superunit, Western Carpathians, Slovakia

**Bačík, P.[1,*], Uher, P.[1], Dikej, J.[1], Fridrichová, J.[1], Miglierini, M.[2], Števko, M.[3]**

*[1] Comenius University in Bratislava, Faculty of Natural Sciences, Department of Mineralogy and Petrology, Ilkovičova 6, 842 15 Bratislava, Slovakia*
*[2] Slovak University of Technology, Faculty of Electrical Engineering and Information Technology, Department of Nuclear Physics and Technology, Ilkovičova 3, 812 19 Bratislava, Slovakia*
*[3] Pribišova 15, 841 05 Bratislava, Slovakia*
** E-Mail: bacikp@fns.uniba.sk*

Tourmaline-supergroup minerals are common gangue minerals on many hydrothermal veins in the Gemeric Superunit, Eastern Slovakia. They were described from many occurrences of Sb hydrothermal veins (Klimko et al. 2009; Bačík et al. 2017a), siderite-quartz-sulphide hydrothermal veins (Bačík et al. 2017b) and also from a magnesite-talc deposit (Bačík et al. 2011).

Tourmalines are abundant in the Betliar – Straková, Čučma – Gabriela and Rožňava – Peter-Pavol Sb vein deposits in the Rožňava area, Slovakia. They form relatively large prismatic to radial aggregates of parallel black to greyish-black crystals. Tourmaline-supergroup minerals from Betliar – Straková and Rožňava – Peter-Pavol are compositionally almost homogeneous with intermediate schorl-dravite composition. Čučma – Gabriela tourmalines have distinct zoning with massive cores of schorl-to-feruvite shifting to schorl-to-dravite composition, and dravite to magnesio-foitite rim. The tourmaline composition is influenced by two main substitutions, namely $Ca(Mg,Fe)Na_{-1}Al_{-1}$ and $^{X}\square AlNa_{-1}$ $(Mg,Fe)_{-1}$. Betliar – Straková and Rožňava – Peter-Pavol tourmaline-supergroup minerals exhibit only small extents of the $^{X}\square AlNa_{-1}(Mg,Fe)_{-1}$ substitution. In Čučma – Gabriela tourmalines, this substitution is more extended and shifts its composition to magnesio-foitite. In contrast, extensive $Ca(Mg,Fe)Na_{-1}Al_{-1}$ substitution results in the decrease of Al in the core of Čučma – Gabriela tourmalines. The unit-cell dimensions of all investigated tourmaline-supergroup minerals indicate an octahedral disorder with the $^{Z}(Fe^{3+}+Mg)$ proportion calculated from empirical equations varying between 0.85 and 0.87 apfu (atoms per formula unit). Based on Mössbauer spectra, the $^{Z}Fe^{3+}$ content varied between 0.25 apfu in Betliar – Straková tourmalines and 0.45 apfu in Čučma – Gabriela samples. Based on the Fe/(Fe+Mg) ratios, Betliar – Straková tourmalines are slightly enriched in Fe compared to Rožňava – Peter-Pavol, suggesting the impact of the host-rock composition; the former grew in Fe-richer acidic metarhyolitic rocks, the latter in metapelites. In Čučma – Gabriela tourmalines, the variations in Fe/(Fe+Mg) very likely reflect the change in fluid composition. Magnesio-foitite is the product of second-stage crystallization forming rims and crack fillings. The relatively low $Fe^{3+}/Fe^{2+}$ ratio indicates only minor proportions of meteoric fluids in tourmaline crystallization.

Tourmalines occur in a large number of Cretaceous siderite-quartz-sulphide hydrothermal veins in the Gemeric Unit, Slovak Ore Mountains, Slovakia, such as Dobšiná, Vlachovo, Rožňavské Bystré, Hnilčík, Rakovnica, Novoveská Huta, Gretla, Rudňany, and Bindt. Tourmalines form selected deposits belong mostly to the alkali group, schorl-dravite series, whereas foitite (Vlachovo and Bindt) and oxy-dravite compositions (Hnilčík) occur only rarely. Rim zones of some schorlitic tourmalines show high

concentrations of Ti (up to 2.35 wt. % $TiO_2$, 0.30 apfu; Rožňavské Bystré). The chemical composition is mostly controlled by alkali-deficient $^{X}\square AlNa_{-1}(Mg,Fe)_{-1}$ and proton-deficient $AlO(Mg,Fe^{2+})_{-1}(OH)_{-1}$ substitutions. Titanium is incorporated into the structure by $^{Y}Ti^{Y}(Mg,Fe)^{Y}Al_{-2}$, $^{Y}Ti^{Z}Mg^{Y}Al_{-1}{}^{Z}Al_{-1}$, $^{Y}TiO^{Y}Al_{-1}(OH)_{-1}$, and $^{X}Ca^{Y}Ti^{Z}MgO_2{}^{X}\square_{-1}{}^{Y,Z}Al_{-2}(OH)_{-2}$ substitutions.. The unit-cell parameter *a* varies between 15.960 and 15.985 Å; variations in *c* are larger, between 7.177 and 7.236 Å, indicating the presence of $Fe^{3+}$ and $Mg^{2+}$ at the *Z* site. Mössbauer spectroscopy has shown variable $Fe^{3+}$ proportions (0.17-0.55 apfu) in all samples. The highest $Fe^{3+}$ concentrations occur in samples from Rudňany and Gretla in the external part of the Gemeric unit, suggesting higher oxidation and greater impact of meteoric fluids during longer fluid transport. The determined $X_{Mg}$ ratios in the samples are correlated with the compositions of the host rocks; schorl to foitite occurs in veins located in the meta-rhyolites host, while tourmalines with the highest Mg contents occur in metabasalts.

Brown tourmalines were found in the Gemerská Poloma talc-magnesite deposit. Acicular tourmalines form aggregates along with talc on the slip surface of carbonate rock consisting of dolomite and magnesite. The tourmalines are almost unzoned and have compositions corresponding to dravite with very high $X_{Mg}$ (0.95 – 0.96). In contrast, samples have very low *X*-site vacancies (up to 0.17) and Ca contents (up 0.05 apfu). The Fe contents are also very low (up to 0.14 apfu) and the contents of Al variy between 5.97 and 6.27 apfu. The calculated $^{W}O^{2-}$ contents correlate with that of Al, which suggests a quite significant role of the $AlOMg_{-1}(OH)_{-1}$ substitution. Other substitutions are negligible, tourmaline compositions are very uniform. However, the dravite studied is significantly Al-Mg disordered with $^{Z}Mg/(^{Z}Mg+^{Y}Mg) = 0.45\text{-}0.50$, as suggested by distribution of Al and Mg among octahedral sites calculated from lattice parameters [*a* = 15.9289(7) Å; *c* = 7.2132(17) Å]. Dravite from Gemerská Poloma was likely a side-product of talc formation from original carbonate rock during the Permian granite intrusion. Dravite formed from granite-derived Si- and B-bearing fluids on the slip surface during/after brittle deformation of carbonate which results in its finely acicular habitus. Its high-magnesian composition is controlled by the geochemical properties of the host rock.

Based on crystal-chemical data from various hydrothermal-tourmaline occurrences, it is possible that the factors influencing the evolution of tourmaline include the composition of the solutions, the origin of the fluid, the length of their transport and the host-rock environment in which the tourmaline crystallizes.

***Acknowledgments:*** *This work was supported by the Slovak Research and Development Agency under the contract No. APVV-0375-12 and and the Ministry of Education of Slovak Republic grant agency under the contracts VEGA-1/0079/15 and VEGA-1/0499/16.*

## References:

Bačík P, Dianiška I, Števko M, Sečkár P (2011) Brown acicular dravite from talc-magnesite deposit Gemerská Poloma (Gemeric Superunit, Slovakia). Bull Mineral-Petrol Odd Nár Muz (Praha) 19:164–170 (in Slovak)

Bačík P, Dikej J, Števko M, Fridrichová J, Miglierini M (2017a) Crystal chemistry and evolution of tourmalines from the Sb hydrothermal veins in Rožňava area, Western Carpathians, Slovakia. Miner Petrol 111:609–624

Bačík P, Uher P, Dikej J, Puškelová Ľ (2017b) Tourmalines from the siderite-quartz-sulphide hydrothermal veins, Gemeric unit, Western Carpathians, Slovakia: crystal chemistry and evolution. Miner Petrol, published online (DOI 10.1007/s00710-017-0500-8)

Klimko T, Chovan M, Huraiová M (2009) Hydrothermal mineralization of stibnite veins in the Spiš-Gemer Ore Mts. Miner Slov 41:115–132 (in Slovak)

# Zircon grains in A-type granite and their inclusions as recorder of upper mantle conditions in the Croatian segment of the Late Cretaceous collisional zone between Europe and Adria

**Balen, D.[1], Schneider, P.[1,*], Massonne, H.-J.[2], Opitz, J.[2], Putiš, M.[3], Luptáková, J.[4], Petrinec, Z.[1]**

*[1] Department of Geology, Faculty of Science, University of Zagreb, Croatia*
*[2] Institut für Mineralogie und Kristallchemie, Universität Stuttgart, Germany*
*[3] Faculty of Natural Sciences, Comenius University, Bratislava, Slovakia*
*[4] Earth Science Institute, Slovak Academy of Sciences, Banská Bystrica, Slovakia*
** E-Mail: petra.schnajder@gmail.com*

Zircon, one of the ubiquitous accessory minerals in granites is a valuable indicator of various geological processes. In addition, it includes and preserves various types of inclusions and serves as a natural preservation capsule allowing inside views into earlier stage(s) of the (geodynamic) evolution. The so-called Sava(-Vardar) Zone is one of the still geologically intriguing areas in the SE Europe with a suture zone after closing the western Neotethys branch following collision of the southern margin of the European plate with the Adria plate (Pamić 1993; Schmid et al. 2008; Ustaszewski et al. 2010). This zone shows rare outcrops of various types of granitic rocks. Among them is the peculiar red-coloured Cretaceous granite from Mt. Požeška Gora (N Croatia). This granite, associated with rhyolites, crops out as several small intrusive bodies covering a total area of approx. 6-7 km$^2$ (Pamić 1987) and caught our attention due to its geotectonic position, appearance, colour, accessory mineral content and still disputable age (Pamić et al 1988; Jamičić 2007).

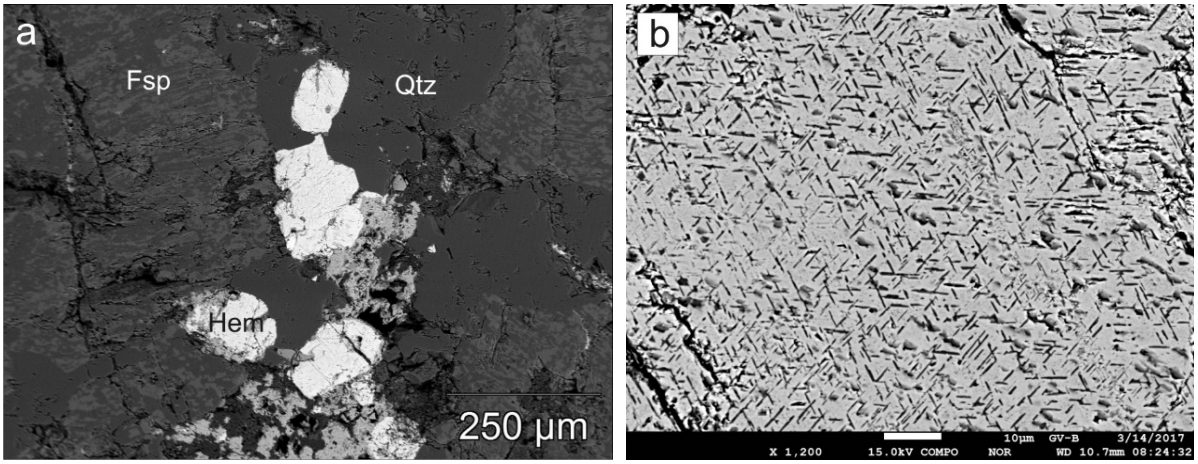


***Fig. 1.*** *BSE images of* ***a*** *Mt. Požeška gora granite texture; Fsp=alkali feldspar, Hem=hematite, Qtz=quartz.* ***b*** *hematite with crystallographically oriented ilmenite exsolutions*

The Mt. Požeška Gora granite is massive with a fine- to coarse-grained granitic texture. It is mainly composed of alkali feldspar and quartz (Fig. 1a), with small amounts of plagioclase, white mica and hematite with crystallographically oriented ilmenite exsolutions (Fig. 1b). Alkali feldspar is dominantly perthite whereas plagioclase is almost pure albite. Quartz-alkali feldspar intergrowths and micrographic textures are common.

Accessory minerals found by polarizing microscope include zircon, apatite and Fe-(Ti)-oxides.

The analyzed zircon population consists of 184 grains ranging from 60-75 μm in the long and 25-35 μm in the short axis. Aspect ratios range from 1.7:1 to 2.9:1, with the median value of 2.2:1. The external morphology is governed by predominantly developed {100} prisms and {101} >> {211} bipyramids (Fig. 2a), among them prevail D (50 % of the total population), J5 (30 %) and J4 (11 %) types after Pupin's (1980) zircon typology (Fig. 2b). Zircon crystals are colourless to slightly yellowish with high transparency and birefringence. Cathodoluminescence (CL) and back-scattered electron (BSE) images reveal clear signs of growth oscillatory zoning typical of magmatic growth conditions without any signs of dissolution of the surface, which indicates saturation of Zr in the melt. The morphology of the zircon grains separated out of the Mt. Požeška Gora granite combined with whole rock granite geochemistry points to a high-temperature, dry A-type granite (Balen et al. 2017).

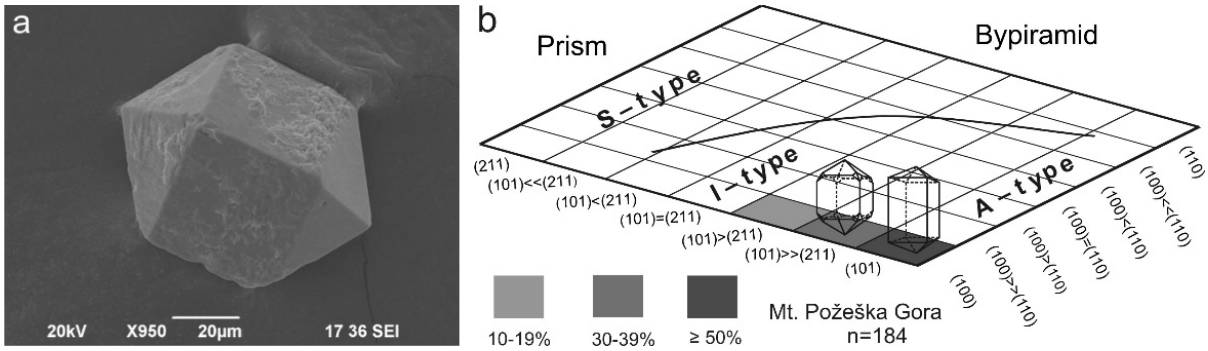


***Fig. 2. a*** *Typical morphology of Mt. Požeška Gora zircon.* ***b*** *Modified zircon typology diagram*

Zircon grains are found included in the lately crystallized minerals, alkali feldspar and quartz, and some of them comprise inclusions of hematite, apatite and early zircon. The Raman spectra of inclusions (Fig. 3) in zircon (preliminary findings) also revealed tiny (<10 μm) minerals of kokchetavite and kumdykolite(?) (polymorphs of K-feldspar and albite, respectively) representing metastable phases in melt inclusions that require rapid cooling (Ferrero et al. 2016). The findings set magma genesis to the depth (most likely) corresponding to the upper mantle source, as predicted by zircon typology and reveal the early path of A-type granite magma evolution.

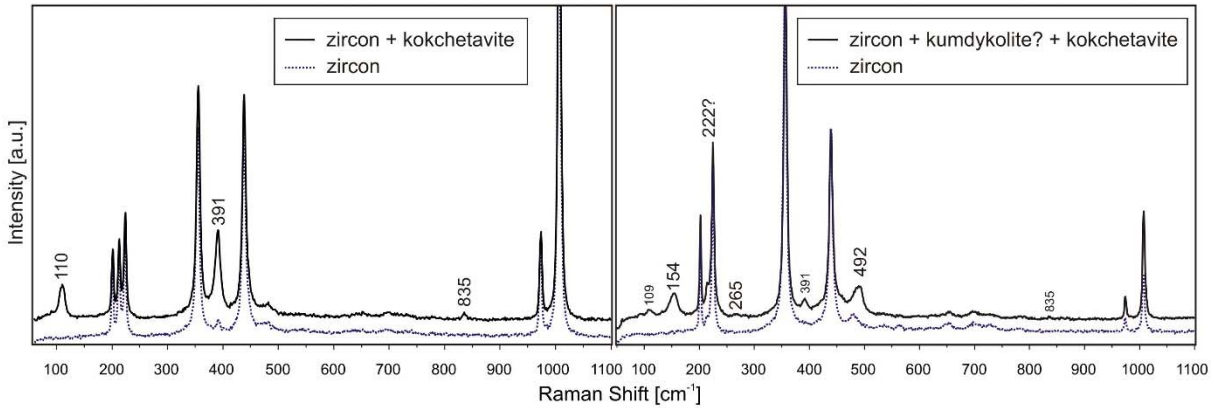


***Fig. 3.*** *Raman spectra of kokchetavite and kumdykolite(?) from inclusions in zircon*

All analyzed zircons from the Mt. Požeška Gora granite have variable uranium (398-1988 ppm) and thorium (263-1371 ppm) contents, with Th/U ratios ranging from 0.61 to

0.97, consistent with a magmatic origin (Hoskin and Schaltegger 2003). According to their external typology, internal structure, and chemical composition (high $U_{mean}$=903 ppm and $Th_{mean}$=666 ppm, Th/U=0.74, Zr/Hf=54.96) it is suggested that they crystallized in deep magma chambers at relatively high and constant temperature. The calculated Zr saturation temperatures of the magma and the onset of the zircon crystallization (Watson and Harrison 1983) show values of up to 878 °C, indicating its formation in a high-temperature environment. Existence of hematite (norm 2.7 wt. %), that paints the granite reddish, indicates an oxidised magma type. The positive Ce anomaly in zircon REE patterns (Fig. 4a) also provides evidence of a positive oxidation potential of the magma. Exsolution lamellae of ilmenite in hematite with crystallographically oriented texture resulted from relatively rapid cooling and/or pressure drop.

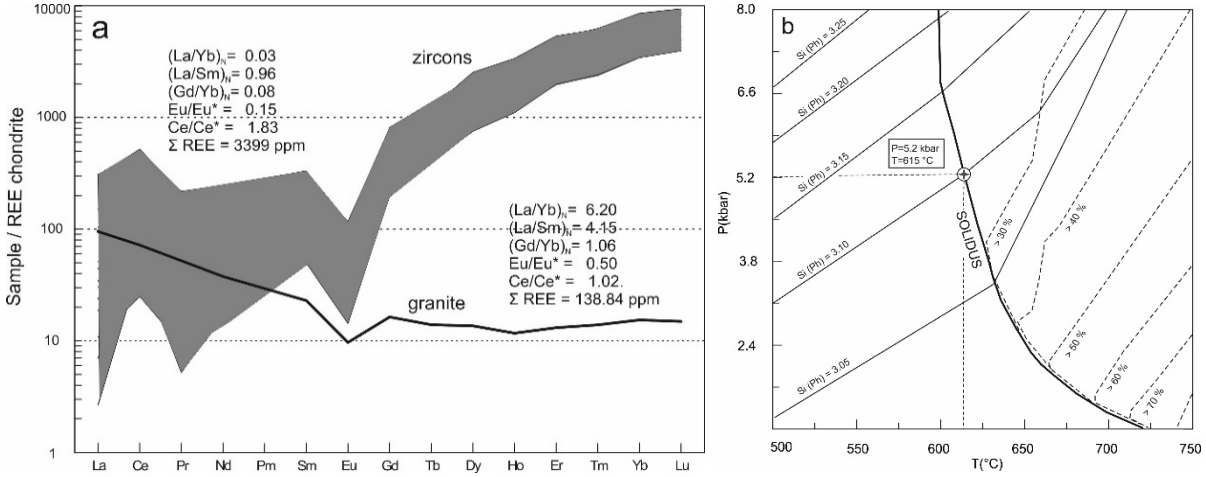


***Fig. 4. a*** *REE patterns normalized to chondrite (Boynton 1984) for zircons and host granite.* ***b*** *P-T diagram showing the granitic solidus and isopleths for the Si content in white mica and melt volume. The intersection of the solidus and a specific Si isopleth for white mica indicates the intrusion level of the host granite*

Emplacement P-T conditions were estimated with PERPLE_X calculations of the intersection of the specific Si isopleth (3.10 Si p.f.u.), according to late-crystallized white mica, with the solidus for the host granite in a P-T diagram (Fig. 4b). The obtained values are 5.2 kbar and 615°C, which correspond to a crustal intrusion level of ca. 20 km, and fit the P-T ranges resulting from the application of the Or-Ab-Qtz (300-1000 MPa) and An-Ab-Or (600-650°C) ternary systems.

The finding of red granite pebbles at the base of the Santonian-Campanian-Maastrichtian geological column (e.g. Jamičić 2007) was in contradiction with the previously reported Maastrichtian age (71.5±2.8 Ma, Rb/Sr isochron) for three granite and two cogenitic rhyolite samples (Pamić et al. 1988). Ages obtained in our study on zircon using a LA-ICP-MS are $^{207}Pb/^{235}U$=85.8±1.1 Ma, $^{206}Pb/^{238}U$=86.1±1.5 Ma and $^{208}Pb/^{232}Th$=87.7±1.9 Ma (RMSD), which are in agreement with stratigraphic constraints.

The Late Cretaceous subduction of the western Neotethyan branch in the study area was terminated and changed to a post-subduction rift-like tectonic process. The subsequent extension caused rhyolite volcanism along deep faults and younger extension-related basaltic volcanism (Belak et al. 1998). The A-type granite with its specific zircon typology originated at great depths and high-temperatures (upper mantle conditions) and intruded rapidly mid- to shallow-crustal levels. The presented evidence fits this scenario that invokes a geodynamic change from a compressional to an extensional regime during the Late Cretaceous.

***Acknowledgments:*** *This work has been fully supported by Croatian Science Foundation under the project IP-2014-09-9541. The authors are grateful to T. Theye (Stuttgart) for help during microprobe work; further analytical work is supported by APVV-15-0050 and ITMS 26220120064.*

## References:

Balen D, Schneider P, Massonne H-J, Opitz J, Petrinec Z (2017) A Cretaceous A-type granite from the Europe-Adria collisional zone: a marker of geodynamic changes. Goldschmidt 2017 Abstract

Belak M, Halamić J, Marchig V, Tibljaš D (1998) Upper Cretaceous-Palaeogene Tholeiitic Basalts of the Southern Margin of the Pannonian Basin: Požeška gora Mt. (Croatia). Geol Croat 51:163–174

Boynton WV (1984) Geochemistry of the rare earth elements: meteorite studies. In: Henderson P (ed) Rare earth element geochemistry. Elsevier, Amsterdam, pp 63–114

Ferrero S, Ziemann MA, Angel RJ, O´Brien PJ, Wunder B (2016) Kumdykolite, kokchetavite, and cristobalite crystallized in nanogranites from felsic granulites, Orlica–Snieznik Dome (Bohemian Massif): not evidence for ultrahigh–pressure conditions. Contrib Mineral Petrol 171:3 doi: 10.1007/s00410-015-1220-x

Hoskin PWO, Schaltegger U (2003) The composition of zircon and igneous and metamorphic petrogenesis. Rev Mineral Geochem, vol 53, Mineral Soc Am, pp 27-62

Jamičić D (2007) Upper Cretaceous deposits of the Požeška gora Mt. (Croatia). Natura Croatica 16:105–120

Pamić J (1987) Mladoalpinski alkalijsko-feldspatski graniti (aljaskiti) Požeške gore u Slavoniji (Young-Alpine alkali feldspar granites (alaskites) from Mt. Požeška Gora in Slavonia, northern Yugoslavia). Geologija 30:183–205

Pamić J (1993) Eoalpine to Neoalpine magmatic and metamorphic processes in the northwestern Vardar Zone, the easternmost Periadriatic Zone and the southwestern Pannonian Basin. Tectonophysics 226:503–518

Pamić J, Lanphere M, McKee E (1988) Radiometric ages of metamorphic and associated igneous rocks of the Slavonian Mountains in the southern part of the Pannonian Basin, Yugoslavia. Acta Geol 18:13–39

Pupin JP (1980) Zircon and granite petrology. Contrib Mineral Petrol 73:207–220

Schmid SM, Bernoulli D, Fügenschuh B, Matenco L, Schefer S, Schuster R, Tischler M, Ustaszewski K (2008) The Alps–Carpathians–Dinarides connection: a compilation of tectonic units. Swiss J Geosci 101:139–183

Ustaszewski K, Kounov A, Schmid SM, Schaltegger U, Krenn E, Frank W, Fügenschuh B (2010) Evolution of the Adria-Europe plate boundary in the northern Dinarides: From continent-continent collision to back-arc extension. Tectonics 29:TC6017 doi: 10.1029/2010TC002668

Watson EB, Harrison TM (1983) Zircon saturation revisited: temperature and composition effects in a variety of crustal magma types. Earth Planet Lett 64:295–304

# Peralkaline and metaluminous granitoids and volcanics of the Neoproterozoic rift-related Robertson River igneous suite, Northern Virginia, USA: Nb-Ta oxides and their alteration

**Belkin, H.E.**

*U.S. Geological Survey (ret.), 11142 Forest Edge Drive, Reston, VA 20190 USA*
*E-mail: harveybelkin@gmail.com*

The Robertson River suite is the largest Neoproterozoic A-type granite body emplaced along the eastern Blue Ridge flank during regional Rodinia crustal extension. Eight plutons constitute the elongate (110 km by ≤5 km) Robertson River batholith (Tollo and Lowe 1994). U–Pb isotopic analyses of zircons indicate emplacement in two magmatic pulses: about 735–722 and 704–697 Ma. Metaluminous magmas were emplaced during both pulses and form most of the batholith. Peralkaline magmas constitute the Amissville granite and the Battle Mountain volcanic centre (Tollo 1994) that erupted unknown quantities of rhyolite during the final phase of activity. The igneous body appears to be a multiply intruded large dike-shaped sheet emplaced episodically into Mesoproterozoic basement during regional Rodinian crustal extension.

The first pulse rocks are metaluminous and includes the Rivanna granite, Laurel Mills granite, Arrington Mountain alkali feldspar granite, White Oak alkali feldspar granite, and the Cobbler Mountain alkali feldspar quartz syenite. The second pulse includes the metaluminous Hitt Mountain alkali feldspar syenite and the peralkaline Amissville alkali feldspar granite and the Battle Mountain feldspar granite, rhyolite, and felsite. The Robertson River plutons exhibit compositional and mineralogical characteristics typical of A-type granites. Composition variations include a striking enrichment in HFSE such as Zr, Nb, Y, and REE, high Ga/Al and $FeO^T$/MgO, and low Ba and Sr. Both metaluminous and peralkaline rocks have a plethora of accessory minerals such as Nb-Ta oxides, chevkinite mineral group, allanite, fluorcarbonates, gadolinite, zircon, monazite, apatite, calcite, siderite, and sphalerite; fluorite is ubiquitous. The major REE-bearing phases are fluorocarbonate, chevkinite group mineral, allanite, gadolinite, and a variety of Nb phases with variable REE content.

The Nb-Ta oxides occur in a wide variety of chemistry, habits, and typically show multiple generations, and alteration and deposition by late-stage fluids. To date, five major groups of Nb-Ta oxides have been identified by EPMA analysis; columbite group, fergusonite group, euxenite group, aeschynite group, and the pyrochlore super group. The nomenclature distinctions except columbite were based on the three-group model of Ercit (1995). No crystallographic investigations were attempted and we assume considering their U and Th content that most are metamict. The columbite group represented by columbite-(Fe) and columbite-(Mn) has been observed in both metaluminous and peralkaline units. Ta/(Ta+Nb) is very low, all below 0.06; $TiO_2$ averages 2.5 wt% and ΣREE+Y is ≤1 wt%. Most columbite is in the range of 0.3 to 0.6 Mn/(Mn+Fe), however, the Rivanna granite columbite-(Fe) has MnO ≤ 0.1 wt%. The fergusonite group is the most abundant Nb-Ta oxide and has been observed in most of the Robertson River suite. The only member, fergusonite-(Y) is HREE enriched, with $FeO^T$ 0.1 to 4 wt%, $TiO_2$ 0.2 to 3 wt%, PbO 0.3 to 0.5 wt%, CaO 0.1 to 1 wt%, ΣREE averages 16 wt%, $Y_2O_3$ averages 28 wt% with variable amounts of $UO_2$ and $ThO_2$, usually ≤1 wt%. The aeschynite group, to

date, has been found only in the peralkaline granites. Three members, all LREE enriched, have been identified based on dominant cation in the A and B sites, aeschynite-(Nd), nioboaeschynite-(Ce), and nioboaeschynite-(Nd). All have CaO 1 to 3 wt%, $FeO^T$ 1 to 2 wt%, $ThO_2$ 0.5 to 5 wt%, ΣREE averages 30 wt%, and $Y_2O_3$ averages 3 wt%. The euxenite group was recognized in both the metaluminous and peralkaline units; two members polycrase-(Y) and euxenite-(Y) were distinguished based on the dominant B-site cation. Both members have $FeO^T$ 0.1 to 4 wt%, PbO 0.3 to 0.5 wt%, CaO 0.4 to 4 wt%, ΣREE averages 10 wt%, $Y_2O_3$ averages 20 wt% with variable amounts of $UO_2$ and $ThO_2$ that range from 0.2 to 4 wt%. Members of the pyrochlore super group have been identified in both the metaluminous and peralkaline units. This group is the most chemically variable; fluorcalciopyrochlore, calciopyrochlore, and a probable mixed pyrochlore species were observed. Nb is the dominant B-site cation in all analyses. In all members, $TiO_2$ ranges from 5 to 8 wt%, with variable $UO_2$ and $ThO_2$ 0.5 to 12 wt%, PbO 0.1 to 6 wt% and ΣREE ranges from 0.2 to 8 wt%.

The Robertson River suite is enriched in HFSE and Ga. The maximum values are as follows: Ga varies from 41 to 54 ppm in the metaluminous rocks and 58 and 87 ppm in the peralkaline Amissville and Battle Mountain units respectively, Zr ranges from 178 to 2402 ppm in the metaluminous suite and from 2469 to 4055 in the peralkaline rocks, Nb ranges from 47 to 97 ppm in the metaluminous units to 203 to 312 ppm in the two peralkaline units, and ΣREE+Y vary from 367 to 1685 ppm in metaluminous rocks to 1167 and 8253 ppm in the Amissville and Battle Mountain peralkaline units, respectively. The Nb/Ta w/w whole rock ratio varies from 7 to 30, however, most are below chondritic value of 19.9 and range from 10 to 18. This is in contrast to the Zr/Hf w/w whole rock values where most are superchondritic, >34.4. In both cases, their ratios are not correlated to abundance. The Nb/Ta w/w values of the Nb-Ta oxide minerals are far more varied than those in the host rocks, especially in the fergusonite and euxenite groups. The Nb/Ta w/w values in both fergusonite and euxenite groups vary from 11 to 300 with many with Ta analyses below the EPMA detection limit of 0.1 wt%.

Alteration in all the Nb-Ta groups except columbite is pervasive and can make interpretation of EPMA data sometimes difficult. The fergusonite, euxenite, and aeschynite groups appear to alter mainly by hydration with the addition and loss of major constituents. Si, Al, and Fe typically increase with Ti, Th, U and Pb increasing in some grains. Losses in Y and REE are major, although Nb tends to be less affected in some grains. The significant loss of Y and REE together with the identification of very late stage Y-REE phases suggest that using Y and REE related ratios to distinguish among magma sources may be questionable. Pyrochlore group alteration is by hydration and A-site cation loss and addition, especially Ca and Pb. The alteration systematics of the Nb-Ta minerals suggests that a late-stage, highly reactive aqueous fluid moved through the rock during the early cooling process. Ta appears to have been relatively mobile, although the details of its movement and precipitation are yet unknown.

**References:**

Ercit TS (2005) Identification and alteration trends of granitic-pegmatite-hosted (Y,REE,U, Th)-(Nb,Ta,Ti) oxide minerals: A statistical approach. Can Mineral 43:1291–1303

Tollo RP (1994) Definition and nomenclature of the Robertson River Igneous Suite, Blue Ridge Province, Virginia. In: Stratigraphic Notes, 1992. U.S. Geol Survey, Bull 2060, pp 19–24

Tollo RP, Lowe TK (1994) Geologic map of the Robertson River Igneous Suite, Blue Ridge Province, Virginia. U.S. Geol Survey Misc Field Studies Map MF-2229, scale 1:100,000. 15 pp

# Accessory mineral assemblage and their dependence on the melt character in the S-type granites: an example from the Western Carpathians

**Broska, I.*, Kubiš, M.**

*Earth Sciences Institute of the Slovak Academy of Sciences, Dúbravská cesta 9, 840 05 Bratislava*
** E-mail: igor.broska@savba.sk*

Volatile-rich S-type granite melts during their cooling and fractionation may significantly change the accessory mineral assemblage. Moreover, such granite systems strongly modify also the composition of some accessory phases. Therefore, the accessory minerals can be used as an important discriminative parameter for revealing circumstances or PTX conditions in such type of granite evolution. Generally the fluids and especially the presence of boron in the felsic melt significantly decrease the melt viscosity (e.g. Dingwell et al. 1993), minerals have more time for their growth, and unusual chemistry conditions during long fractionation give them special compositional features.

The Permian S-type granites from the Alpine Gemeric unit in the Western Carpathians are an excellent example of specialised accessory mineral evolution (Broska et al. 2002). Because of high concentration of boron the granites commonly contain schorlitic tourmaline and due to specific volatile and trace element contents (F, B, Rb, Nb, Ta, W, Sn) they are named specialised S-type granites. The content of tourmaline increases upwards changing also its form of occurrence - tourmaline in the deeper granite part forms scattered grains but within upper part it can be also nodular and dendritic.

The count of typomorphic minerals in the S-type granites, represented mainly by zircon, monazite, xenotime-(Y) ± garnet and tourmaline, is significantly enlarged in the differentiated upper part of granite body or in the granite cupolas. There is strong alteration of granites, including greisenisation. The granites in cupolas are tin-bearing because the extended S-type accessory mineral assemblage includes also Sn, Nb, Ta, W mineral phases or various Nb-Ta oxides, wolframites and economically important cassiterite, but on the contrary there is the decrease of frequency of REE accessory minerals. The apex granites can be qualified as rare-metal granites. Zircon in the rare-metal granite compared to deeper seated biotite granites shows a larger xenotime-(Y) molecule and also a different morphology, which result in lower IT parameter. Zircon composition or $Zr/Hf_{wt}$ ratio in zircon from deeper biotite granite varies from 29 to 45, for upper rare-metal granites an increase in Hf contents toward $Zr/Hf_{wt}$ results in a ratio of 5. The cheralite component in monazite from biotite granites does not exceed 12 mol. %, but in rare-metal granites the monazites contain up to 14 to 20 mol. % of cheralite and in some places even more than 40 mol. %. Accumulation of P along with high activity of F in granite cupolas stabilised aluminophosphates and topaz instead of primary apatite and albite (Petrík et al. 2011). Tiny, late pure apatite precipitates by exsolution of P from albites.

The very high flux regime in the differentiated granite cupolas which influences on frequency of the accessory mineral paragenesis, documents a formation of the tetrad effect on REE`s chondrite normalised patterns (Fig. 1). According to Bau (1996) the tetrad effect is caused by complexation of the REE`s with $H_2O$, $CO_2$, $F^-$, and Li. In such circumstances the behaviour of the REE`s is not more dependent on the ionic radii, but on filling of 4f orbitals. Thus, the REE`s with 0/4 (La), 1/4 (Nd, Pm), 2/4 (Gd), 3/4 (Ho, Er) and 4/4 (Lu) filling 4f orbitals can be fractionated from the other REE`s resulting in the

tetrad pattern. Generally, the tetrad effect occurs in highly evolved igneous rocks as an indicator of the transition between magmatic to high-temperature hydrothermal systems.

The relationship between accessory mineral paragenesis and the extreme volatile rich-granite system documents the tetrad effect or significant increase of the frequency of accessory mineral phases also in the granites from the Gemeric unit in Western Carpathians. The normalised REE pattern of the basic (undifferentiated) S-type granite with paragenesis represented by monazite-(Ce), xenotime-(Y), tourmaline ± garnet without bulk rock tetrad effect. On the other hand, rare metal granites in upper part of granite body are almost free of the REE accessory minerals which is in contrary to the more variable other accessory minerals including cheralite-(Ce), Nb-Ta-W minerals (Nb-Ta rutile, ferrocolumbite, manganocolumbite, ixiolite, Nb-Ta ferberite), cassiterite, topaz, molybdenite, arsenopyrite and rare accessory aluminophosphates (arrojadite, lacroixite, goyazite, gorceixite and viitaniemiite).

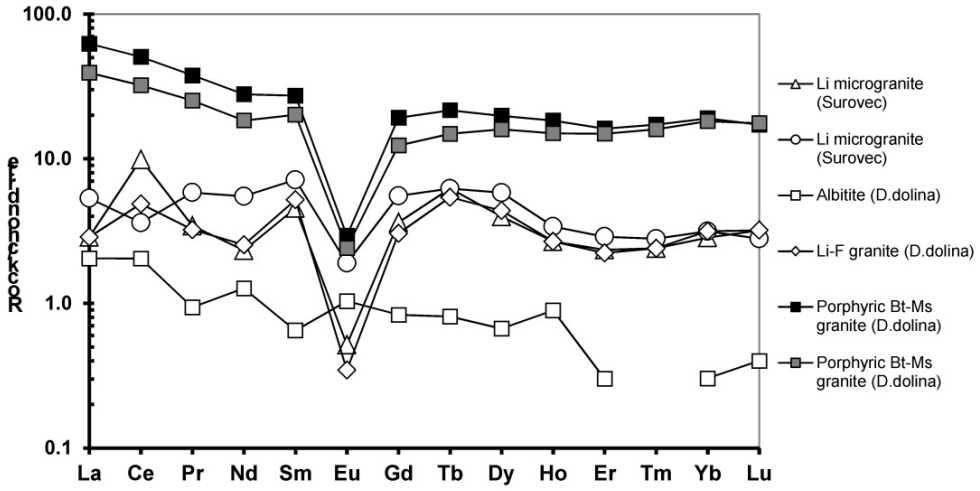


***Fig. 1.*** *Comparison of REE chondrite normalised patterns in deeper seated granites and upper rare-metal granites. The tetrad effect (open marks) in chondrite normalised granites indicates the high flux of volatiles in rare-metal granite cupolas which is connected with high frequency of accessory minerals with exception of REE minerals. Secondary albitites show the lowermost content of REE`s (locations are in brackets)*

***Acknowledgments:*** *This study was funded by the Slovak Scientific Grant Agency (VEGA 2/0084/17) and by APVV 140278.*

## References:

Bau M (1996) Controls on the fractionation of isovalent trace elements in magmatic and aqueous systems: evidence from Y/Ho, Zr/Hf, and lanthanide tetrad effect. Contrib Mineral Petr 123:323–333

Broska I, Kubiš M, Williams C, Konečný P (2002) The compositions of rock-forming and accessory minerals from the Gemeric granites (Hnilec area, Gemeric Superunit, Western Carpathians). Bull Czech Geol Survey 77:147–155

Dingwell DB, Knoche R, Webb SL (1993) The effect of F on the density of haplogranite melt. Am Mineral 78:325–330

Petrík I, Kubiš M, Konečný P, Broska I, Malachovský P (2011) Rare phosphates from the Surovec topa-Li-mica microgranite, Gemeric unit, Western Carpathians, Slovak Republic: role of $F/H_2O$ of the melt. Can Mineral 49:521–540

# Geochemistry of the Chaltén Plutonic Complex (Patagonia) mafic rocks and the influence of accessory minerals on trace element signature of arc magmas

**Bustamante, D.*, Ramírez de Arellano, C.**

*Facultad de Ingeniería, Escuela de Ciencias de la Tierra, Universidad Andres Bello*
** E-Mail: d.bustamantepa@gmail.com*

Several studies have shown that the trace elements signature of arc magmas is conditioned by the terrigenous material introduced into the mantle wedge during sediment subduction and subduction erosion. Like arc magmas, this terrigenous material is extremely rich in lithophile elements relative to mantle rocks. The way how these lithophile elements are transferred to the mantle wedge had been traditionally modelled considering the physical features of elements, such as ionic ratio and charge, resulting in a different behaviour (incompatibility and mobility) for each group of elements (e.g. LILE and HFSE) during the dehydration and melting processes that occur in the subduction zone. However, during the last decade, different authors have emphasized the importance of accessory minerals in the petrogenesis of arc magmas (e.g. Hermann and Rubatto 2009). The crustal rocks and sediments contain accessory minerals capable of capturing elements such as REE, U, Th, Zr, Hf, among others. For example, monazite usually has high Th and U concentrations; zircon has high concentration of Zr and Hf; garnet and titanite concentrate medium to heavy rare earth elements (MREE and HREE), while allanite concentrates light REE (LREE) and Th. In continental subduction zones, during the dehydration and melting of the oceanic crust and the overlying sediments, these minerals could remain as residual phases after the melting of terrigenous material, retaining the mentioned elements. Therefore, the trace element signature of terrigenous material could not be completely transmitted to the mantle wedge and arc magmas.

We analyse next the geochemical data from a mafic unit belonging to the Chaltén Plutonic Complex (CHPC), located at the Chile-Argentina border in Patagonia formed in a context of fast subduction and high subduction erosion rates during the Miocene in the Austral Andes (Ramírez de Arellano et al. 2012). Within this complex, the Laguna Sucia mafic group (γ1 series), unlike the others units, shows a marked depletion in U, Th, Zr and Hf, and a flat LREE pattern.

Trace element ratios such as Th/La, which is typically inherited from subducted sediments (Plank 2005) does not correlate with any of the trench sediments, nor the forearc units. Therefore, we argue that the trace element signature of these rocks is not inherited from the continental crust. The degree of differentiation and the isotopic composition of these rocks indicate that only little assimilation occurred. Moreover, fractional crystallization modelling shows that there are no phases capable to generate such anomalies (Bustamante 2017). Considering these results, we argue that the U, Th, Zr and Hf anomalies observed in the analysed samples can be attributed only to processes occurred during the contamination of the mantle wedge with a subduction component generated by the partial melting of eroded crust.

Hence, trace element signature of arc magmas is influenced by the accessory minerals contained in terrigenous material, depending on whether they are melted or not. Petrography (optical microscopy and back scattered images), EDS and X ray diffraction analyses indicate the presence of zircon, Zr-oxides, monazite and large volume of garnet

in rocks from the forearc region (metamorphic complexes and Patagonian Batholith), supporting this hypothesis.

Unlike the Laguna Sucia mafic group (γ1 series), the rest of the CPCH mafic units, which do not exhibit strong U, Th, Zr and Hf negatives anomalies, represents situations in which zircon has been melted instead of remaining as residual phases after melting of terrigenous material. Thus, the melting of subducted terrigenous material (sediment or eroded crust) occurs at temperatures around of the zircon equilibrium condition (800-900°C; Watson and Harrison 1983). This is consistent with the sediment melting model proposed by Behn et al. (2011), where terrigenous material is detached from the slab and rise, forming diapirs and reaching higher temperatures in the mantle wedge.

***Acknowledgments:*** *Geochemical data presented here was generated during the PhD thesis of co-author C.R.d.A. and financed by the Swiss National Science Foundation (SNSF) under the direction of Benita Putlitz. Petrographic description, SEM and XRD analysed were performed in the Solid Analysis Laboratory (LAS) of Andres Bello University, financed by 1161818 Fondecyt Project and by UNAB Regular Project N°753.*

## References:

Behn MD, Kelemen PB, Hirth G, Hacker BR, Massonne HJ (2011) Diapirs as the source of the sediment signature in arc lavas. Nat Geosci 4:641-646. doi: 10.1038/NGEO1214

Bustamante D (2017) Anomalías de U, Th, Zr y Hf en magmas de arco y su posible relación con la contaminación del manto, producto de la subducción de parte de la corteza continental. Undergraduated thesis, Universidad Andrés Bello. Santiago, Chile

Hermann J, Rubatto D (2009) Accessory phase control on the trace element signature of sediment melts in subduction zones. Chem Geol 265(3-4):512–526

Plank T (2005) Constraints from Thorium/Lanthanum on Sediment Recycling at Subduction Zones and the Evolution of the Continents. J Petrol 46(5):921-944. doi.org/10.1093/petrology/egi005

Ramírez de Arellano C, Putlitz B, Müntener O, Ovtcharova M (2012) High precision U/Pb zircon dating of the Chaltén Plutonic Complex (Cerro Fitz Roy, Patagonia) and its relationship to arc migration in the southernmost Andes. Tectonics 31(4), TC4009. doi: 10.1029/2011TC003048

Watson EB, Harrison TM (1983) Zircon saturation revised: temperature and compositions effects in a variety of crustal magma types. Earth Planet Sc Lett 64(2):295-304. doi: 10.1016/0012-821X(83)90211-X

# Chevkinite-(Ce) from São Miguel, Azores Islands: monitoring the crystal structure from primary crystallization to late-stage hydrothermal events

**Carbonin, S.[1]*, Liziero, F.[1], Ridolfi, F.[2], Renzulli, A.[3], Belluso, E.[4]**

*[1] Dipartimento di Geoscienze, University of Padova - Italy*
*[2] Leibniz Universität Hannover - Germany*
*[3] Dipartimento di Scienze Pure e Applicate, University of Urbino - Italy*
*[4] Dipartimento di Scienze della Terra, University of Torino -Italy*
** E-Mail: susi.carbo@hotmail.co.uk*

Chevkinite-(Ce), a REE-Ti-Fe silicate with general formula $^{X\text{-}VIII}A_4{}^{VI}B{}^{VI}C_2{}^{VI}D_2Si_4O_{22}$, is an accessory phase in silica-saturated-oversaturated syenite clasts (weakly peralkaline) contained in the plinian pumice fall erupted at 5 ka from the Agua de Pau volcano (Fogo A deposit; São Miguel, Azores Islands) (Ridolfi et al. 2003). Ten crystals from 3 rock-samples were investigated by means of single-crystal X-ray structure refinement, combined with electron microprobe chemical analysis, in order to obtain accurate cation distribution. Previous extensive characterization by means of transmission electron microscopy (TEM) showed these minerals to exhibit high crystallinity and few defects, confirming that they are non-metamict. Azores chevkinite is characterized by significant quantities of HFSE besides the main constituent Ti, namely Nb (4 wt.% $Nb_2O_5$) and to a lesser extent Zr (1 wt.% $ZrO_2$). Substitution of $REE^{3+}$ by $Ca^{2+}$ in the A sites is accompanied by substitutions at the octahedral sites for charge compensation: the overall compositional variation is best represented by the relationship (Ca+Ti+Zr) ↔ (REE+$Fe^{2+}$+Nb), thus Nb and Zr are inversely correlated with each other.

Structural refinements were carried out in space group *C2/m* without chemical constraints, taking care to properly select the scattering curves for site occupancy refinement in the A, B, C and D sites. Subsequently, both X-ray diffraction data and microprobe analyses were taken into account to achieve cation distribution by means of the minimization of an error function. The result is that Nb and Zr are found located in the D sites. Niobium site preference for the D sites is corroborated by an earlier prediction of Calvo and Faggiani (1974) who calculated that some pentavalent substitution in the D sites of chevkinite would enhance the chance for its appearance. Moreover, judging from Nb mineral/melt values, São Miguel chevkinite is particularly enriched in Nb relative to its host rock (Ridolfi et al. 2003) as was already noted by MacDonald et al. (2002) for two Kenyan samples. In addition, inspection of Nb content both in the bulk analysis and in chevkinite from the literature, allows us to speculate that chevkinite behaves as a "trash-bin" mineral for this element. With respect to the B site occupancy, Fe is dominant but in the most Ca-Ti-Zr-rich samples small quantities of Ca and Zr reside here. The C sites are mainly occupied by Ti and Fe. The 8- and 10-coordinated A sites, A1 and A2 respectively, are occupied dominantly by REE and Ca, and the cation distribution shows that they are unequally populated, mainly as a function of the ionic size.

In the studied chevkinites, the exchange reactions seem to be more complex than those suggested by Vlach and Gualda (2007 and references therein), i.e. $(Ca+Sr)_A+(Ti+Zr)_C$ ↔ $(REE,Y)_A+(M^{3+,2+})_C$, which take into account only the A and C sites.

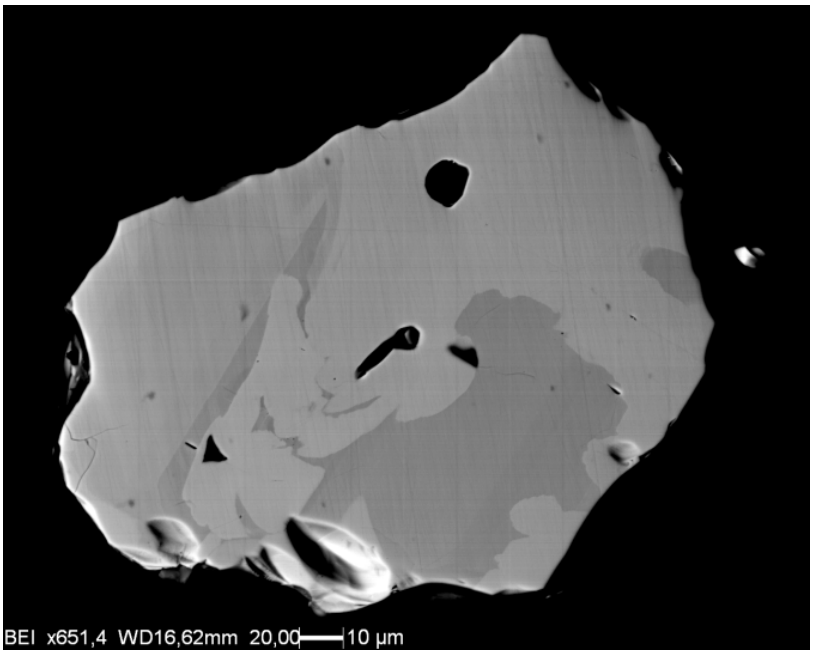


***Fig. 1.*** *Back-scattered electrons (BSE) image of one structurally refined zoned crystal; brighter areas are characterized by high REE, Nb and Fe abundances; darker zones are more enriched in Ca, Ti and Zr*

In the ten crystals studied, 2 show complex, patchy zoning indicating resorption and recrystallization. Notably, one of them (Fig 1) shows the best structure refinement (R= 0.018 for 1327 reflections) meaning that recrystallization did not affect its crystallinity. Primary crystallization occurred from peralkaline melts enriched in REE, Nb and Fe; subsequently chevkinite interacted with hydrothermal fluids more enriched in Ca, Ti and Zr. Areas enriched in Ca (and to a lesser extent Ti and Zr) display normal analytical totals from which good-quality mineral formulae can be derived. The charge balance relationship (Ca+Ti+Zr) ↔ (REE+$Fe^{2+}$+Nb) is continuous with that of the other crystals studied. The total number of electrons determined from site occupancy refinement in the A, B, C and D sites is in good agreement with that derived from chemical composition averaged between the REE-and the Ca-rich areas. Chevkinite, that evolved in such a way from REE-rich to Ca-rich compositions, should have recorded a late stage deuteric alteration resulting from a closed-system, magmatic-hydrothermal stage of crystallization, rather than metasomatic contributions.

***Acknowledgments:*** *CNR-IGG is thanked for the maintenance of the electron microprobe laboratory in Padova. Thanks are extended by SC to G. Menegazzo for writing the minimization program, to. A. Fioretti for the BSE image, and to S. Boesso for heavy liquid concentrations of chevkinite minerals.*

## References:

Calvo C, Faggiani R (1974) A Re-investigation of the Crystal Structures of Chevkinite and Perrierite. Am Mineral 59:1277-1285

Macdonald R, Marshall AS, Dawson JB, Hinton RW, Hill PG (2002) Chevkinite-group minerals from salic volcanic rocks of the East African Rift. Miner Mag 66(2):287-299

Ridolfi F, Renzulli A, Santi P, Upton BGJ (2003) Evolutionary stages of crystallization of weakly peralkaline syenites: evidence from ejecta in the plinian deposits of Agua de Pau volcano (São Miguel, Azores Islands). Miner Mag 67(4):749-767

Vlach SRF, Gualda GAR (2007) Allanite and chevkinite in A-type granites and syenites of the Graciosa Province, Southern Brazil. Lithos 97:98-121

# Insight from high common Pb monazite: Llallagua Tin Ore Deposit (Bolivia) and Amelia Pegmatite (Virginia, USA)

**Catlos, Elizabeth J.[1,*], Miller, Nathan R.[1]**

*[1] The University of Texas at Austin, Jackson School of Geosciences, 1 University Station C1100, Austin, TX, 78756, USA*
** E-mail: ejcatlos@jsg.utexas.edu*

Monazite [(Ce,Th)$PO_4$] is commonly reported to contain low amounts of common Pb and thus is ideal for U-Th-Pb geochronology. However, the Llallagua tin ore deposit in Bolivia and a pegmatite in the Amelia mining district of Virginia have monazite with unusually large and variable amounts of bulk abundance of common Pb or percentage of common to radiogenic Pb. Understanding if common Pb is accommodated in the monazite structure deserves attention because the mineral is a commonly used geochronometer in methods that avoid the measurement of Pb isotopes. Herein, we analyze monazite from these locations by electron microprobe (EMP), laser ablation-inductively coupled plasma mass spectrometry (LA-ICP-MS), and secondary ion mass spectrometry (SIMS) to determine whether common Pb resides within the primary monazite structure, along microcracks, or as contamination by other mineral phases.

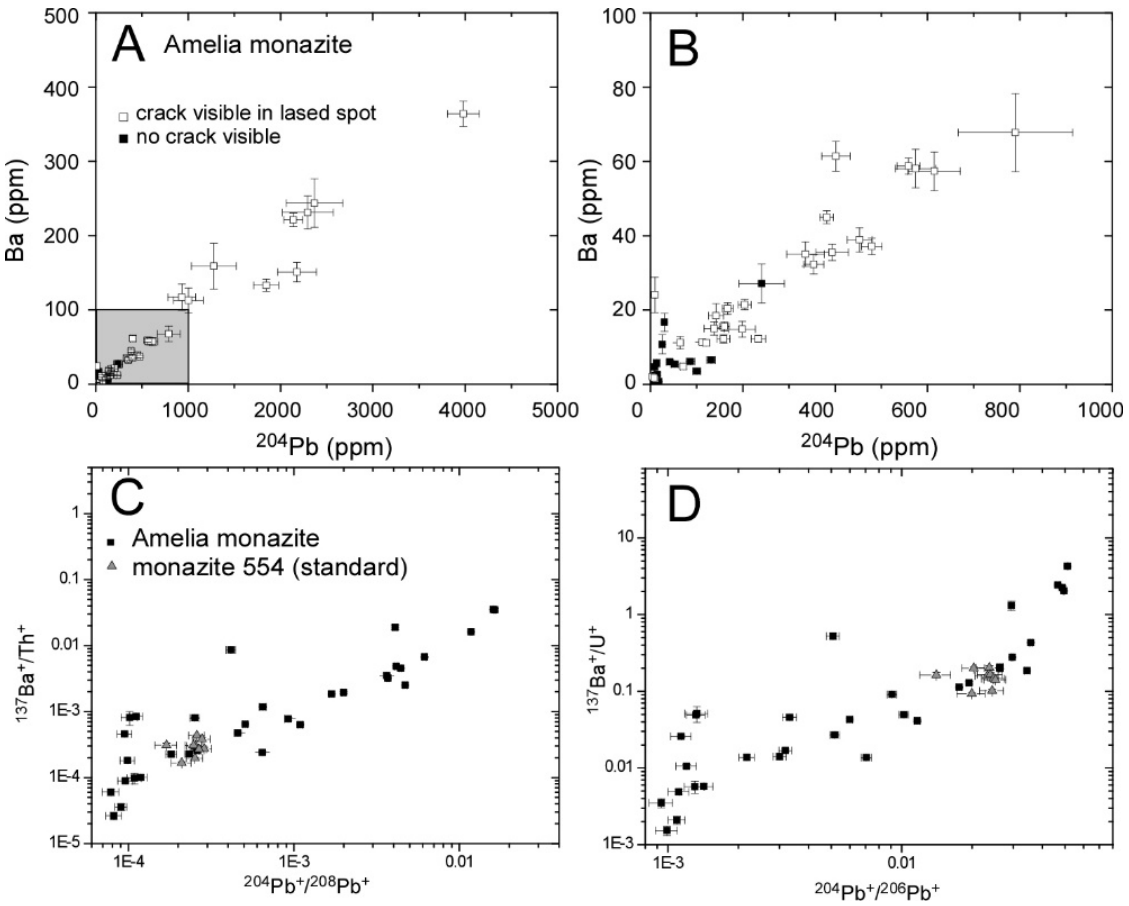


***Fig. 1.*** *(A) 204Pb (ppm) vs. Ba (ppm) from the Amelia monazite obtained using LA-ICP-MS. The shaded region is shown in panel (B). (C) $^{204}Pb+/^{208}Pb+$ vs. $^{137}Ba+/Th+$ and (D) $^{204}Pb+/^{206}Pb+$ vs. $^{137}Ba+/U+$ from the Amelia monazite obtained using SIMS (after Catlos and Miller, 2016)*

A large single crystal of Amelia monazite is high in Th (8.54±1.63 wt%) and has numerous microcracks adjacent to compositional discontinuities with respect to primary zoning, consistent with recrystallization (see Catlos and Miller, 2016 for details). The amount of $^{204}Pb$, a proxy for common Pb in the Amelia monazite, linearly correlates with Ba, suggesting the presence of a stoichiometric phase or possible substitution mechanism (Fig. 1).

Common Pb in the Amelia monazite may be related to the presence of gorceixite [$(BaAl_3(PO_4)(PO_3OH)(OH)_6$], Ba-bearing plumbogummite [$PbAl_3(PO_4)_2(OH)_5{\cdot}H_2O$], or other Ba-bearing phase in association with microcracks as the result of alteration.

Monazite from the Llallagua tin ore deposit in Bolivia formed via direct precipitation from hydrothermal fluids as evidenced by oscillatory zoning, low radiogenic element contents, field evidence, and textural relationships (Fig. 2). Monazite compositions should thus provide insight into characteristics of the fluids from which it formed. As expected, the Llallagua monazite has low and variable concentrations of radiogenic elements, with higher amounts of U (177±42 ppm) than Th (63±30 ppm). This is commonly observed with hydrothermal monazite and presents analytical challenges for geochronology. High common Pb reported for this monazite is likely due to the difficulty of measuring low levels of Pb in the mineral overall (near instrument detection limits).

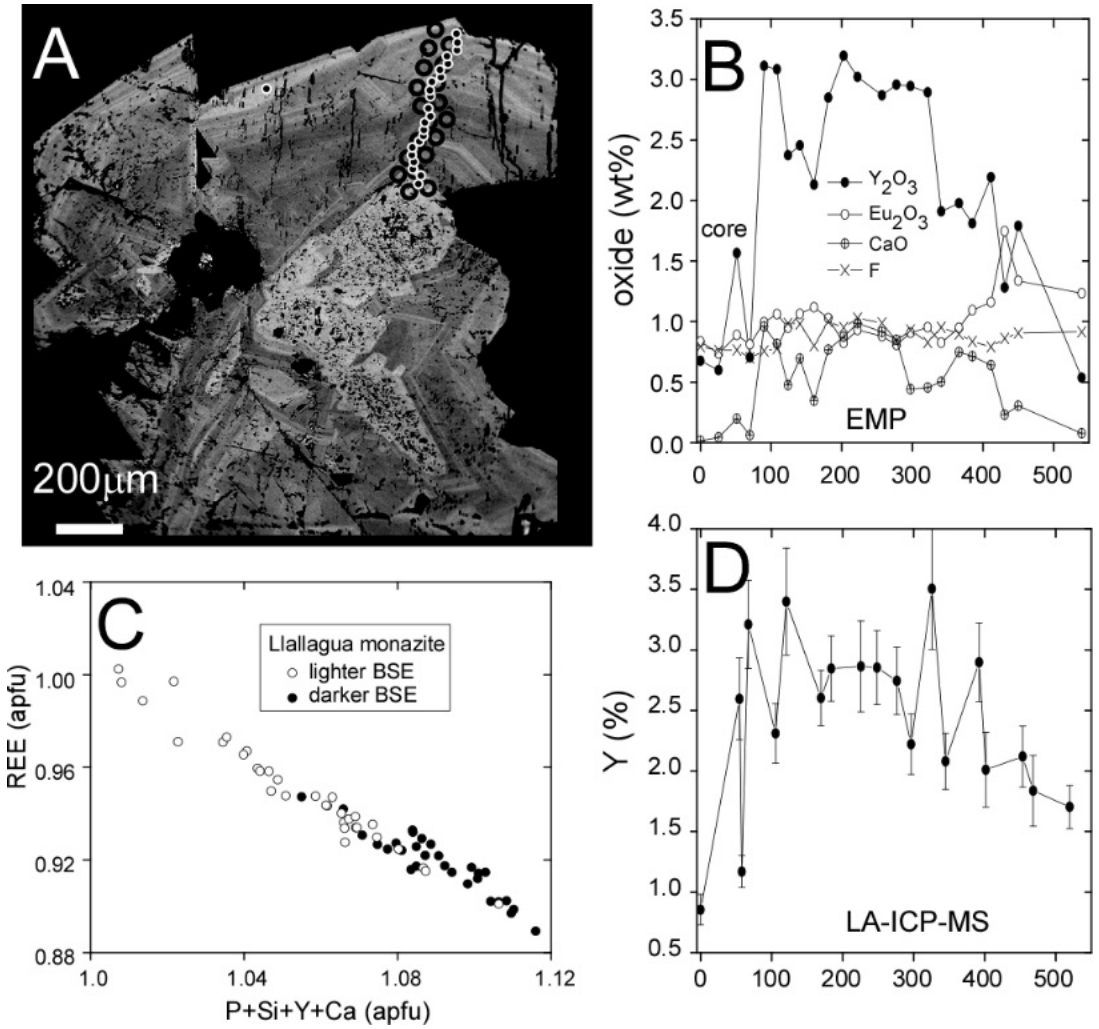


***Fig. 2.*** *(A) BSE image a Llallagua monazite grain. Dark circles are locations of LA-ICP-MS spots, whereas white circles are EMP analyses. (B) Transects across this grain in $Y_2O_3$, $Eu_2O_3$, CaO or F obtained using an electron microprobe. (C) P+Si+Y+Ca vs. REE (apfu). (D) Transect in Y obtained using LA-ICP-MS*

The Llallagua grains contain some of the highest amounts of fluorine ever reported for monazite (0.88±0.10 wt%) (Fig. 2B), indicating fluids from which it precipitated were likely rich in F, an effective mobilizer of REE, Y, and Th. The monazite also has high Eu contents and positive Eu anomalies, consistent with formation in a highly reducing back arc environment. Fluorine, Ca, Si and REE may have been supplied via the dissolution of pre-existing fluorapatite. Both minerals share substitution mechanisms and positive Eu anomalies. Monazite oscillatory zoning is controlled by an interplay of low (P + Ca + Si + Y) and high atomic number (REE) elements.

Common Pb in monazite may be hosted in fractures, along grain boundaries, and/or as surface contamination, rather than in the monazite structure. The results reported here have implications for those seeking to avoid common Pb and, as both study localities are historically important mining districts, detailed compositional data from these monazite grains may aid new evaluations of these localities as potential ore resources for rare earth elements.

## References:

Catlos, E.J., Miller, N.R. (2016) Ion microprobe $^{208}Th$–$^{208}Pb$ ages from high common Pb monazite, Morefield Mine, Amelia County, Virginia: Implications for Alleghanian tectonics. American Journal of Science 316: 470-503

# Dry annealing of radiation damaged zircon: Which "degree of reconstitution" is probed by which analytical technique?

**Chanmuang, C.[1,*], Ende, M.[1], Nasdala, L.[1], Wirth, R.[2]**

*[1] Institut für Mineralogie und Kristallographie, Universität Wien, Althanstr. 14, 1090 Wien, Austria*
*[2] Sektion 4.3, Helmholtz-Zentrum Potsdam, Deutsches GeoForschungsZentrum GFZ, Telegrafenberg, 14473 Potsdam, Germany*
** E-Mail: chutimun.chanmuang@univie.ac.at*

Radiation damaged zircon recovers upon dry thermal annealing. Several aspects of the structural recovery, however, are still controversial. For several applications, it is crucial to estimate the extent to which the initial radiation damage has been recovered. For instance, CA (chemical abrasion) prior to TIMS analysis (Mattinson 2005) is well known to yield less biased U–Pb geochronology results, however, it is crucial to understand which temperature treatment leads to which degree of structural reconstitution, before the chemical treatment is done (Mattinson et al. 2007). Another example is the gradual change in He-retention performance upon thermal annealing (Guenthner et al. 2013), whose understanding requires quantitative estimation of the structural recovery.

We report here first results of a systematic dry-annealing study that involves zircon samples ranging from mildly to severely radiation damaged. We have observed that "degrees of recovery" estimated from diffraction techniques (e.g. unit-cell dimensions and volumes, sharpness of electron-diffraction spots) tend to be much higher than "degrees of recovery" detected by short-range-order methods (e.g., sharpening of Raman bands and luminescence lines; Fig. 1). For instance, annealing of zircon #GZ8 at 700 °C (96 h) has caused more than 80 % of the total unit-cell reduction. The very same annealing resulted in only ~50 % of the total Raman-bandwidth reduction (Fig. 2a). This apparent mismatch indicates that long-range and short-range methods are not just complementary techniques but detect different types of annealing-induced changes.

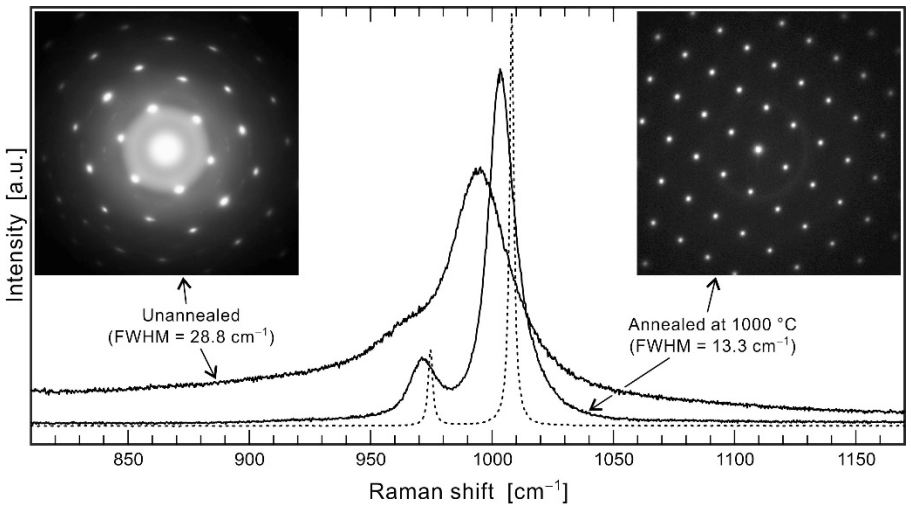


***Fig. 1.*** *Apparently incongruent recovery of the long-range and short-range order of the severely radiation damaged zircon #G3 upon dry annealing, visualised by the comparison of Raman spectra and electron diffraction patterns (dotted: reference spectrum of crystalline $ZrSiO_4$). Note that annealing at 1000 °C has resulted in decidedly incomplete relaxation of the Raman band broadening whereas fairly sharp electron diffraction spots imply that the long-range lattice order is widely recovered*

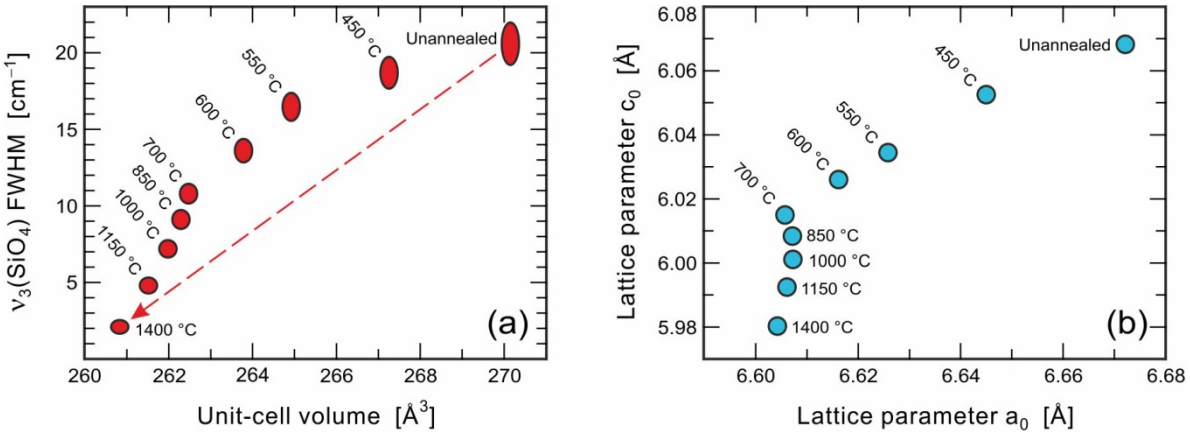


***Fig. 2. a*** *Apparently incongruent degrees of thermal annealing of the moderately radiation-damaged zircon #GZ8, as detected by Raman and X-ray diffraction. Note that the proportionate decrease of the unit-cell volume exceeds appreciably that of the full width at half maximum (FWHM) of the main Raman band near 1000 cm$^{-1}$.* ***b*** *Mismatch in the proportionate reduction of the unit-cell dimensions parallel and perpendicular to the c axis upon dry annealing*

The apparently "quick" unit-cell reduction is controlled by extensive changes in lattice parameter $a_0$ in initial annealing stages. It is well known that upon accumulation of radiation damage, the unit cell expands preferentially along c whereas its a dimension experiences significant increase at more elevated damage-accumulation steps (Holland and Gottfried 1955). Upon dry annealing of radiation damaged zircon, the "mismatch" between $a_0$ and $c_0$ is even more striking: Initial annealing is dominated by $a_0$ decrease (virtually completed at 700 °C) whereas $c_0$ continues to decrease until nearly complete recovery is achieved at 1400 °C (Fig. 2b). The preferred relaxation of the initial expansion along the a axis (Weber 1990) can be used to distinguish untreated and partially annealed zircon (Nasdala et al. 2004).

Overall, there are vast differences in the "degrees of annealing" as detected by different techniques. Moderately heat-treated zircon (i.e. annealing at moderate temperatures and/or for short durations) may appear widely recovered when studied with diffraction methods but still show significant degrees of disturbance of the short-range order. We present first results of the ongoing, combined Raman and X-ray and electron diffraction study; interpretations and possible implications are discussed.

***Acknowledgments:*** *Zircon G3 was made available by Allen K. Kennedy and its annealing was done by James M. Mattinson. Financial support by the Austrian Science Fund (FWF) through project P24448–N19 to L.N. is gratefully acknowledged.*

## References:

Guenthner WR, Reiners PW, Ketcham RA, Nasdala L, Giester G (2013) Helium diffusion in natural zircon: Radiation damage, anisotropy, and the interpretation of zircon (U-Th)/He thermochronology. Amer J Sci 313:145–198

Holland HD, Gottfried D (1955) The effect of nuclear radiation on the structure of zircon. Acta Cryst 8:291–300

Mattinson JM (2005) Zircon U–Pb chemical abrasion (CA-TIMS) method: combined annealing and multi-step dissolution analysis for improved precision and accuracy of zircon ages. Chem Geol 220:47–56

Mattinson JM, Nasdala L, Lengauer C, Wirth R (2007) Inside CA-TIMS zircon analysis; the interplay among natural radiation damage, annealing, solubility, and U-Pb isotopic systematics. Eos Trans Am Geophys Union 88(52), Suppl, abstract V31G-06

Nasdala L, Reiners PW, Garver JI, Kennedy AK, Stern RA, Balan E, Wirth R (2004) Incomplete retention of radiation damage in zircon from Sri Lanka. Am Mineral 89:219–231

Weber WJ (1990) Radiation-induced effects and amorphization in zircon. J Mater Res 5:2687–2697

# Special case of cation ordering in octahedral sites in natural epidote-supergroup minerals

**Cibula, P.[1,*], Bačík, P.[1], Kozáková, P. [1], Miglierini, M.[2]**

*[1] Comenius University in Bratislava, Faculty of Natural Sciences, Department of Mineralogy and Petrology, Ilkovičova 6, 842 15 Bratislava, Slovakia*
*[2] Slovak University of Technology in Bratislava, Faculty of Electrical Engineering and Information Technology, Institute of Nuclear and Physical Engineering, Ilkovičova 3, 812 19 Bratislava, Slovak Republic*
** E-Mail: cibula9@uniba.sk*

Crystals of natural dark green epidote from Sobotín, Czech Republic (ES) and natural brown-green clinozoisite from Baluchistan, Pakistan (CP) were studied for crystal-chemical variations before and after heating. Two samples from each other were not heat treated and were used as a standard while the eight other parts were heated in the muffle furnace in the air atmosphere for 12 hours and then cooled down to the ambient temperature for 12 h.

The average chemical composition of epidote in ES-0 – ES-9 is $Ca_{2.000}A1_{2.211}Fe_{0.742}Si_{2.994}O_{12}(OH)$ and clinozoisite (CP-0 – CP-9) is $Ca_{2.017}A1_{2.626}Fe_{0.319}Si_{3.002}O_{12}(OH)$. The main difference between samples is in Fe/Al ratio. Epidote from Sobotín is $^{M3}Fe^{3+}$-dominant (0.68–0.80 apfu), while $Fe^{3+}$ (between 0.29–0.33 apfu) is lower in clinozoisite samples. The content of other cations including Mg, Ti, V and Cr is very low or below the detection limit in both types of samples.

The unit-cell dimensions of both samples strongly depend on the $Fe^{3+}$-Al ratio. Original samples fall into the trend of epidote-clinozoisite solid solution very well with larger all *a*, *b*, *c* and *V* in $Fe^{3+}$-dominant epidote in ES sample compared to clinozoisite in CP. However, in heated samples, deviations from the trend can be observed. It is better pronounced in the CP samples with a vertical trend of increase in all *a*, *b*, *c* and *V* in heated samples. This trend could be partly attributed to small variations in $Fe^{3+}$-Al ratio but interestingly, sample heated at 900°C display significant increase in *b*. In contrast, the ES samples displays similar vertical trend only in *c* and partly in *a*; variations in *b* and *V* have no significant vertical trend.

The position of $Fe^{3+}$ in the epidote-clinozoisite structure can be read from the Mössbauer spectra; spectra of both sample sets heated below 1000°C contain doublets related to $Fe^{3+}$ in octahedral coordination. However, there is a slight difference in doublets if both sample sets are compared. The ES spectra are symmetrical and can be interpreted as one doublet of $Fe^{3+}$ in the *M*3 site. However, CP samples display slight asymmetry of Mössbauer spectra. This can be explained by presence of more components in spectra. First two components have isomer shift (IS) and quadrupole splitting (QS) typical for *M*3 site. Third doublet is close to $Fe^{3+}$ in *M*1 site and takes area of 12-15 % corresponding to ca. 0.04 apfu in samples heated up to 500°C and increases up to 19 % (0.06 apfu) in samples heated at more than 500°C.

Incorporation of small amounts of $Fe^{3+}$ in *M*2 can explain the presence of doublets with IS 0.31- 0.37 mm/s and QS 0.80-1.00 mm/s in the Mössbauer spectra of epidote-clinozoisite solid solution (Liebscher, 2004). In our samples, doublets of the CP samples original and heated up to 800 °C have a similarly low QS but distinctly higher IS. Therefore, their interpretation as $Fe^{3+}$ in *M*2 is not entirely clear but also not ruled out.

The *M*1 site links the oxygen atoms O1, O4, and O5. The O4–O5 edge is shared between individual octahedra forming chains to which the individual *M*3 octahedra are attached.

*M*1 and *M*3 are connected by a common O1–O4 edge. The *M*1 octahedron is fairly regular and its mean bond length is about 1.90 to 1.94 Å (Franz & Liebscher, 2004). Up to about $X_{Ep}$ = 0.6 the *M*1 octahedron exhibits only minor structural changes with increasing Fe content: the mean bond length, the volume, and the distance between the two apical O1 atoms slightly increase as response to the expansion of the attached *M*3 due to increased Fe content on *M*3 (Bonazzi & Menchetti, 1995).

Based on the site occupancy, attention must be paid to *M*1 and *M*3 octahedra, if the crystal chemistry of epidote-clinozoisite solid solution is going to be studied. The *M*3 octahedron coordinates the oxygen atoms O1, O2, O4, and O8 and is the largest and most disorder site with the largest variability in occupancy (Ito et. al., 1954; Stregiou et. al., 1987; Grodzicki et. al., 2001). Increasing Fe content increases its mean bond length from 1.98 to 2.06 Å (Franz & Liebscher, 2004). This mostly results from increase in the distance between the apical O4 and O8 due to the significant shift of O8; in clinozoisite it is considerable smaller than the comparable O1–O1 distance in *M*1, but increases significantly with increasing Fe content. Structural changes of *M*3 are most pronounced for $X_{Ep} < 0.6$ and are in a clear linear relationship with Fe content. If $X_{Ep}$ is higher than 0.6, the structural changes are less obvious and non-linear (Franz & Liebscher, 2004).

In the Mössbauer spectra, $Fe^{3+}$ in *M*1 is manifested by doublets with IS 0.22-0.36 mm/s and QS 1.46-1.67 mm/s (Bird et. al., 1988; Fehr & Heuss-Assbichler, 1997; Heuss-Assbichler, 2000). Doublets in our CP-0 – CP-8 samples have slightly higher IS and QS but their interpretation as $Fe^{3+}$ in *M*1 is relatively reasonable. Moreover, Fehr & Heuss-Assbichler (1997) observed two doublets in the Mössbauer spectra that both displayed the main characteristics of $Fe^{3+}$ on *M*3 but with small differences in their QS. These were attributed to two slightly different *M*3 sites, labelled *M*3 and *M*3´, which belong to two different monoclinic epidote phases, one with Al-$Fe^{3+}$ disorder on *M*3 (*M*3 doublet) and one with an ordered distribution of Al and $Fe^{3+}$ at *M*3 (*M*3´ doublet); the latter represents the intermediate composition with $X_{Ep}$ = 0.5 (Fehr & Heuss-Assbichler, 1997; Heuss-Assbichler, 2000).

However, this interpretation is relatively questionable, although, it can explain asymmetry of doublets in the CP samples very effectively. The Al-$Fe^{3+}$ disorder between the *M*1 and *M*3 octahedral sites occurs at total $Fe^{3+}$ contents higher than about $X_{Ep}$ = 0.6 and is restricted to the *M*1 and *M*3 sites (Giuli et. al., 1999). This obviously is not our case because CP clinozoisite contain only up to 0.3 $Fe^{3+}$ apfu. On the other hand, variable degree of disorder in specific areas of clinozoisite structure may result not only in occurrence of probable *M*1 doublet but also in above mentioned splitting of *M*3 doublets which may be interpreted for instance as *M*3 doublet for isolated $^{M3}Fe^{3+}$ and *M*3´ doublet for the pair of $^{M1}Fe^{3+}$ and $^{M3'}Fe^{3+}$ in neighbouring octahedra.

***Acknowledgments:*** *This work was supported by the Ministry of Education of Slovak Republic grant agency under the contracts VEGA-1/0079/15 and VEGA-1/0499/16.*

## References:

Bird DK, Cho M, Janik CJ, Liou JG, Caruso LJ (1988) Compositional order - disorder and stable isotope characteristics of Al–Fe epidote state 2-14 drill hole Salton Sea Geothermal System. J Geophys Res 93:13135–13144

Bonazzi P, Menchetti S (1995) Monoclinic members of the epidote group: effect of the Al↔$Fe^{3+}$↔$Fe^{2+}$ substitution and of the entry of $REE^{3+}$. Mineral Petrol 53:133–153

Fehr KT, Heuss-Assbichler S (1997) Intracrystalline equilibria and immiscibility along the join clinozoisite–epidote: An experimental and $^{57}Fe$ Mössbauer study. Neues Jahrbuch für Mineralogie Abhandlungen 172:43–76

Franz G, Liebscher A (2004) Introduction to Physical and Chemical Properties of the Epidote Minerals. Rev Mineral Geoche 56: 1–82

Giuli G, Bonazzi P, Menchetti S (1999) Al-Fe disorder in synthetic epidotes: a single-crystal X-ray diffraction study. Am Mineral 84:933–936

Grodzicki M, Heuss-Assbichler S, Amthauer G (2001) Mössbauer investigations and molecular orbital calculations on epidote. Phys Chem Miner 28(9):675–681

Heuss-Assbichler S (2000) Ein neues Ordnungsmodell für die Mischkristallreihe Klinozoisit-Epidot und das Granat-Epidot-Geothermometer. Habilitationthesis, Munich p105

Ito T, Morimoto N, Sadanga R (1954) On the structure of Epidote. Acta Crystallogr 7:53–59

Liebscher A (2004) Spectroscopy of Epidote Minerals. Rev Mineral Geochem 56: 125–170

# Investigating Pb loss in baddeleyite

**Davies, J.H.F.L.[1,*], Seydoux-Guillaume, A.-M.[2], Schaltegger, U.[1]**

*[1] Department of Earth Sciences, University of Geneva, rue des Maraîchers 13, CH-1205 Geneva, Switzerland*

*[2] 2Laboratoire Magmas et Volcans LMV, UMR 6524 CNRS-UBP-UJM-IRD, Faculté de Sciences et Techniques, 23 rue du Dr. Paul Michelon, 42023 Saint Étienne, France*

** E-Mail: joshua.davies@unige.ch*

Baddeleyite ($ZrO_2$) is a trace phase that can be found in small evolved melt pockets in mafic rocks. Baddeleyite incorporates U into its crystal structure during growth and rejects Pb, much like zircon, $ZrSiO_4$ (its silicate equivalent), making it an excellent mineral for U-Pb dating. Initial studies to date mafic rocks discovered that baddeleyite is much more robust to secondary Pb loss than zircon. When zircon and baddeleyite were dated from the same samples, zircon often suffered from Pb loss, yielding discordant results, whereas baddeleyite typically was concordant or close to concordant (e.g. Heaman and LeCheminant 1993). However, after the introduction of the chemical abrasion technique to remove the areas of zircon affected by Pb loss and get reliable and concordant U-Pb ages (Mattinson, 2005), it became apparent that baddeleyite crystals, which are not amenable to chemical abrasion (see Rioux et al. 2010), are more prone to Pb loss than previously thought (Schaltegger and Davies, 2017).

Here we investigate the possible mechanisms for Pb loss in baddeleyite. We use Raman spectroscopy and transmission electron microscopy to determine the cumulative effects of U decay on the structure, we also use trace element geochemistry and electron imaging to assess the effects of secondary alteration on baddeleyite crystals. We show that baddeleyite is much more robust to radiation damage than zircon, and shows almost no long range disorder due to alpha recoil, this is similar to monazite. However short range disorder is observed in Raman spectra with band broadening which roughly correlates to alpha dose. We also show that alpha recoil ejection can be a viable mechanism for Pb loss from baddeleyite in some cases, since typical baddeleyite have a high surface area to volume ratio. However, most investigated baddeleyite crystals do not show consistent trends between geochemistry, structure and Pb loss suggesting that fast pathway diffusion may be the most viable mechanism for Pb mobility in most cases.

***Acknowledgments:*** *We acknowledge funding from the SNSF (project number 162341). We also acknowledge the radiogenic isotope group at the University of Genève for useful discussions throughout the completion of this work.*

## References:

Heaman, L.M., LeCheminant, A.N. (1993) Paragenesis and U–Pb systematics of baddeleyite ($ZrO_2$), Chemical Geology, 110, pp. 95-126

Mattinson, J.M. (2005) Zircon U–Pb chemical abrasion ("CA-TIMS") method: Combined annealing and multi-step partial dissolution analysis for improved precision and accuracy of zircon ages, Chemical Geology, 220, 1–2, 12, pp. 47-66

Rioux, M., Bowring, S., Dudás, F., Hanson, R. (2010) Characterizing the U–Pb systematics of baddeleyite through chemical abrasion: application of multi-step digestion methods to baddeleyite geochronology, Contributions to Mineralogy and Petrology, 160, pp. 777-801

Schaltegger, U. Davies, J.H.F.L. (2017) Petrochronology of Zircon and Baddeleyite in Igneous Rocks: Reconstructing Magmatic Processes at High Temporal Resolution, Reviews in Mineralogy and Geochemistry, 83, pp. 297-328

# $ZrO_2/HfO_2$ in zircon from the Kozhim massif (Subpolar Urals)

**Denisova, Yu. V.**

*Institute of Geology, Komi Science Center, Ural Branch of the Russian Academy of Sciences, 54 Pervomaiskaya str., 167982, Syktyvkar, Russia*
*E-Mail: yulden777@yandex.ru*

Most accessory zircon crystals in rocks of the Kozhim massif are well-light faceted. Type I (about 80–90 vol% of all zircon): Transparent colourless, short-prismatic crystals with smooth and shiny faces. Sizes 0.05–0.15 mm; aspect ratios 1.0–1.8; developed faces (100), (110), (111). Type II (about 5–10 vol% of all zircon): Transparent brown, short-prismatic crystals with smooth and shiny faces. Sizes 0.05–0.10 mm; aspect ratios 1.0–2.0; developed faces (100), (110), (111). Type III (about 5–10 vol% of all zircon): Light transparent, long-prismatic crystals with smooth and shiny faces. Sizes 0.4–0.8 mm; aspect ratios 2.0–4.0; developed faces (100), (110), (111) (Denisova, 2014, 2015).

The quantity of the $ZrO_2/HfO_2$ were calculated and histograms of the $ZrO_2/HfO_2$ distribution compiled (Fig.1). Type II zircon is an early generation (the largest average value of $ZrO_2/HfO_2$ is 53,91). This type was formed in a tectonically quiet conditions (monomodality of the histogram 1. a). Type I is a late generation (the smallest average value of $ZrO_2/HfO_2$ is 43,90). The graphs of types I and III are bimodal and indicate the difficult conditions of crystallization.

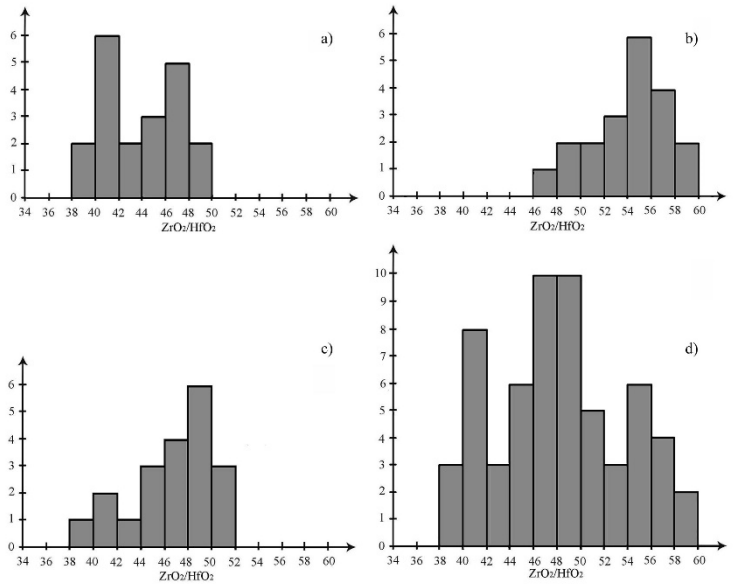


***Fig. 1.*** *Incidence of $ZrO_2/HfO_2$ in zircons of the Kozhim massif: (a) Type I; (b) Type II; (c) Type III; (d) Cumulative distribution (Types I+II+III)*

***Table 1.*** *Testing of the hypothesis about the normal distribution of $ZrO_2/HfO_2$*

| Type | Number of intervals | $\chi^2_{calc}$ | $\chi^2$ |
|---|---|---|---|
| I | 6 | 6.93 | 7.81 |
| II | 7 | 2.67 | 9.49 |
| III | 7 | 4.28 | 9.49 |

Note. $\chi^2_{calc}$ – calculated Pearson criterion; $\chi^2$ - table value of the Pearson criterion

Check the observed distribution of $ZrO_2/HfO_2$ for normality. According to the Pearson criterion, the studied distributions are normal (Table 1; or each type: $\chi^2_{calc} < \chi^2$). This allows you to apply various statistical methods of analysis of distribution.

Check the bimodality of the histogram for I and III morphotypes (table 2) by Goldin. Suppose that these histograms have the material of unimodal distribution of values of $ZrO_2/HfO_2$. According to the data obtained, the magnitude of the $ZrO_2/HfO_2$ for the I type in contrast to the III type have a bimodal distribution ($t_{calc} > t$). This distribution shows the heterogeneity of the environment of mineral formation during crystallization of an early generation of zircon.

***Table 2.*** *Testing of the hypothesis about monomodality the distribution of $ZrO_2/HfO_2$*

| Type | Incidence | | | $t_{1\ calc}$ | t |
|---|---|---|---|---|---|
| | First max | Second max | Min | | |
| I | 6 | 5 | 2 | 2.41 | 2.02 |
| III | 2 | 6 | 1 | 1.89 | 2.02 |

Note. $t_{1\ calc}$ – the calculated Styudent criterion; t - table value of the Styudent criterion

Each studied type of zircon is defined as a separate generation. However, the first and third types are similar in the distribution range of the $ZrO_2/HfO_2$, and the similar peaks. Check hypothesis about equality of average values (table. 3). The hypothesis of equal values was not confirmed ($t_{calc} > t$). Thus, all types of Kozhim zircon can be considered as a separate generation of the mineral.

***Table 3.*** *Testing of the hypothesis about equality of mean values of $ZrO_2/HfO_2$*

| Type | *mean values of* $ZrO_2/HfO_2$ | Dispersion | $t_{2\ calc}$ | t |
|---|---|---|---|---|
| I | 43.90 | 8.94 | 2.64 | 2.02 |
| III | 46.54 | 11.94 | | |
| III | 46.54 | 11.94 | 4.29 | 2.02 |
| II | 53.91 | 10.50 | | |

Note. $t_{2\ calc}$ – the calculated Styudent criterion; t - table value of the Styudent criterion

The beginning of the formation of the Kozhim massif is breaking through rocks of granite magma. The type II zircon started to crystallize during this stage. A sharp increase in the temperature of the melt led to the increase in uniformity of the mineral-forming medium. A change in the conditions contributed to the formation of long-prismatic crystals of zircon (type III). Next, the temperature decreased , the viscosity increased, fluidnation the mineral-forming medium was changed. As a result, the hafnium unstable to accumulate. All these changes led to the formation of later generation of mineral (type ii).

*The work is executed at financial support of the fundamental research Program of RAS № 15-18-5-17.*

## References:

Denisova Yu V (2014) Typomorphic and typochemical accessory zircons sings of the Subpolar Urals granitoids. Vestnik of the Institute of Geology, KomiSC of RAS, Syktyvkar 2014(5):9–16

Denisova Yu V (2015) The petrogenetic value of the $ZrO_2/HfO_2$ relations in zircons (Subpolar Urals). Vestnik of the Institute of Geology, KomiSC of RAS, Syktyvkar 2015(2):23–31

# In situ chemical dating of new accessory minerals from the Evate deposit in Mozambique

**Gajdošová, M.[1]*, Huraiová, M.[1], Hurai, V.[2], Konečný, P.[3]**

*[1] Department of Mineralogy and Petrology, Faculty of Natural Sciences, Mlynská dolina, Ilkovičova 6, 842 15 Bratislava*
*[2] Earth Science Institute, Slovak Academy of Sciences, Dúbravska cesta 9, 840 05 Bratislava*
*[3]Slovak Geological Institute of Dionýz Štur, Mlynská dolina 1, 817 04 Bratislava*
** E-mail: gajdosova86@uniba.sk*

This work is focused on in situ chemical dating of zirconolite, thorianite and monazite from the Evate apatite-magnetite-carbonate deposit in Mozambique.

The deposit is located in the eastern part of the Nampula province in the Monapo structure (Macey et al., 2013). The Evate deposit is one of the most important apatite deposits in Africa discovered during geophysical prospection in 1975, and investigated in 1983 by Bulgarian and finally by Czechoslovakian geologists (Intergeo, 1985). Drilling cores from the exploration work carried out by Geoindustria state enterprise in 1985 represent and unique research material investigated in this study.

The deposit has an elongated shape and is approximately 3 km long and 850 m wide. A total of 155 413 000 t of apatite ores with an average composition of 9.32 wt. % $P_2O_5$ is present.

Original report of Intergeo (1985) mentions apatite, magnetite, forsterite, phlogopite and graphite, with a smaller amount of diopside, amphibole, wollastonite, antigorite, scapolite, spinel, garnet, feldspar, rutile, quartz, sulphides and anhydrite. In current research, we have identified additional accessory minerals such as monazite, baddeleyite, zirconolite, allanite, zircon, thorianite, sulphates (gypsum, celestine, barite).

The aim of this study is to determine the age of zirconolite, thorianite and monazite using an in situ chemical dating, and to interpret new data in the context of the evolution of the Evate deposit. The chemical dating was performed using a CAMECA SX100 electron microprobe at the State Geological Institute of Dionýz Štúr in Bratislava. Calculated ages and individual statistical data were computed using a DAMON computer program (Konečný et al., 2004) with the equations given in the paper of Montel et al. (1996).

Zirconolite $CaZrTi_2O_7$ was present in two forms: younger zirconolite II created grains several μm size. Older zirconolite I created thin rims around magnetite, geikielite, zircon and baddeleyite. Zirconolite I has an increased content of REE+Y (0.323-0.613 *apfu*) and slightly increased content of Nb (0.009-0.180 *apfu*). Th (up to 0.185 *apfu*) and U (up to 0.074 *apfu)* contents are lower. Zirconolite II has low REE+Y (0.082-0.488 *apfu*) and Nb contents (0.012-0.152 *apfu*) and increased content of Th (0.012-0.218 *apfu*) and U (0.002-0.149 *apfu*). Grains of zirconolite I, 30-40 μm size, were used for dating. Their age calculated from 14 analyses corresponds to 443±3.4 Ma.

Thorianite $ThO_2$ was associated in the same sample with zirconolite, zircon, pyrrhotite, phlogopite and magnetite. Thorianite creates grains, 10-50 μm in size, with Th contents from 0.644 to 0.840 *apfu*. U and Pb contents ranged from 0.023 to 0.235 *apfu* and the calculated age from 11 analyses corresponded to 489±2.8 Ma.

Monazites from albitized gneiss underlying the magnetite-apatite deposit have increased LREE contents (0.810-1.000 *apfu*) dominated by Ce (0.37-0.50 *apfu*), being diagnostic of monazite-(Ce). HREE contents are low (0.006-0.08 *apfu*). Studied monazites

have low contents of the huttonite, xenotime and cheralite components. The age of monazite calculated from 6 analyses is 573±13 Ma.

The monazite age is consistent with 584±16.5 Ma old zircon rims correlated either with a cooling-related metasomatic event (Karlsson, 2006) or with a high-pressure metamorphism (Macey et al., 2013). The monazite age is also consistent with a 590 Ma U-Pb age of zircon and baddeleyite from magnetite-apatite-forsterite rocks (Siegfried, 1999; Hurai et al., 2017). Hence, the age of monazite from albitized gneiss is interpreted as that of alkaline metasomatization (fenitization) caused by the penetration of carbonatite-silicate magma during the collapse of Gondwana supercontinent. Ages of zirconolite and thorianite from apatite-magnetite rocks are considerably younger and reflect the several alteration event caused by hydrothermal fluids, which penetrated the deposit during Cambrian and Ordovician tectonic fragmentation.

***Acknowledgments:*** *The work was supported by the Comenius University grant for young scientists (UK/78/2017) and the VEGA grant No. 2/0118/16.*

## References:

Hurai V, Paquette JL, Huraiová M, Slobodník M, Hvožďara P, Siegfried P, Gajdošová M, Milovská S (2017) New insights into the origin of the Evate apatite-iron oxide-carbonate deposit, Northeastern Mozambique, constrained by mineralogy, textures, thermochronometry, and fluid inclusions. Ore Geol Rev 80, 1072–1091

Intergeo (1985) Relatorio Final - Monapo, Prospeccao Regional Geoquimica, Mozambique. Inter. Rep., ING, Maputo, 105 p.

Karlsson JP (2006) An investigation of the felsic Ramiane Pluton, in the Monapo structure, Northern Mocambique. Examensarbeten I Geologi vid Lunds universitet – Berggrundsgeologi 202

Konečný P, Siman P, Holický I, Janák M, Kollárová V (2004) Metodika datovania monazitu pomocou elektrónového mikroanalyzátora. Miner Slov 36, 225–235

Macey PH, Miller JA, Rowe CD, Grantham GH, Siegfried P, Armstrong RA, Kemp J, Bacalau J (2013) Geology of the Monapo Klippe, NE Mozambique and its significance for assembly of central Gondwana. Precambr Res 233, 259–281

Montel JM, Foret S, Veschambre M, Nicollet Ch, Provost A (1996) Electron microprobe dating of monazite. Chem Geol 131, 37–53

Siegfried PR (1999) The Monapo structure and intrusive complex – an example of large scale alkaline metasomatism in northern Mozambique. In: Mineral Deposits: Processes to Processing. Rotterdam, 683-686

# Hydrothermal titanite from the Chengchao iron skarn deposit: Temporal constraints on iron mineralization, and its potential as a reference material for titanite U–Pb dating

**Hao, Hu[1], Jian-Wei, Li[2,*], Christopher R.M., McFarlane[3]**

*[1] State Key Laboratory of Geological Processes and Mineral Resources, China University of Geosciences (Wuhan), Wuhan 430074, China*
*[2] Faculty of Earth Resources, China University of Geosciences (Wuhan), Wuhan 430074, China*
*[3] Department of Earth Sciences, University of New Brunswick, 2 Bailey Drive, Fredericton, NB, E3B 5A3 Canada*
** E-Mail: jwli@cug.edu.cn*

Titanite incorporates moderate amounts of U and Th into its structure and has a high Pb diffusion closure temperature, making it an ideal mineral for U–Th–Pb dating. In the last decade, laser ablation inductively coupled plasma mass spectrometry has been increasingly used for the in situ analysis of U–Pb isotopes and trace elements in titanite samples from a wide range of formation environments, yielding significant insights into the timing and processes of magmatic, metamorphic, and hydrothermal events. However, recent studies have shown that using zircon as the calibrant material can significantly underestimate U–Pb titanite dates. Therefore, a matrix-matched titanite reference material with known high-precision age is required in order to study titanite U–Pb geochronology more reliably.

In this study, U-Pb isotopes and trace elements of titanite from the Chengchao iron skarn deposit (Daye district, Eastern China), were analyzed using laser ablation inductively coupled plasma mass spectrometry to provide temporal constraints on iron mineralization and to evaluate its potential as a reference material for titanite U–Pb geochronology. Titanite grains from mineralized endoskarn have simple growth zoning patterns, exhibit intergrowth with magnetite, diopside, K-feldspar, albite and actinolite, and typically contain abundant primary two-phase fluid inclusions. These paragenetic and textural features suggest that these titanite grains are of hydrothermal origin. Hydrothermal titanite is distinct from the magmatic variety from the ore-related granitic intrusion in that it contains unusually high concentrations of U (up to 2995 ppm), low levels of Th (12.5–453 ppm), and virtually no common Pb. The REE concentrations are much lower, as are the Th/U and Lu/Hf ratios. The hydrothermal titanite grains yield reproducible uncorrected U–Pb ages ranging from 129.7 ± 0.7 to 132.1 ± 2.7 Ma (2σ), with a weighted mean of 131.2 ± 0.2 Ma [mean standard weighted deviation (MSWD) = 1.7] that is interpreted as the timing of iron skarn mineralization. This age closely corresponds to the zircon U–Pb age of 131 ± 1 Ma (MSWD = 0.71) determined for the quartz diorite, and the U–Pb ages for zircon and titanite (130 ± 1 Ma and 131.3 ± 0.3 Ma) in the granite, confirming a close temporal and likely genetic relationship between granitic magmatism and iron mineralization. Different hydrothermal titanite grains have virtually identical uncorrected U–Pb ratios suggestive of negligible common Pb in the mineral. The homogeneous textures and U–Pb characteristics of Chengchao hydrothermal titanite suggest that the mineral might be a suitable internal reference material for U–Pb dating.

***Acknowledgments:*** *The research was co-supported by the National Natural Science Foundation (grants 41502072, 41325007), China Postdoctoral Science Foundation (2016M590728).*

# U-Pb geochronology related to different structural states of zircon crystals

**Kis, A.[1,*], Weiszburg, T.G.[1], Váczi, T.[2], Dunkl, I.[3], Buda, Gy.[1]**

*[1] Department of Mineralogy, Eötvös L. University, Budapest, Hungary*
*[2]Department of Applied and Nonlinear Optics, Institute for Solid State Physics and Optics, Wigner RCP of the H.A.S.*
*[3] Department of Sedimentology and Environmental Geology, University of Göttingen, Germany*
** E-Mail: annamari.kis@gmail.com*

Based on laser ablation inductively coupled plasma mass spectrometry (LA-ICP-MS) studies of 120 selected zircon crystals we refined the genetic picture of Mórágy Subunit (Hungary) and its correlation with Rastenberg Pluton (Austria) for a better paleotectonic reconstruction of the Variscan plutonic rocks across Europe. In previous geochronology-aimed publications (Klötzli and Parrish 1996; Klötzli et al. 2004; Koroknai et al. 2010), the Variscan age of the two magmatic complexes has already been proved. Nevertheless, these investigations left open basic questions with respect to the whole history (the origin of the different rock types and the age of overprinting effect(s)) of the intrusions, mainly because of the ambiguity caused by the uncontrolled textural heterogeneity of the measured zircon crystals. In order to answer the open questions, we needed to clarify and identify the different geological processes based on their preserved traces in zircons textures from two intrusions.

In the current work, we focus on the application of comparative time-resolved U-Pb dating based on zircon ($Zr[SiO_4]$, tetragonal), the most suitable mineral for U-Pb geochronology. One of the main barriers of getting properly time-resolved zircon age data is the frequent internal inhomogeneity of the zircon crystals themselves. To overcome that limitation, some textural pre-examination steps were done before the U-Pb dating.

The detailed textural patterns (primary and secondary) of zircon crystals were identified by scanning electron microscopy (SEM), based on the comparative analysis of the cathodoluminescence (CL) and back-scattered electron (BSE) contrasts. We assigned the primary texture (growth zoning (± xenocrystic core) and sector zoning) areas to the main magmatic event, while the secondary texture (convolute zoning, fluid-mediated reactions) was regarded as the imprint of any post-magmatic event in zircon crystals.

The structural state of zircon zones was determined by Raman spectroscopy. We classified three groups of structural state of the individual zircon zones based on the full width at half maximum (FWHM) of the $\nu_3$ ($SiO_4$) Raman band (Nasdala et al. 1995): 1. well crystallized (< 5 $cm^{-1}$ FWHM), 2. intermediate (5–15 $cm^{-1}$ FWHM), 3. metamict (>15 $cm^{-1}$ FWHM). Our samples are generally characterized by moderate radiation damage, the bulk of the FWHM values fell mainly between 5 $cm^{-1}$ and 15 $cm^{-1}$.

With the help of the detailed texture-related observations (SEM-BSE, SEM-CL, Raman spectroscopy), we marked the promising spots in the zircon crystals for geologically well interpretable age data determination. Accordingly, the strongly radiation-damaged zones (> 15 $cm^{-1}$) could be excluded from the LA-ICP-MS dating, because these zircon zones are not too resistant toward to the fluid-driven replacement processes (Putnis 2009). In the case of the alteration of previously radiation-damaged zircon zones we have to take into account the possibility of Pb-loss during the replacement reaction, which can modify and disturb the precise U-Pb age determination (Nasdala et al. 1998).

LA-ICP-MS analysis of 313 spots was performed on fully mapped zircons from all rock types (host granitoid rock, mafic enclave, hybrid rocks) of the Mórágy intrusion and one (main) rock type of the Rastenberg complex. Out of these, 190 were concordant (< 10 %) for the determination of crystallization age of granitoids and 123 were discordant for the dating of the overprinting event. Out of 123 discordant age data 26 analyses from Mórágy and 19 analyses from Rastenberg, showing slightly discordant age data (10 – 17 %), were plotted and evaluated. The rest, due to high discordance (> 17 %), was not interpreted.

The concordant age of the main rock type (host granitoid) of both the Mórágy and Rastenberg intrusions is the same. Additionally the two other rock types (mafic enclave, hybrid rock) from Mórágy gave the same age as well, indicating in situ unmixing for genetical relationship of the three rock types.

For the further evaluation of the concordant age data, the ISOPLOT UNMIX algorithm was used to calculate statistically distinguishable age components – assuming Gaussian distribution for each – for samples having individual dates that overlap within error. We found a bimodal age distribution for both intrusions (Mórágy: 345.9 ± 0.95 Ma and 335.6 ± 0.74 Ma; Rastenberg: 345.4 ± 3.5 Ma and 333.2 ± 4.8 Ma). These ages were invariant for zircon morphology, zircon primary texture types as well as for rock types.

These age data and our zircon texture observations suggest continuous crystallization of both granitoid plutons through a long time interval (ca. 10 Ma), giving chance for the local formation of hybrid magma during the mixing of the mafic "enclave" and the host granitoid.

The slightly discordant U-Pb age (lower intercept age) of the Rastenberg zircons shows Permian age (268 ± 19 Ma, MSWD: 7.7), while zircons from Mórágy yield Cretaceous age (115 ± 48 Ma, MSWD: 2.3). These data indicate geographically different positions for the two intrusions by the time of the first (Permian) overprinting event.

Finally, we evaluated the age data in terms of different discordance values vs. structural state of zircon zones. We found that above FWHM of 12 $cm^{-1}$ the larger part of the age data shows high discordance (useless for age interpretation), while below that value most of the areas were suitable for age determination. Based on that observation we suggest that for age determination purposes the formerly set intermediate/metamict

crystalline state border in our case should be lifted down by 3 $cm^{-1}$ for the FWHM value of 12 $cm^{-1}$. These results highlight the importance of quantitative textural assessment of radiation damage in the selection of zircon crystals for high-resolution U-Pb age determination.

## References:

Klötzli U, Parrish RR (1996) Zircon U/Pb and Pb/Pb geochronology of the Rastenberg granodiorite, South Bohemian Massif, Austria. Miner Petrol 58:197–214

Klötzli U, Buda Gy, Skiöld T (2004) Zircon typology, geochronology and whole rock Sr-Nd isotope systematics of the Mecsek Mountain granitoids in the Tisia Terrane (Hungary). Miner Petrol 81:113–134

Koroknai B, Gerdes A, Király E, Maros Gy (2010) New U-Pb and Lu-Hf isotopic constraints on the age and origin of the Mórágy Granite (Mecsek Mountains, South Hungary). IMA 20th General Meeting, 21–27 August, Budapest, Hungary, Abstracts, pp. 506

Nasdala L, Irmer G, Wolf D (1995) The degree of metamictization in zircon: a Raman spectroscopic study. Eur J Mineral 7:471–478

Nasdala L, Pidgeon RT, Wolf D, Irmer G (1998) Metamictization and U–Pb isotopic discordance in single zircons: a combined Raman microprobe and SHRIMP ion probe study. Miner Petrol 62:1–27

Putnis A (2009) Mineral replacement reactions. In: Putirka KD, Tepley FJ (eds) Minerals, inclusions and volcanic processes. Rev Mineral Geochem, vol 70. Mineral Soc Am, Chantilly, pp 87–124

# The geochronological pitfalls of the petrochronology of accessory minerals - instrumental elemental fractionation effects and age accuracies

**Klötzli, U.**

*GeoCosmoChronology, Department of Lithospheric Research, University of Vienna*
*Althanstrasse 14, A-1090 Vienna / Austria*
*E-Mail: urs.kloetzli@univie.ac.at*

With the advent of the petrochronology of accessory minerals some ten years ago petrochronological investigations have now developed into a back-bone of hard-rock geology by routinely combining geochronology (mostly age data from radiometric and chemical in-situ U-Th-Pb mineral chronometers) and petrology (both experimental and thermodynamic modelling data) thus allowing to gain deeper insights into the P-T-t evolution of metamorphic and magmatic rocks. Numerous petrochronological studies of mainly metapelitic and granitoid rocks have been published, positively demonstrating the applicability of petrochronology per se.

An underlying assumption of the methodological approach is that both the geochronological and the petrological data used to establish the P-T-t models are both accurate and precise. This assumption is self-evident and has been frequently discussed.

On the other hand, the in-situ dating community has for a long time been aware of the fact that instrumental elemental fractionation effects (IEF), sometimes called „matrix effects“, can be detrimental to the achievable overall accuracy, and to some extent also the precision of in-situ ages. Uncorrected IEF can cause age shifts of several percent, as has been shown for zircon, monazite, xenotime and rutile. The effect of common Pb on in-situ ages (for instance of titanite) are not discussed in the present context.

Primarily, IEF have three different sources: a) variable crystal chemical composition of the analysed mineral, b) crystallographic orientation of the mineral analysed and c) experimental setup. Only IEF source a) is further discussed here.

Numerous corrections schemes have been proposed all of which somehow claim that the procedures successfully correct for IEF thus implying that the age data is accurate and precision is dominated by instrumental parameters only. Applied corrections schemes are mostly one-dimensional. For example are the Th or U concentrations of monazite used to correct the IEF of SIMS dating; Y and REEs concentrations can be used to correct the IEF of xenotime SIMS and LA analyses; zircon SIMS and LA ages can be IEF corrected by the amount of accumulated radioactive dose and the U, Th, Hf concentrations.

But both published data and ongoing work has demonstrated, that these one-dimensional „matrix effect“ corrections are not sufficient to sufficiently correct IEF. Multi-dimensional corrections schemes appear to be recommended to allow properly correcting the IEF for any given mineral composition. This is shown for instance for a large xenotime crystal (Fig. 1) evidently showing a one-phase growth history and LA (white dots on Fig.1) and SIMS in-situ ages which do not support such a simple mineral growth scenario. Evidently multi-dimensional IEFs stemming from the strongly variable crystal composition (spider diagrams on Fig. 1) are responsible for the discrepancy between

obvious growth history and age data. Chemical EMP-CHIME data seem not to be affected, due to rather reduced precisions when compared with the SIMS and LA data.

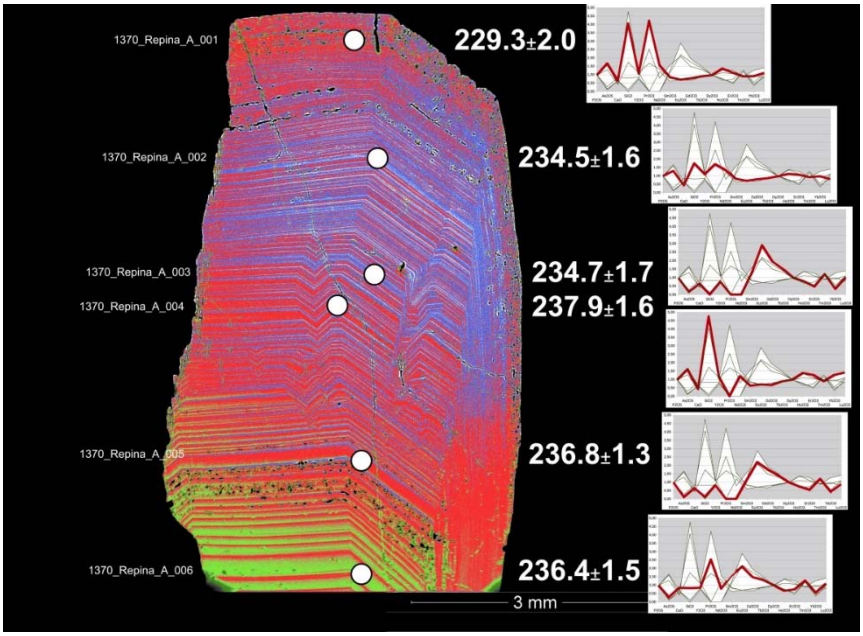


***Fig. 1.*** *Xenotime 1370 from the Ural Mountains showing a well developed chemical oscillatory zonation indicative for a single-phased continuous crystal growth. White spots are LA-MC-ICP-MS analytical points (10 µm) with $^{206}Pb/^{238}U$ ages (± 2 SD) and chemical compositions shown in the spider diagrams, red lines give the respective point composition, the white area shows the overall range in composition. Although the crystal shows one growth phase, LA spot ages evidently vary unsystematically and thus do not represent growth ages proper. Rather the correlation of LA age and mineral chemistry suggest the presence of multi-dimensional IEF during LA-MC-ICP-MS analysis*

We have to assume that such multi-dimensional IEF effects are widespread. This means, that age data gained on minerals showing a large variability in composition are prone to exhibit IEF and thus are not properly corrector for by using published one-dimensional IEF correction schemes. But it is exactly the correlation of changing mineral composition with changes in P-T conditions which are used for petrochronological investigations. This then means that the observed correlation of mineral (growth/recrystallization) ages and P-T conditions can be spurious and thus geologically misleading. In other words: the crystal chemical evolution of datable accessories minerals with changing P-T conditions leads to changing IEFs. So observed age differences can at last in parts be analytically caused (by IEF) and do not necessarily reflect, for instance, protracted mineral growth on a certain part of a P-T evolution. So the interpretation of IEF influenced and not properly IEF corrected age data in a purely petrochronological way might lead to wrong geological interpretations.

It is thus proposed that petrochronological age data be thoroughly tested for IEF and that multi-dimensional corrections scheme are a) established and b) routinely used. This ask for a common community effort to established the appropriate reference materials for SIMS, LA and EMP techniques to allow for multi-dimensional IEF corrections.

***Acknowledgments:*** *This contribution has benefitted from vital input of numerous students and colleagues: J. Burda,, A. Cernok, A. Ganwa, G. Habler, D. Harlov, C. Hauzenberger, D. Hippler, M. Horvat, P. Kanjanapayont, E. References:Klötzli-Chowanetz, J. Kosler, E. Kovaleva, M. Mandl, I. Misur, B. Neugschwentner, M. Oester, M. Pańczyk, C. Read, S. Repina, S. Sinigoi, G. Ujvari, N. Wirth, S. Zavadskis.*

# Seismically-deformed zircon: crystalline Pb nano-spheres and other enigmas

**Kovaleva, E.[1], Kusiak, M.A.[2,3,*], Wirth, R.[3], Habler, G.[4], Klötzli, U.[4]**

*[1] Department of Geology, University of the Free State, Bloemfontein, South Africa*
*[2] Institute of Geological Sciences, Polish Academy of Sciences, Warsaw, Poland*
*[3] GeoForschungsZentrum, Potsdam, Germany*
*[4] Department of Lithospheric Research, University of Vienna, Austria*
** E-Mail: mkusiak@twarda.pan.pl*

Among all accessory minerals, zircon is the most often used as a main tool for isotope geochronological studies due to properties that allow a wealth of geological information to be encrypted in its microstructure. Deformed zircons from granulitic metapelites of the Ivrea-Verbano Zone (Southern Alps, Northern Italy) showing planar deformation bands (PDB) and planar fractures (PF) are hosted by (ultra)mylonites, and are associated with pseudotachylytic veins. The frictional melts and related ultramylonites were formed at ~10 km depth as a result of high differential stresses and strain rates released by seismic slip and coeval shearing at elevated temperatures (Pittarello et al. 2008). The peak metamorphic temperatures in this area reached > 900 °C and 1.0-1.2 GPa (Pittarello et al. 2012; Redler et al. 2012), however, the emplacement of pseudotachylite is estimated at 550-650 °C and 0.4-0.6 GPa (Pittarello et al. 2012). Our finding demonstrates that formation of planar features in zircon is not only possible during shock deformation, but also happens in a seismically active environment. Moreover, the newly discovered PDBs and PFs are suggested to represent new evidence for seismicity, providing that the host rocks are derived from deep tectonic settings.

The studied zircon grains range from 30 to 150 μm in length and, besides of characteristic PDBs and PFs, reveal curviplanar fractures (CFs) and crystallographic evidence of crystal-plastic deformation (Fig. 1). PDBs in zircon appear as parallel lamellae in orientation contrast images and in electron backscatter diffraction (EBSD) maps, and represent planar lattice volumes, rotated ≤ 3° with respect to the host grain. PDBs are usually parallel to the zircon {100} crystallographic planes, are 0.3-1 μm wide and have spacing from < 1 to 25 μm (Kovaleva et al. 2015).

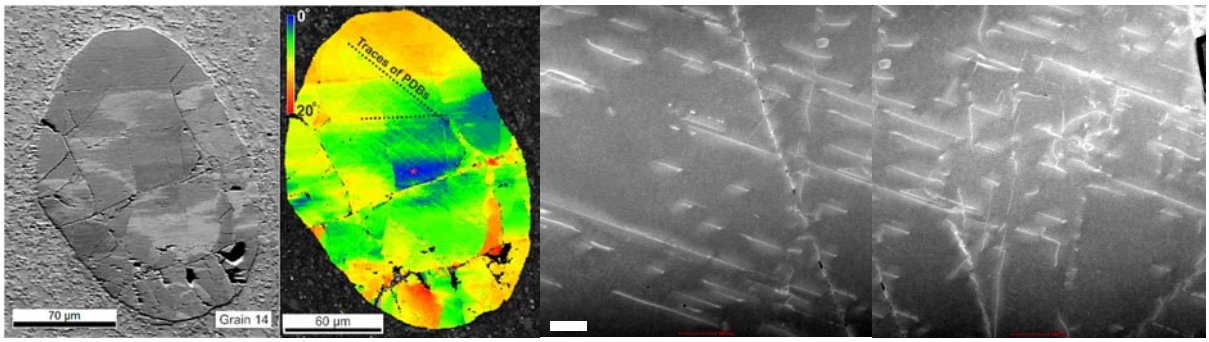


***Fig. 1.*** *Grain 14 with PDBs; from left to right: orientation contrast image; EBSD map; TEM image with visible straight dislocation lines. Scale bar is 500 nm*

Zircon grains with PDBs were investigated with secondary ion mass spectroscopy (NanoSIMS), in order to study the effect on trace elements distribution. Furthermore, transmission electron microscopy (TEM) was applied in order to decipher the geometry

of strain-related dislocations and to investigate the nature of radiogenic Pb clusters that had been found to be associated with PDBs as a result of NanoSIMS mapping. PDBs cause re-distribution and loss of radiogenic lead isotopes which are supposed to result in isotopic age resetting within the affected domains. PDBs also facilitate diffusion of REE (Y, Yb and Ce) and P in the affected grains (Kovaleva and Klötzli 2017).

The TEM investigations revealed arrays of long (up to 3 μm) straight dislocations (Fig. 1) indicating crystal-plastic deformation by dislocation glide and lack of subsequent annealing.

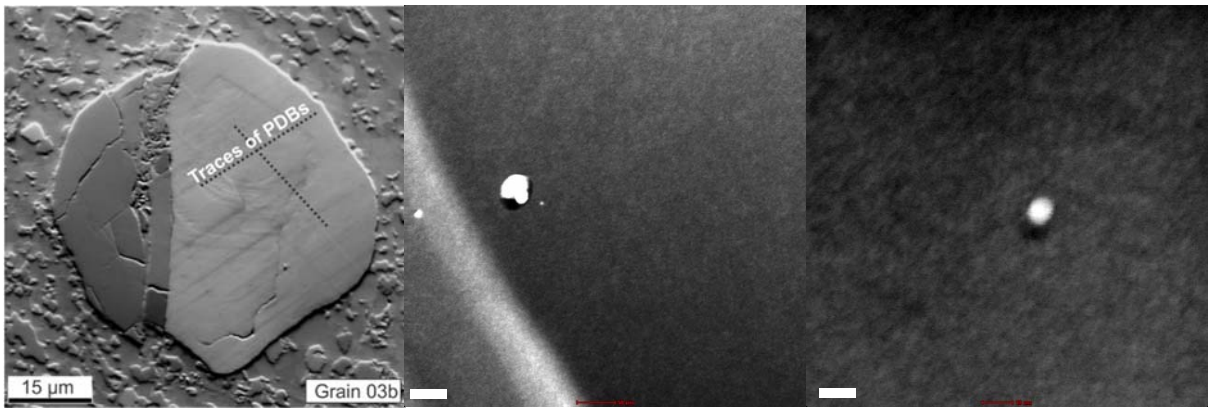


***Fig. 2*** *Grain 3b with PDBs; from left to right: orientation contrast image; TEM mages that reveal Pb spheres found in deformed zircon lattice. Scale bar is 50 nm (middle image) and 10 nm (right)*

Another important feature documented with TEM is the occurrence of 5-7 nanometer-sized crystalline Pb spheres (Fig. 2). These Pb spheres are commonly associated with Si, Al, Na, and Ca. In contrast to the native Pb spheres discovered in zircons from the UHT Enderby Land (East Antarctica) (Kusiak et al. 2015), the spheres found in zircon grains from IVZ represent a Pb oxide. In order to provide relevant interpretations for the described phenomena, further studies on these zircon grains are being conducted.

***Acknowledgments:*** *This study was conducted thanks to the Alexander for Humboldt Fellowship awarded to M.A.K. This study was partly funded by the University of Vienna (doctoral school "DOGMA", project IK 052). The authors acknowledge access to the Laboratory for scanning electron microscopy and focused ion beam applications, Faculty of Earth Sciences, Geography and Astronomy at the University of Vienna (Austria).*

## References:

Kovaleva E, Klötzli U (2017) NanoSIMS study of seismically deformed zircon: Evidence of Y, Yb, Ce and P re-distribution and resetting of radiogenic Pb. Am Mineral in press

Kovaleva E, Klötzli U, Habler G, Wheeler J (2015) Planar microstructures in zircon from paleo-seismic zones. Am Mineral 100:1834–1847

Kusiak MA., Dunkley DJ, Wirth R, Whitehouse MJ, Wilde SA, Marquardt K (2015) Metallic lead nanospheres discovered in ancient zircons. PNAS 112:4958-4963

Pittarello L, Di Toro G, Bizzarri A, Pennacchioni G, Hadizadeh J, Cocco M (2008) Energy partitioning during seismic slip in pseudotachylyte-bearing faults (Gole Larghe Fault, Adamello, Italy). Earth Planet Sci Lett 269:131–139

Pittarello L, Pennacchioni G, Di Toro G (2012) Amphibolite-facies pseudotachylytes in Premosello metagabbro and felsic mylonites (Ivrea Zone, Italy). Tectonophysics 580:43–57

Redler C, Johnson TE, White RW, Kunz BE (2012) Phase equilibrium constraints on a deep crustal metamorphic field gradient: metapelitic rocks from the Ivrea Zone (NW Italy). J Metamorph Geol 30:235–254

# High-Hf zircon from rare-metal pegmatites from the Vasin-Mylk deposit (Kola region, Russia)

**Kudryashov, N.M.[1,*], Voloshin, A.V. [1], Udoratina, O.V. [2]**

*[1] Geological Institute, Kola Science Centre, Russian Academy of Sciences, 184209 Apatity, Russia*
*[2]Institute of Geology, Komi Science Center, Ural Branch of the Russian Academy of Sciences, 54 Pervomaiskaya str., 167982, Syktyvkar, Russia*
** E-mail: nik@geoksc.apatity.ru*

The Vasin-Mylk deposit is located within the Kolmozero-Voronya greenstone belt composed of sedimentary-volcanogenic rocks of 2.9-2.7 Ga Late Archean age. The massifs of tourmaline and microcline granites, together with granite pegmatites, intrude all the above complexes of the belt, completing its long evolution. An estimate of the age of pegmatites in the Vasin-Mylk deposit was determined by the U-Pb (ID TIMS) isotope composition of microlite and was 2454±8 Ma (Kudryashov at al. 2015).

The pegmatite field of the Vasin-Mylk deposit with the lepidolite-albite-microcline-spodumen-pollucite association is located among amphibolites in the northwestern part of the belt and is one of the largest cesium deposits in the world. The bulk of Cs is concentrated in the pollucite, the associated useful components of pegmatites are Li, Be, Ta, Nb. Among the great variety of accessory minerals in pegmatites, alongside with the pollucite, there are minerals of the columbite-tantalite group, simpsonite, torolite, behierite, holtite, microlite, zircon.

High-Hf zircon was found in the areas of fine-grained greisen with the albite-lepidolite-quartz composition. The zircon crystals are closely associated with holtite and stibiotantalite, representing idiomorphic, almost featureless, octahedral grains of about 500 μm with pinkish-yellow and yellow-orange color. High-Hf zircon is characterized by a very low content of uranium (<1 ppm) and rare-earth elements.

The researches of the internal structure of high-Hf zircon showed the presence of both a thin euhedral zonation, characterized by the alternation of the finest dark and light bands, and a rough zonation (Fig. 1). Light zones have increased Hf content compared to the dark ones. The nodules in zircon are mainly represented by tantalite, there are also small quartz and apatite nodules.

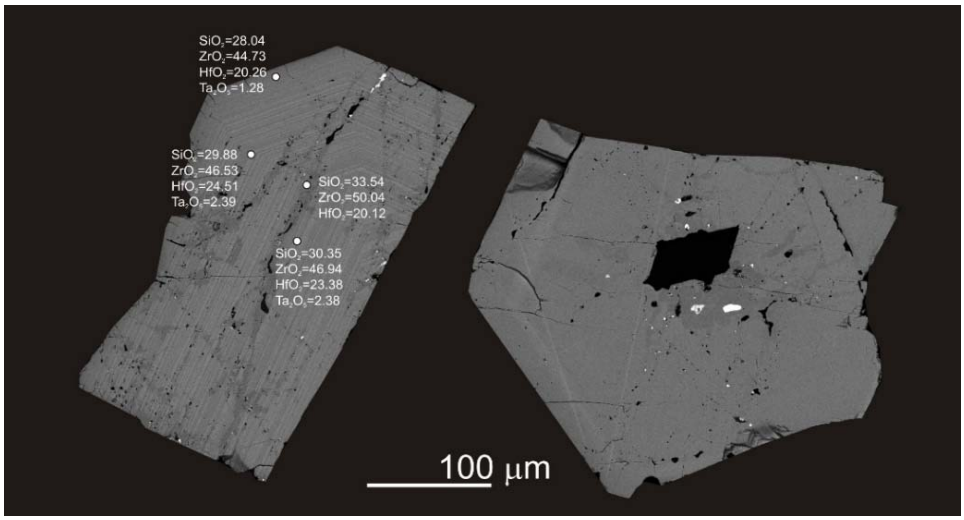


***Fig. 1.*** *Microimages of zircon crystals in the reflected electrons mode. 1 - zircon with fine euhedral zoning; 2 - zircon with a rough zoning. The points are microprobe analysis areas and chemical composition*

The comparison of the position of Raman peaks of high-Hf zircon with the reference zircon and hafnon shows that the main peaks of the studied zircon are shifted toward higher values in relation to the reference zircon and toward lower values relative to the reference hafnon, thereby occupying the middle position (Fig. 2).

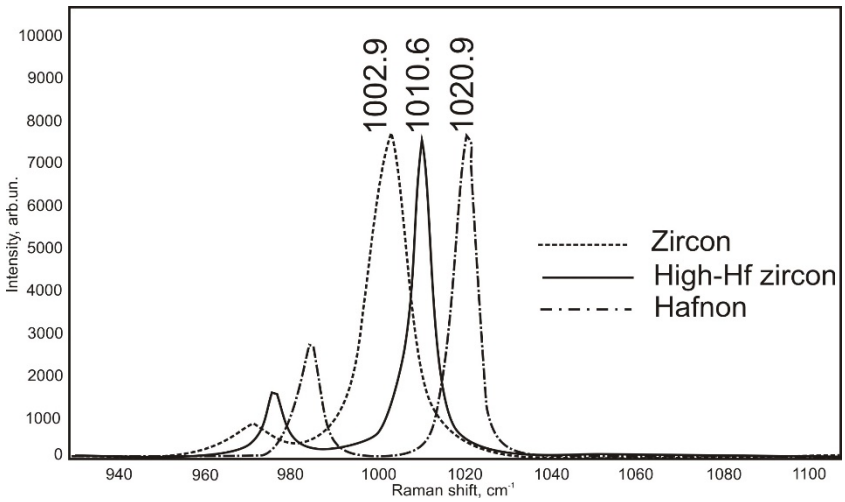


***Fig. 2.*** *Raman spectra of the main peak for high-Hf zircon, reference zircon and hafnon*

Hafnium has a higher affinity for granite melt than zirconium. High concentrations of hafnium usually reflect Zr/Hf fractionation in granite magma, where zircon from pegmatites is considerably enriched by hafnium compared to granite (Černý et al. 1985). The main factor that can influence the solubility of zircon and hafnon in melts is the fractional crystallization of granite magma, where the composition of the melt and its temperature change. Other factors may be the buffer effects of Zr-bearing phases and the role of such fluxes as Li, F and B. The experimental works also showed that a low temperature of high-aluminous melt can result in high hafnium content in zircon (Linnen, Keppler, 2002).

The studied high-Hf zircon crystallized in Al-saturated melt because it was closely associated with albite, spodumene, lepidolite and holtite. Using a Ti-thermometer (Watson at al. 2006), the crystallization temperatures of high-hf zircon were measured in the range of 350-470 °C. This temperature is almost half the temperature of the zircon crystallized from magmatic melt. In the zones of development of high-Hf zircon, B-containing minerals including elbaite and holtite are widely distributed. Thus, the crystallization of aluminous minerals (spodumene, lepidolite) from alumina saturated melt with fluxing elements (B, Li and F) contributed to the strong fractionation of Zr/Hf ratio and the crystallization of the zircon with a high hafnium content during the late stages of the evolution of rare metal pegmatites at the Vasin-Mylk deposit.

***Acknowledgments:*** *The studies were carried out with RFBR financial support, Grant 16-05-00367. The state project 0231-2015-0005.*

## References:

Černý P, Meintzer RE, Anderson AJ (1985). Extreme fractionation in rare-element granitic pegmatites: selected examples of data of mechanisms. Canadian Mineralogist 23: 381–421

Kudryashov NM, Lyalina LM, Apanasevich EA (2015). Age of Rare-Metal Pegmatites from the Vasin-Myl'k Deposit (Kola Region): Evidence from U–Pb Geochronology of Microlite. Doklady Earth Sciences 461: 321-325

Linnen RL, Keppler H (2002). Melt composition control of Zr-Hf fractionation in magmatic processes. Geochimica et Cosmochimica Acta 66: 3293-3301

Watson EB, Wark DA, Thomas JB (2006). Crystallization thermometers for zircon and rutile. Contributions to Mineralogy and Petrology 151: 413-433

# Zircon U-Pb-Lu-Hf isotopes of granitoids and enclaves from Ladakh Batholith, Trans-Himalaya, India: Implication on timing and source of magmatism and India-Asia collision

**Santosh Kumar[1,*], Brajesh Singh[2], Wei-Qiang Ji[3], Fu-Yuan Wu[3], Manjari Pathak[1]**

*[1] Department of Geology, Centre of Advanced Study, Kumaun University, Nainital 263 002, India*
*[2] Mineral Sales Private Limited, Hospet, Bangalore, India*
*[3] Institute of Geology and Geophysics, Chinese Academy of Sciences, Beijing 100029, China*
** E-Mail: skyadavan@yahoo.com*

Felsic magmatic pulses in the north of Indus-Tsangpo Suture Zone (ITSZ) of northwest Indian Himalaya, referred herein Ladakh granitoids, and associated mafic to hybrid microgranular enclaves and syn-plutonic dykes constitute the bulk of the Ladakh Batholith (Kumar, 2010a), which is an integral part of the Trans-Himalayan gigantic batholiths stretched from Namche Barwa in the east to the Nanga Parbat in the west (see the inset map of Fig.1). The Ladakh granitoids and associated enclaves (microgranular enclaves and xenoliths) have been subjected to zircon U-Pb-Lu-Hf isotopic investigations in order to constrain timing and source of magmatism and its implication on the prcise timing of India-Asia collision.

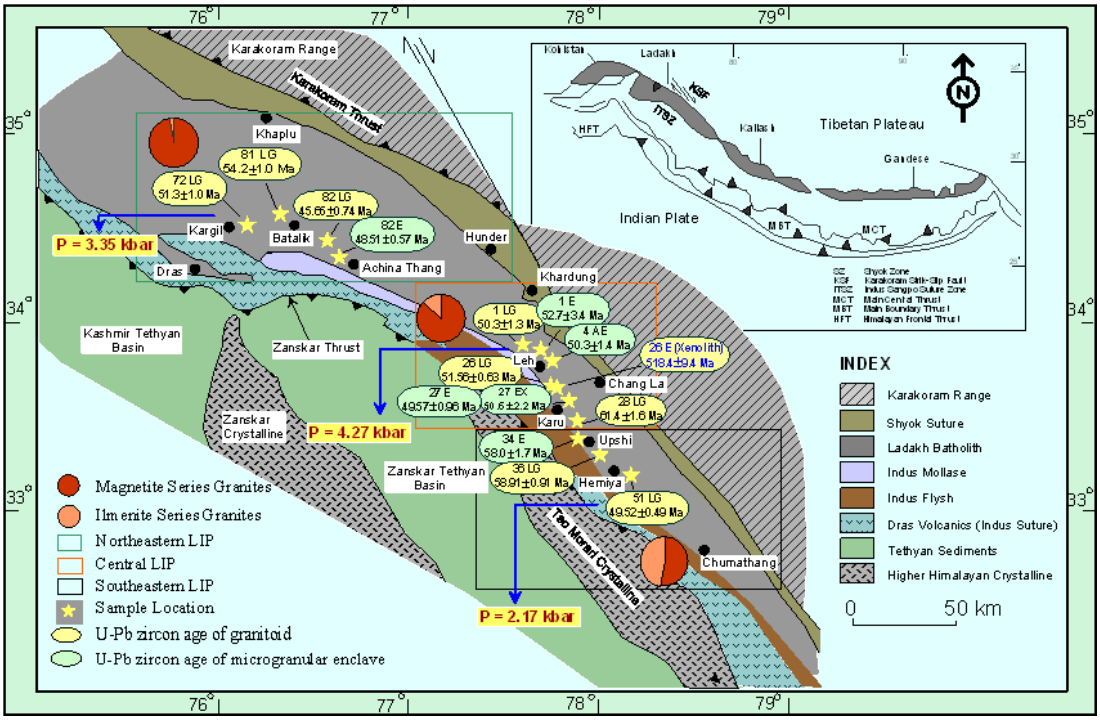


***Fig. 1:*** *Geological structure of Himalaya showing location of Ladakh Batholith in the north of Indus-Tsangpo Suture Zone (ITSZ). Main Central Thrust (MCT) and Main Boundary Thrust (MBT) are also shown (after Gansser, 1977) (Inset map). Geological map of the Ladakh Batholith and associated litho-groups (Sharma and Choubey, 1983; Thakur, 1987). Locations of various places, pressures (P) of magma emplacement, U-Pb zircon ages of granitoids, microgranular enclaves and xenolith are shown on the map. Relative abundance of magnetite series (oxidized type) and ilmenite series (reduced type) granitoids in western, central and eastern parts of the Ladakh Batholith, northwest Indian Himalaya is also shown as wheel diagrams (Kumar, 2008)*

The Ladakh granitoids are calc-alkaline, largely metaluminous (I-type) to a few peralumous type, magnetite to ilmenite series granitoids whereas morcogranular enlclaves are highly metaluminous and magnetite series granitoids (Kumar, 2008, 2010b). Al-in-hornblende geobarometers (P= 3.35 kbar in the west, P=2.99 kbar in the central, and P=2.17 kbar in eastern parts of batholith) suggest differential unroofing of Ladakh granitoid magma chambers (Fig. 1). Fifteen samples (8 Ladakh granitoids and 6 microgranular enclaves including one xenolith) were treated for insitu zircon U-Pb-Lu-Hf isotopes. U-Pb zircon data suggests coeval nature of the Ladakh granitoids and respective enclave globules encloed therein in the Kargil-Batalik-Achinathang (ca 45, 51, 54 Ma, 48.5 Ma), Leh-Karu (ca 50, 61 Ma) and Upshi-Himiya (ca 50, 58 Ma). A magmatic xenolith hosted in the Ladakh granitoids near Karu region has yielded surprisingly an age of ca 518 Ma representing the Gondwana component whereas zircons from its host calc-alkaline granitoids yield a weighted mean age of ca 51 Ma. Most Lu-Hf isotopic data of zircons have shown positive $\varepsilon_{Hf}(t)$ values and young Hf model ages (200-980 Ma) comparable well to those observed for Gangadese Batholith (Ji et al. 2009), which strongly suggest involvement of juvenile magma sources in their genesis and mixing between felsic and mafic magmas. However, one sample of Ladakh granitoid (50 Ma) in the eastern part of the batholith exhibits heterogeneous zircon Hf isotopic ratios and negative εHf(t) values suggesting contribution of ancient continental crust, probably northermost parts of the Indian lithoshpere, in their evolution. This view is further supported by a xenolith (ca 518 Ma) hosted in a Ladakh granitoid (51 Ma), which provides heterogeneous zircon Hf model ages (1685-1740 Ma) and high negative εHf(t) values pointing to the involvement of Columbia Supercontinent related magmatic component in the evolution of eastern part of Ladakh granitoids that must have happened after the collision. The obtrained ages of ca 50-51 Ma may thus mark the onset of the India-Asia collision. The Ladakh Batholith is a product of multistage magma mixing of multiple pulses of mantle- and crustal-derived magmas concomitant fractional differentiation, mingling and diffusion mechanism.

***Acknowledgments:*** *The work is supported under UGC-CAS-I, DST-FIST, and DST-ITS grants.*

## References:

Gansser A (1977) The great suture zone between Himalaya and Tibet: a preliminary account. Sci. Terre Himalaya CNRS, 268:181–192

Ji WQ, Wu FY, Chung SL, Li, Jin X, Liu CZ (2009) Zircon U-Pb geochronology and Hf isotopic constraints on petrogenesis of the Gangadese Batholith, southern Tibet. Chem Geol 262:229-245

Kumar S (2008) Magnetic susceptibility mapping of Ladakh granitoids, Northwest Higher Himalaya: implication to redox series of felsic magmatism in the subduction environments. Mem Geol Soc India 72:83–102

Kumar S (2010a) Mafic to hybrid microgranular enclaves in the Ladakh batholith, Northwest Himalaya: implications on calc-alkaline magma chamber processes. J Geol Soc India 76:5–25

Kumar S (2010b) Magnetite and ilmenite series of granitoids of Ladakh batholith, Northwest Indian Himalaya: implications on redox conditions of calc-alkaline felsic magma chambers. Curr Sci 99:1260–1264

Sharma KK, Choubey VM (1983) Petrology, geochemistry, and geochronology of the southern margin of the Ladakh batholith between Upshi and Chumathang. In: Thakur VC, Sharma KK (eds) Geology of Indus Suture Zone of Ladakh. Wadia Institute of Himalayan Geology, Deharadun, pp 41–60

Thakur VC (1987) Plate tectonic interpretation of the western Himalaya. Tectonophysics 134:91–102

# Nanostructure of 4.2 Ga zircon from the Acasta Gneiss

**Kusiak, M.A.[1,2,*], Wirth, R.[2], Iizuka, T.[3], Dunkley, D.J.[1], Schmidt, C.[2]**

*[1] Institute of Geological Sciences, Polish Academy of Sciences, Warsaw, Poland*
*[2] Deutsches GeoForschungsZentrum (GFZ), Potsdam, Germany*
*[3] Department of Earth and Planetary Sci., Tokyo Institute of Technology, Japan*
** E-Mail: mkusiak@twarda.pan.pl*

Following recent discoveries of metallic Pb nanospheres in zircon grains from ultra-high temperature (UHT) metamorphic rocks in Antarctica (Kusiak et al., 2015) and granulites in southern India (Whitehouse et al., submitted), xenocrystic zircon from Acasta Gneiss was examined with transmission electron microscopy (TEM). The Acasta Gneiss Complex in the Slave Craton of northwestern Canada contains the oldest known rocks on Earth, with ages of 3.94-4.03 Ga (Bowring and Williams 1999). These protoliths underwent high-temperature metamorphism of amphibolite facies at ca. 3.4-3.6 Ga, coincident with granitic magmatism. In a ca. 3.9 Ga tonalitic gneiss, a 4.2 Ga xenocrystic core inside the 3.9 Ga igneous zircon was found (Iizuka et al., 2006), containing 621-699 ppm U and 48-347 ppm Th. This zircon has been interpreted by the authors as providing direct evidence for the formation of Early Archean continental crust by remelting of ca. 4.2 Ga crust. Four FIB (focused ion beam) foils were cut from the xenocrystic zircon and examined by TEM to reveal the micro- and nanostructure of the grain and the distribution of radiogenic Pb.

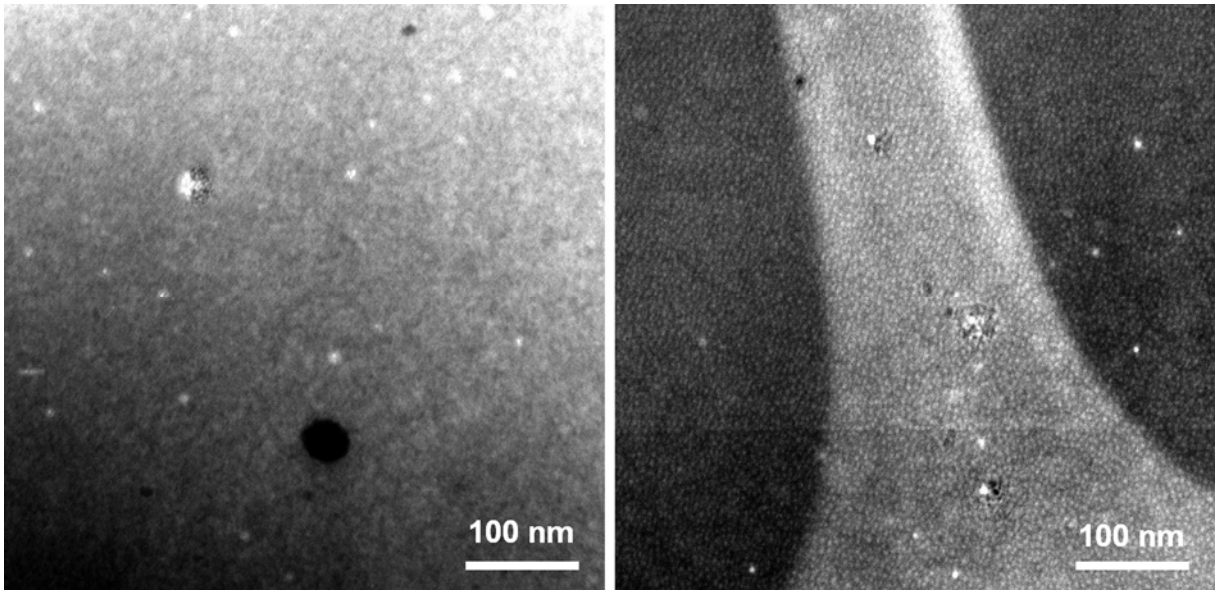


***Fig. 1.*** *TEM images of two foils presenting Pb nanospheres in Acasta zircon*

On the nanoscale, the zircon contains a mixture of metamict and crystalline domains. Raman spectroscopic analyses reveal that the core of the crystal is on average more crystalline than the rim, with the amorphous fraction varying between about 0.5 and 3.5%. Metamict areas contain porosity, most probably caused by radiation damage. The FIB foils reveal nano-scale fluid filled porosity in the zircon, which also shows small cracks with traces of Al and F. Nanopores also contain traces of Y and U.

TEM imaging also reveals that xenocrystic zircon contains Pb nanospheres (small bright spots on the Fig. 1) together with Fe-oxide particles. Although the Pb spheres are present in both, more and less crystalline parts, the latter contain more spheres.

The spheres are smaller (up to 10 nm only) than those in zircon from Enderby Land in East Antarctica and the Kerala Khondalite Belt (KKB) in southern India. The spheres from the Acasta Gneiss are not observed together with coexisting Si or Ti-Al phases as was observed in composite nanoinclusions in zircon grains from Enderby Land. There is no indication of dissolution-reprecipitation process.

These results indicate that ultra-high-temperature (UHT) conditions are not required for Pb nanospheres formation. Further work is conducted to shed more light for this feature.

***Acknowledgments:*** *This research was conducted in the frame of the Alexander von Humboldt Fellowship granted to MAK.*

## References:

Bowring SA, Williams IS (1999) Priscoan (4.00-4.03 Ga) orthogneisses from northwestern Canada. Contributions to Mineralogy and Petrology 134:3–16

Iizuka T, Horie K, Komiya T, Maruyama S, Hirata T, Hidaka H, Windley BF (2006) 4.2 Ga zircon xenocryst in an Acasta gneiss from northwestern Canada: Evidence for early Continental crust. Geology 34:245–248

Kusiak MA, Dunkley DJ, Wirth R, Whitehouse MJ, Wilde SA, Marquardt K (2015) Metallic lead nanospheres discovered in ancient zircons. PNAS 112:4958–4963

Whitehouse MJ, Kusiak MA, Wirth R, Rawindra Kumar RD (2017) Metallic Pb nanospheres in ultra-high temperature metamorphosed zircon from southern India. Miner Petrol 111:467–474

# On the way to a quantification of radiation damage in accessory minerals using $REE^{3+}$ photoluminescence spectroscopy

**Lenz, C.[1,2,*], Lumpkin, G.R.[1], Thorogood, G.J.[1], Nasdala, L.[2]**

*[1] Australian Nuclear Science and Technology Organisation, Lucas Heights, Sydney, Australia*
*[2] Institut für Mineralogie und Kristallographie, Universität Wien, Austria*
** E-Mail: christoph.lenz@univie.ac.at*

The long-term impact of natural radioactivity may cause severe structural damage in minerals. Self-irradiation-induced structural damage is created mainly in alpha-decay events in the $^{232}$Th, $^{235}$U, and $^{238}$U decay chains, by the nuclear interaction (atomic "knock-ons") of recoiled heavy daughter nuclei (e.g., Weber et al. 1990). Many accessory minerals incorporate variable amounts of actinides, whose radioactive decay creates structural disorder, in their crystal structure. The generally increased susceptibility of radiation-damaged minerals to chemical alteration or aqueous leaching is of enormous importance, as these processes may for instance bias results of chemical and isotopic age determinations (e.g., Kuiper 2005; Zamyatin et al. 2017).

The investigation of gradually radiation damaged and metamict minerals, and their synthetic analogues, has increased appreciably over the past two decades, stimulated by the potential use of mineral-like ceramics as waste forms for the immobilisation of reprocessed spent nuclear fuel and other radioactive waste (e.g., Lumpkin 2016). Information obtained from studies on radiation-damage-assisted alteration in accessory minerals has important implications for the validation of the long-term performance of analogue nuclear waste forms for the disposal in geological repositories, as radiation damage affects negatively the ability of solids to immobilise radionuclides. In both research fields, however, a fast and inexpensive technique that operates on the micrometre-scale and provides direct quantitative information on the structural disorder, may open up new opportunities in the characterisation of radiation damage.

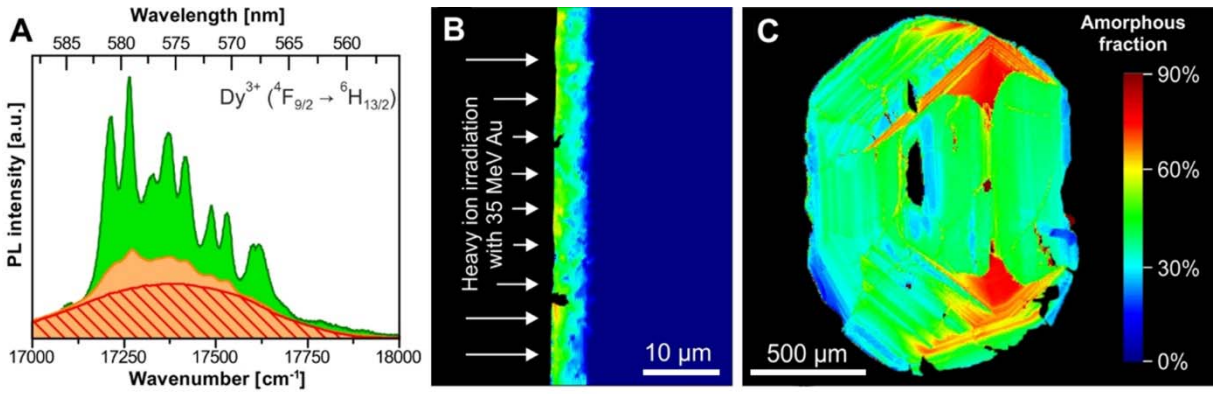


***Fig. 1.*** *Use of PL spectra of $Dy^{3+}$ to quantify radiation damage in zircon. (**A**) PL spectra of mildly (green) and strongly (ochre) radiation damaged zircon, normalized to an "amorphous" model spectrum (red). The integrated area of the amorphous model in relation to that of the observed spectrum may be used as an estimate for the amorphous fraction (e.g., 75% for the ochre and 40% for the green spectrum). (**B**) Colour-coded, hyperspectral PL map of a cross-section of an Au-irradiated $ZrSiO_4$ ceramic pellet. (**C**) Colour-coded, hyperspectral PL map of a zircon single-crystal from Plešovice, Czech Republic (Sláma et al. 2008). High concentrations of U and Th result in high damage accumulation over geological periods of time*

Recently, confocal photoluminescence (PL) spectroscopy of rare-earth elements ($REE^{3+}$) incorporated in natural zircon crystals, has been used as structural probe for the characterisation of radiation damage due to the self-irradiation by decay of trace U and Th (Lenz and Nasdala 2015). Similar to results from Raman spectroscopy (Nasdala et al. 1995), the width of PL emission lines has been used as a measure of radiation damage accumulated. One major challenge for using linewidths of PL signals for a quantitative measure of radiation effects, is its calibration using reference samples of known amorphous fraction or α-dose. Attempted calibrations based on the study of naturally radiation-damaged minerals, however, are often biased. This is because of insufficient knowledge of their thermal and, hence, annealing history (Nasdala et al. 2001).

Here, we present a new concept based on the luminescence emission of $REE^{3+}$, which aims at the direct determination of the amorphous fraction from a single PL measurement using state-of-the-art confocal spectrometers with spatial resolution in the µm-range. Careful investigation of PL spectra from self-irradiated zircon samples from Sri Lanka as well as artificially irradiated single crystals and analogous polycrystalline ceramics (heavy-ion Au irradiation with energies up to 35 MeV) revealed that the detected luminescence emission of e.g., $Dy^{3+}$ in zircon is basically a superposition of emissions from Dy ions in various, structurally different sites. The latter comprise ions in fully ordered crystallographic environment and/or sites from stressed, but still crystalline remnants and from completely altered sites within the amorphous fraction. We found that the relative integrated area of a fitted model spectra from an amorphous reference sample in relation to the full integrated area of the luminescence emission obtained gives a good estimate of the amorphous fraction present in the probed sample volume (Fig. 1a). The application of the latter approach for the interpretation of point-by-point hyperspectral maps opens up the possibility to investigate the accumulation of radiation damage in natural zircon single crystals (Fig. 1b) in very detail and give rise to direct comparison with damage accumulation in heavy ion irradiation experiments (Fig. 1c). In addition to the emission of $Dy^{3+}$ in zircon, we succesfully tested this concept for further accessory mineral-type phases, such as for $Nd^{3+}$ in xenotime ($YPO_4$) and zirconolite ($CaZrTi_2O_7$).

***Acknowledgments:*** *C.L. gratefully acknowledges the use of instrumentation funded through honorary associate agreement with the ARC CFSS/GEMOC at Macquarie University, Sydney. Ion accelerators at ANSTO are supported through NCRIS. Financial support of C.L. and L.N. by the Austrian Science Fund (FWF) projects J3662-N19 and P24448-N19, respectively, are kindly acknowledged.*

## References:

Kuiper YD (2005) Isotopic age constraints from electron microprobe U-Th-Pb dates, using a three-dimensional concordia diagram. Am Mineral 90:586–591

Lenz C, Nasdala L (2015) A photoluminescence study of $REE^{3+}$ emissions in radiation-damaged zircon. Am Mineral 100:1123–1133

Lumpkin GR (2006) Ceramic waste forms for actinides. Elements 2:365–372

Nasdala L, Wolf D, Irmer G (1995) The degree of metamictization in zircon: a Raman spectroscopic study. Eur J Mineral 7:471–478

Nasdala L, Wenzel M, Vavra G, Irmer G, Wenzel T, Kober B (2001) Metamictisation of natural zircon: accumulation versus thermal annealing of radioactivity-induced damage. Contrib Mineral Petr 141:125–144

Sláma J, Košler J, Condon DJ, Crowley JL, Gerdes A, Hanchar JM, Horstwood MSA, Morris GA, Nasdala L, Norberg N, Schaltegger U, Schoene B, Tubrett MN, Whitehouse MJ (2008) Plešovice zircon – a new natural reference material for U–Pb and Hf isotopic microanalysis. Chem Geol 249:1–35

Weber W J (1990) Radiation-induced defects and amorphization in zircon. J Mater Res 5:2687–2697

Zamyatin D, Shchapova YV, Votyakov SL, Nasdala L, Lenz C (2017): Alteration and chemical U-Th-total Pb dating of heterogeneous high-uranium zircon from a pegmatite from the Aduiskii Massif, Middle Urals, Russia. Miner Petrol 111:475–497

# Chemical and isotopic changes during metasomatic alteration of apatite

**Xiao-Chun, Li[1,*], Mei-Fu, Zhou[1], Xin-Fu, Zhao[2], Li-Ping Zeng[2]**

*[1] Department of Earth Sciences, The University of Hong Kong*
*[2] Faculty of Earth Resources, China University of Geosciences, Wuhan 430074, China*
** E-Mail: njulxc@163.com*

Apatite is a common mineral in iron-oxide copper gold (IOCG) and iron-oxide apatite (IOA) deposits. It normally contains various trace elements [e.g., halogens, S, Sr, and rare earth elements (REE)], which can be used to document the mineralizing conditions. In addition, Sr, Nd and O isotopes of apatite can be effectively employed to trace the source and evolution of the ore-forming fluids. However, it has been documented that apatite can be partially or completely metasomatically altered by hydrothermal fluids, which raises questions about the interpretation of elemental and isotopic compositions (Harlov et al. 2002; 2005). Major and trace element compositions, and Sr, Nd and O isotopic ratios, were determined on altered apatite from several IOCG and IOA deposits in China, to investigate the metasomatic effect on chemical and isotopic changes (Li and Zhou 2015; Zeng et al. 2016).

Our studies show that the hydrothermal alteration of apatite can occur either shortly after the formation of apatite, or hundreds of millions of years after the formation of apatite. We also found that apatite may have undergone multiple stages of alteration. Hydrothermal alteration of apatite can result in the leaching of REE and other trace elements, such as U, Th, Sr and Ba (Fig. 1). There are also apatite grains which have experienced leaching and immediate re-precipitation of REE, so they may contain abundant REE-rich mineral inclusions in or adjacent to altered regions (Fig. 2). Hydrothermal alteration of apatite can also lead to significant shifts of the $^{87}Sr/^{86}Sr$ and $^{18}O/^{16}O$ ratios. The $^{143}Nd/^{144}Nd$ ratios are either weakly or strongly changed during metasomatism, and the Sm/Nd ratio can be significantly changed. These will hinder obtaining the primary initial Nd isotopic composition.

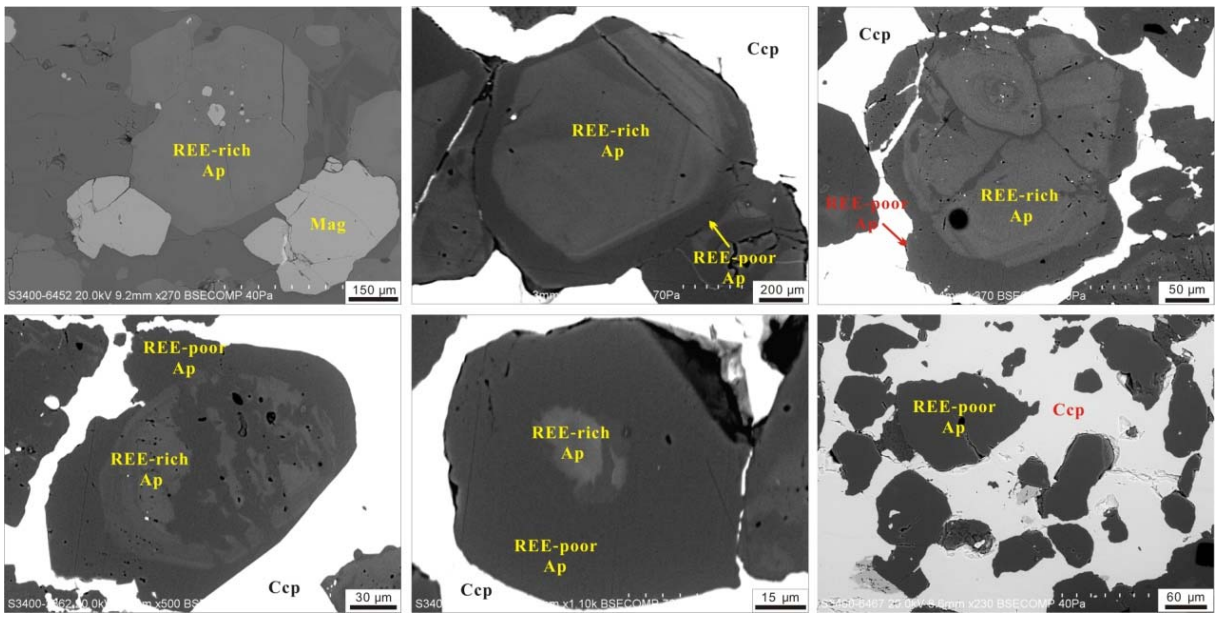


***Fig. 1.*** *Variable degrees of REE leaching during metasomatic alteration of apatite*

Our study highlights that elemental and isotopic compositions of fluorapatite can be significantly modified by hydrothermal fluids during ore-forming events. Thus, instead of traditional bulk-rock analysis, in situ microanalysis is important to provide accurate constraints on the magmatic and/or hydrothermal evolution of complex ore-forming systems.

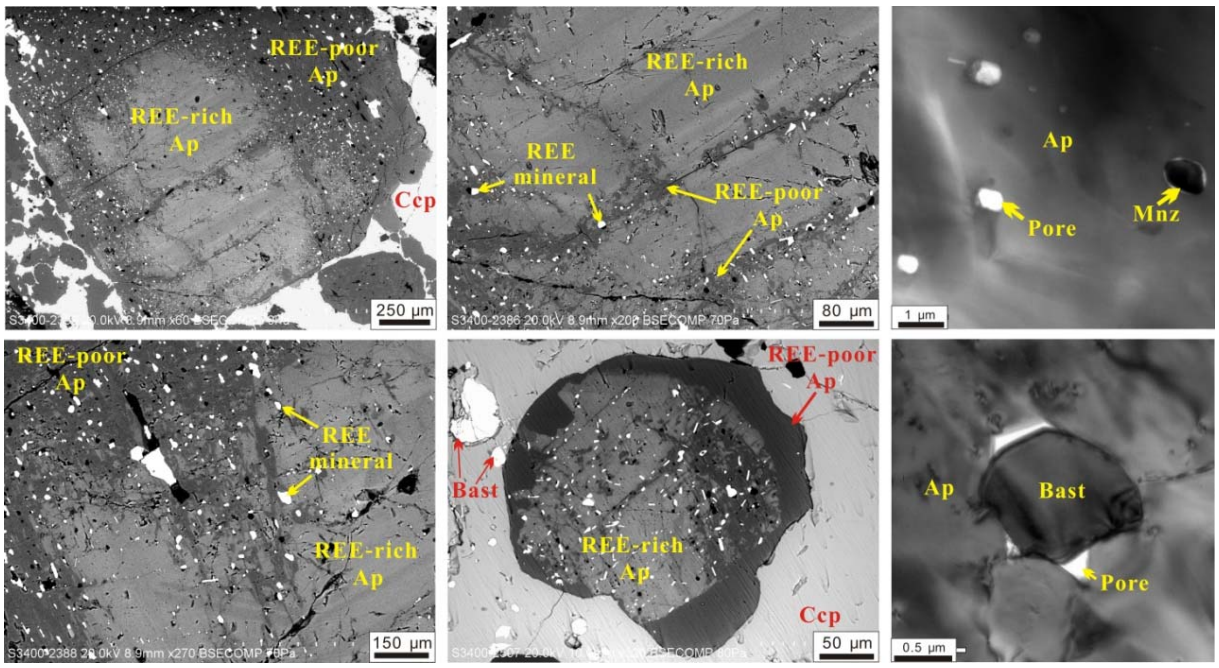


***Fig. 2.*** *Leaching and immediate precipitation of REE during metasomatic alteration of apatite*

***Acknowledgments:*** *Mr. Yu Fan Chan from HKU, Dr. Jingyuan Chen from CAU, and Dr. Wenlan Zhang from NJU are thanked for assistance with the laboratory work. Prof. Daniel E. Harlov from GFZ is greatly appreciated for fruitful discussion.*

## References:

Harlov DE, Förster HJ, Nijland TG (2002) Fluid-induced nucleation of REE-phosphate minerals in apatite: nature and experiment. Part I. Chlorapatite. Am Mineral 87:245–261

Harlov DE, Wirth R, Förster HJ (2005) An experimental study of dissolution-reprecipitation in fluorapatite: fluid infiltration and the formation of monazite. Contrib Mineral Petr 150:268–286

Li XC, Zhou MF (2015) Multiple stages of hydrothermal REE remobilization recorded in fluorapatite in the Paleoproterozoic Yinachang Fe-Cu-(REE) deposit, Southwest China. Geochim Cosmochim Ac 166:53–73

Zeng LP, Zhao XF, Li XC, Hu Hao, Christopher M (2016) In situ elemental and isotopic analysis of fluorapatite from the Taocun magnetite-apatite deposit, Eastern China: Constraints on fluid metasomatism. Am Mineral 11:2468-2483

# The Nuclear Fuel Cycle: Role of Accessory Minerals in Problem Solving

**Lumpkin, G.R.[1,*]**

*[1] Australian Nuclear Science and Technology Organisation, Lucas Heights, NSW 2234, Australia*
** Email: grl@ansto.gov.au*

The nuclear fuel cycle involves mining of uranium minerals, e.g., uraninite, coffinite, and brannerite, followed by ore processing, enrichment of the fissile component, and production of fuel pellets that are encapsulated in rods and used in nuclear reactors to generate electricity. Fuel rods are used in either a once-through cycle and removed from the reactor core for storage (awaiting ultimate disposal) or they are reprocessed and used again in reactors.

Historically, studies of Th-U minerals and ore deposits have played a major role in providing background information relevant to the geological disposal of nuclear wastes arising from both domestic electricity generation and national defence programs. As shown in Figure 1 for the example of natural pyrochlore and zirconolite, Th-U minerals may provide useful information on the performance of nuclear waste forms in terms of the crystal chemistry, radiation damage effects produced primarily by alpha decay processes, and their stability when exposed to a range of natural aqueous fluids. This example is discussed in some detail in the companion paper for this conference (Lumpkin et al. 2017). Additional examples are reviewed by Lumpkin and Geisler-Wierwille (2012), including a range of oxide, silicate, and phosphate minerals of interest to the nuclear waste disposal community.

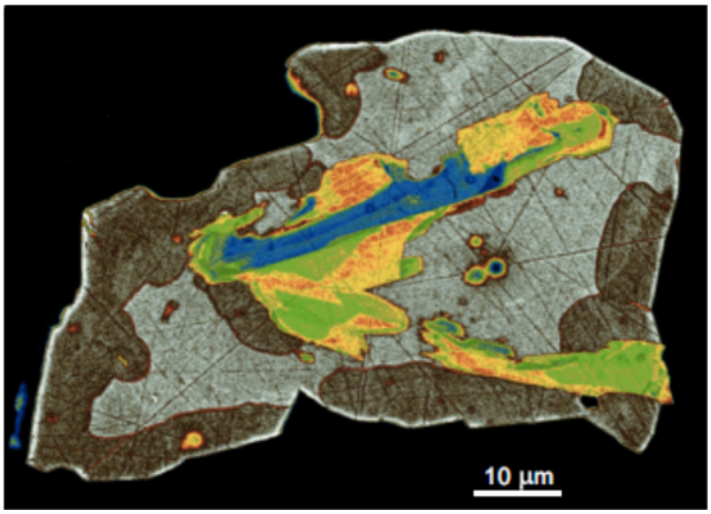


***Fig. 1.*** *False color backscattered SEM image of zirconolite and oxycalciobetafite in Ti-rich hydrothermal veins in the contact aureole of the Adamello massif, northern Italy*

Radiation damage in the minerals and their synthetic analogues occurs on time scales ranging from picoseconds to millions of years and longer in very old rocks. A combination of atomistic modelling, light and heavy ion irradiation, and doping of synthetic samples with short-lived actinides has been very effective in delineating the damage mechanisms and recovery processes. Atomistic simulations using molecular dynamics and density functional theory have been instrumental in understanding the damage and recovery

mechanisms on picosecond time scales and the energetics of some of the processes (e.g., defect formation and migration). These studies range from model systems such as the $TiO_2$ polymorphs to detailed studies of minerals such as perovskite, pyrochlore, and zircon, among others.

In particular, experimental and geological studies of Th-U minerals have revealed long-term recovery processes occurring at elevated temperature and pressure for minerals including pyrochlore, zirconolite, zircon, perovskite, brannerite, and crichtonite, among others. Studies of natural zircon have been particularly important beginning with the ground-breaking work of Holland and Gottfried (1955) and the work of others in the early 1950s. These studies set the stage for understanding the crystalline to amorphous transformation in zircon and other minerals and had a profound impact on future laboratory studies using samples doped with $^{238}Pu$ or $^{244}Cm$ with alpha-decay half-lives of ~ 88 and 18 years, respectively. More recently, it has been pointed out that the thermal history of zircon plays a major role in the amount of radiation damage that is retained today (Nasdala et al. 2004). Additional examples will be illustrated here using thermo-chronology data for specific geological localities.

All of these studies, together with related work have contributed to knowledge about nuclear waste disposal. Furthermore, investigations of meteorites have provided some data on the trapping of noble gases in carbon compounds (amorphous, graphite, diamond, etc.) and this has some relevance to fission gas trapping in nuclear reactor materials (both fission and fusion).

***Acknowledgments:*** *Many individuals with whom I have worked over the years have made this contribution possible. Early work during my PhD years was supported by the USDOE and subsequently by the Australian Nuclear Science and Technology Organisation. I am greatly indebted to all of these individuals and organizations. In particular, I would like to mention my parents for their support over the years – their love of nature planted the seeds of my interest in following a career in earth sciences. I am also greatly indebted to my PhD supervisor and colleague, Prof. Rod Ewing, for supporting our work on radioactive minerals, and for a life-long friendship. Special thanks go to Reto Gieré and Lutz Nasdala in making it possible to deliver a manuscript and presentation.*

## References:

Holland HD and Gottfried D (1955) The effect of nuclear radiation on the structure of zircon. Acta Cryst 8:291-300

Lumpkin GR, Gieré R, Williams CT, McGlinn P, Payne T.E. (2017) Petrography and chemistry of tungsten-rich oxycalciobetafite in hydrothermal veins of the Adamello contact aureole, northern Italy. Miner Petrol 111:499–509

Lumpkin GR, Geisler-Weirwille T (2012) Minerals and natural analogues. In: Konings RJM (ed) Comprehensive Nuclear Materials, vol 5. Elsevier, Amsterdam, pp 563-600

Nasdala L,Reiners PW, Garver JI, Kennedy AK, Stern RA, Balan E, Wirth R (2004) Incomplete retention of radiation damage in zircon from Sri Lanka. Am Mineral 89:219–231

# Genetic relationship between batievaite-(Y) and hainite-(Y) from Sakharjok nepheline syenite pegmatite, Keivy alkaline province, NW Russia

**Lyalina, L.M., Zozulya, D.*, Selivanova, E., Savchenko, Ye.**

*Geological Institute, Kola Science Centre, Russian Academy of Sciences, 184209 Apatity, Russia*
** E-Mail: zozulya@geoksc.apatity.ru*

The Keivy alkaline province, Kola Peninsula, NW Russia, consists of vast alkali granite massifs and several dike-like nepheline syenite bodies. The studied pegmatite body occurs within the contact zone between Sakharjok nepheline syenite and essexite, outcrops up to 30 $m^2$ in area, and consists of nepheline, albite, pyroxenes (mainly aegirine-augite), amphiboles (mainly hastingsite), biotite and analcime. Common accessory minerals observed in the pegmatite are the apatite supergroup minerals, batievaite-(Y), calcite, fluorite, hainite-(Y), meliphanite, thomsonite-Ca, zircon (Lyalina et al. 2015; 2016).

*REE* and actinides distribution in host nepheline syenite (Zozulya et al. 2015), *REE* and F variations in the britholite group minerals from pegmatite (Zozulya et al. 2017) indicate that the late-magmatic (including pegmatitic) and hydrothermal fluids were alkaline (mainly sodium), with significant, but varying, amounts of F and $CO_2$.

Batievaite-(Y), $(Ca_2Y_2[(H_2O)_2\square]Ti(Si_2O_7)_2(OH)_2(H_2O)_2)$, and hainite-(Y), $((Ca_3Y)Na(NaCa)Ti(Si_2O_7)_2(OF)F_2)$, belong to rinkite group of seidozerite-supergroup minerals, their crystal structures based upon the same *HOH* block (Lyalina et al. 2016). Batievaite-(Y) can be considered as the Na-deficient yttrium analogue of hainite-(Y). Crystalo-chemical link between hainite-(Y) and batievaite-(Y) could be expressed by following isomorphic scheme: $2Na^+ + 2Ca^{2+} + O^{2-} + 3F^- \leftrightarrow Y^{3+} + \square + 2(OH)^- + 4H_2O$. It could be suggested from structural properties of batievaite-(Y) (cation deficiency, vacancies, substitution of cations by $H_2O$ molecules), that mineral is related to transformational mineral species (Khomyakov 1992), formed by solid state transformation with inheritance of the main structural elements of the primary full-cation phase such as hainite-(Y) and removal of alkali cations from the structure during low-temperature hydrothermal alteration.

Typically, batievaite-(Y) and hainite-(Y) form intergrowths. Grains of batievaite-(Y) (euhedral or tabular crystals with length 0.25–0.3 mm) are surrounded by hainite-(Y) rims of 0.01–0.15 mm thickness (Fig. 1). The hainite-(Y) rim is separated from the batievaite-(Y) core by aggregates of analcime and calcite. The resorption of batievaite-(Y) and patches of altered batievaite-(Y) are observed therewith. The paragenesis of analcime and calcite crystallized after batievaite-(Y) and before hainite-(Y) indicates the $CO_2$ saturation of pegmatitic fluid due to temperature drop down to 250-100°C. During this stage the Ca activity in fluid decreases provided the relative rise of Na activity that is favorable to crystallization of hainite-(Y).

The study of *REE* composition in batievaite-(Y) and hainite-(Y) confirms the assumptions driven from textural data. An informative geochemical indicators of fluid composition in postmagmatic *REE*-bearing mineral formation are $(La/Nd)_n$ and Y/Dy ratios. It was shown (Smith et al. 2000) that the fractionation of La and Nd depends on the $CO_2$ content in the mineral-forming solutions and affects the $(La/Nd)_n$ in *REE* minerals (> 4 for $CO_2$-rich solution, <4 for $H_2O$-rich solution). It is known, that Y-fluoride complexes

are more stable than Dy-fluoride complexes (Gramaccioli et al. 1999), thus the variations of Y/Dy ratios in minerals may indicate the change of F content in fluid.

In case of Sakharjok, the average values of $(La/Nd)_n$ are successively decreasing in the range batievaite-(Y) – altered batievaite-(Y) – hainite-(Y): 5.6, 5.0 and 1.7, respectively. Batievaite-(Y) has a Y/Dy average value of 24.3; altered batievaite-(Y) – 20.3; hainite(Y) – 20.6. The lowest Y/Dy ratio observed in hainite-(Y) apparently indicates that the mineral crystallized from F-rich fluid, comparing to composition of crystallization media for batievaite-(Y).

On the whole, it is deduced from textural information and composition of minerals that batievaite-(Y) crystallized from $CO_2$-rich and F-poor fluid, while the hainite-(Y) from $CO_2$-poor and F-rich fluid. The content of a significant amount of water in the structure of batievaite-(Y) can explain later postcrystallization transformation (hydration).

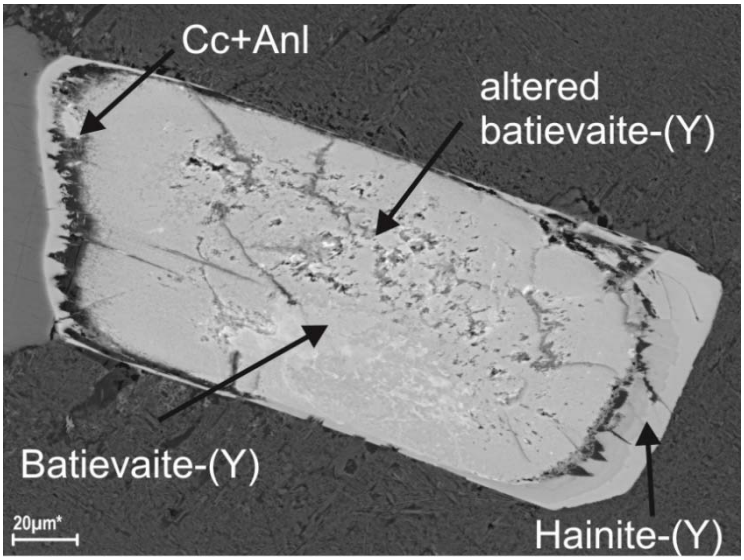


***Fig. 1.*** *Relationship between batievaite-(Y) and hainite-(Y) in the Sakharjok nepheline syenite pegmatite. SEM, BSE image. Cc – calcite, Anl – analcime*

***Acknowledgments:*** *The study was supported by the Russian Foundation for Basic Research grant 16-05-00427 and Russian government grant 0231-2015-0009*.

## References:

Gramaccioli CM, Diella V, Demartin F (1999) The role of fluoride complexes in REE geochemistry and the importance of 4f electrons: some examples in minerals. Eur J Mineral 11:983–992

Khomyakov AP (1992) Transformation mineral species and their use in palaeomineralogical reconstructions. 29th IGC Kyoto, Japan 3/3:704

Lyalina L, Zolotarev Jr A, Selivanova E, Savchenko Ye, Zozulya D, Krivovichev S, Mikhailova Yu (2015) Structural characterization and composition of Y-rich hainite from Sakharjok nepheline syenite pegmatite (Kola Peninsula, Russia). Miner Petrol 109(4):443–451

Lyalina L, Zolotarev Jr A, Selivanova E, Savchenko Ye, Krivovichev S, Mikhailova Yu, Kadyrova G, Zozulya D (2016) Batievaite-(Y), $Y_2Ca_2Ti[Si_2O_7]_2(OH)_2(H2O)_4$, a new mineral from nepheline syenite pegmatite in the Sakharjok massif, Kola peninsula. Russia. Miner Petrol 110(6):895-904

Smith MP, Henderson P, Campbell LS (2000) Fractionation of the REE during hydrothermal processes: constraints from the Bayan Obo Fe-REE-Nb deposit, Inner Mongolia, China. Geochim Cosmochim Ac 64(18):3141–3160

Zozulya DR, Lyalina LM, Savchenko YE (2015) Britholite ores of the Sakharjok Zr–Y–REE deposit, Kola peninsula: geochemistry, mineralogy, and formation stages. Geoch Int+ 53(10):892–902

Zozulya D, Lyalina L, Savchenko Ye (2017) Britholite-group minerals as sensitive indicators of changing fluid composition during pegmatite formation: evidence from the Keivy alkaline province, Kola Peninsula, NW Russia. Miner Petrol 111:511–522

# The chevkinite group and its extraordinary range of compositions and occurrences

**Ray Macdonald**

*Institute of Geochemistry, Mineralogy and Petrology, University of Warsaw, Poland*
*Environment Centre, Lancaster University, Lancaster LA1 4YQ*
*E-Mail: r.macdonald@lancs.ac.uk*

Minerals of the chevkinite group (CGM) are commonly considered to be "rare accessory minerals in alkaline rocks". They are, in fact, known from hundreds of terrestrial localities and have also been recorded in lunar and Martian rocks. The main occurrences are in igneous rocks ranging from kimberlites through mafic and intermediate lithologies to metaluminous and (per)alkaline felsic rocks. They also occur in metamorphic rocks, including granulites, metacarbonates and jadeitites, and in metasomatic rocks and ore deposits. CGM have formed over the pressure range 5 - <1 GPa, and at temperatures of ~1260°C (?) to ~350C (?). Their formation appears to be *relatively* insensitive to $pH_2O$ and $fO_2$.

CGM are dominantly REE-Ti silicates ($(REE,Ca)_4Fe^{2+}(Fe^{2+},Fe^{3+},Ti)_2Ti_2(Si_2O_7)_2O_8$), with $REE_2O_3$ contents up to 50 wt%, but Sr-, Nb-, Th-, Zr- and Cr-rich types are also known. Altogether a total of 56 elements, ranging in abundance from ppm to percent levels, have been recorded in the group. Eleven members have been approved by the CNMNC IMA but more will undoubtedly be identified. Overall compositional variation can be expressed (Vlach and Gualda 2007) as:

$$(Ca+Sr)_A + (Ti + Zr)_C = (REE, Y)_A + (M^{2+,3+})$$

which represents an amalgam of several cation substitution schemes.

Chevkinite and perrierite are overwhelmingly the most abundant CGM. In igneous parageneses they tend to occur in rocks of different compositions. Chevkinite is found mainly in rather evolved, Ca-poor hosts (e.g. syenites, trachytes, granites and rhyolites), whereas perrierite has been recorded in more mafic lithologies (e.g. basalts, trachyandesites, calcic granites and latites).

The stability of CGM *vis-à-vis* other REE-Ti-bearing accessories is poorly understood. There is, for example, experimental and observational evidence that it precedes allanite in the crystallization of certain granites. However, in A-type granites of the Graciosa Province, Brazil, allanite-(Ce) formed in metaluminous to weakly peraluminous granites whereas chevkinite-(Ce) formed in granites of the alkaline association (Vlach and Gualda 2007). Monazite generally forms in peraluminous rocks but in the Miocene Joe Lott Tuff, Utah, CGM from the highest level in the pre-eruptive magma chamber was replaced as the main REE-bearing phase at greater depth by monazite, which in turn was replaced by a CGM.

The CGM are often the major carriers of REE and actinides and they have a high potential for fractionating the (L)REE and Th from U. Very little systematic work has been done in determining CGM-melt partition coefficients, with the exception of the work of Padilla and Gualda (2016) on the Peach Springs Tuff, south-west USA, yet such data are critical in, *inter alia*, geochemical modelling. Similarly, CGM are amenable to geochronology due to their high Th abundances, commonly at the several percent level. Vasquez (2008) showed, for example, that for young chevkinite (<350 ka) the

compositional variations in single crystals can be linked to absolute age through $^{238}U$-$^{230}U$ dating by ion microprobe analysis.

In common with other REE-bearing accessories, CGM are prone to alteration by hydrothermal fluids. The nature and extent of the alteration is primarily determined by the composition of the fluids. Fluids poor in ligands tend to generate a Ti-enriched phase whose nature is unknown but is probably amorphous. With increasing F + $CO_2$ levels, complex replacement assemblages are formed, usually in more than one step, e.g. chevkinite-(Ce) → ferriallanite + davidite-(La) + aeschynite → rutile + titanite + quartz + aeschynite assemblages. Although observational evidence of the effects of alteration and element mobility is accumulating and chemical equations can be constructed to approximate the reactions, there is still no firm geochemical basis for understanding element redistribution.

## References:

Padilla AJ, Gualda GAR (2016) Crystal-melt elemental partitioning in silicic magmatic systems: An example from the Peach Spring Tuff high-silica rhyolite, southwest USA. Chem Geol 440:326-344

Vasquez JA (2008) Allanite and chevkinite as absolute chronometers of rhyolite differentiation. Geol Soc Am Abstr with Programs 40:74

Vlach SRF, Gualda GAR (2007) Allanite and chevkinite in A-type granites and syenites of the Graciosa Province, southern Brazil. Lithos 97:98-121

# High-Hf zircon from the Snezhnoe deposit (Altai-Sayan province)

**Machevariani, M.[1,*], Melnik, A.[1,2], Skublov, S.[2,1], Lukashova, M.[3], Müller, D.[4], Lupashko, T.[5], Ilchenko, K.[5]**

*[1] Saint-Petersburg Mining University, Russia*
*[2]Institute of Precambrian Geology and Geochronology, Russian Academy of Sciences*
*[3] Tescan Orsay Holding, Russia*
*[4] Ludwig-Maximilians-Universität München, Germany*
*[5] M.P. Semenenko Institute of Geochemistry, Mineralogy and Ore Formation, National Academy of Science of Ukraine*
** E-Mail: wmdmaria@gmail.com*

This work presents a mineralogical study on high-Hf zircon (collection of Shuriga T.N.) from the albitized granite of Snezhnoe deposit, one of the richest beryllium deposits of the Altai-Sayan province with additional isolated tantalum-niobium mineralisation area (Kupriyanova and Shpanov 2011).

Literature review on high-Hf zircon from granite pegmatites and granitoids shows that maximum level of $HfO_2$ content in zircon from rocks of both types is quite similar: 18-44 wt% and 16-35 wt%, respectively (Kempe et al. 2004; Yin et al., 2013). The studied zircon contains up to 27 wt% $HfO_2$, which is sufficient for entry in series of rare mineralogical findings. All the Hf-rich zircon grains show a patchy internal texture, sometimes combined with thin remnants (~5μm) of oscillatory zoning on the edge of crystals (Fig.1). Since the "spongy" texture is considered to be specific for aqueous-fluid precipitated zircon (Corfu et al. 2003), the abundance of holes and cavities within all zircon grain with less corroded and vacuolized oscillatory rims suggested hydrothermal overgrowth after altered magmatic cores. Various mineral inclusions of albite, magnetite, limonite, xenotime, bastnaesite-(Y), and thorite are preserved within the zircon crystals and limited to zones with porous texture.

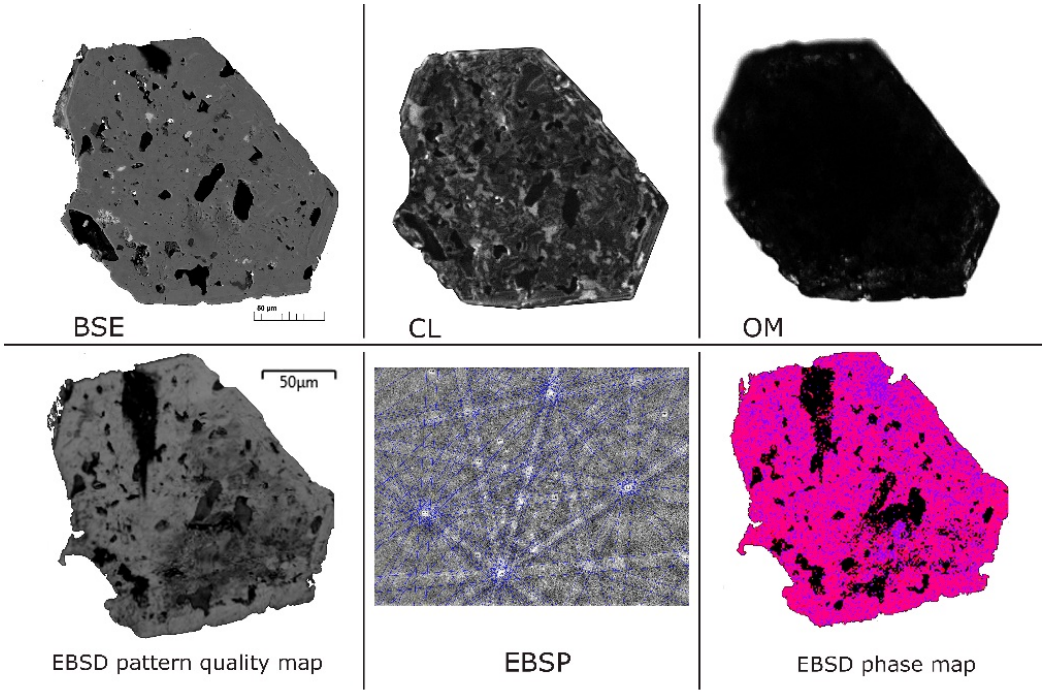


***Fig. 1.*** *BSE, CL, OM images and EBSD maps for zircon grain from the Snezhnoe beryllium deposit*

The chondrite-normalised REE patterns of zircon appear to be typical for zircon of late magmatic or hydrothermal origin and are characterised by the steep positive slope from Sm to Lu with Ce/Ce*~2.7 and Eu/Eu*~0.2. The LuN/LaN varies within wide limits from 422 to 27098 and shows strong positive correlation with Hf content (r=0.85). Yet, all data points for the Hf-zircons fall within or near the field of hydrothermal zircons in the discriminant diagram of SmN/LaN – Ce/Ce* coordinates (Fu 2009). The Zr/Hf ratio varies from 1.3 up to 5.0 and, consistently, the 100*Hf/(Zr+Hf) characteristic ratio is between 17 and 42, which classifies zircon from the Snezhnoe deposit as hafnium one, according to nomenclature proposed by Correia Neves and Lopes Nunes (1974).

The Raman spectroscopy and EBSD data were used to identify the degree of crystallinity within the zircon grains, which could be a clue to understand if high-Hf zones are related to primary growth structures or affected by the secondary alterations. The positions of the most intensive zircon Raman peaks $\nu_3(SiO_4)$ and $\nu_1(SiO_4)$, generally being used to evaluate zircon crystallinity degree (Nasdala 1995; Marsellos and Garver 2010), range within 1000.1-1009.7 $cm^{-1}$ and 967.1-975.7 $cm^{-1}$, respectively, and show strong positive correlation with Hf content (r=0.7 in both cases). Hafnium concentration also negatively correlate with FWHM of $\nu_3$ and $\nu_1$ peaks: the bandwidth reduces and the Raman shift value of this bands increases substantially with elevation of Hf concentration. Since band parameters, significantly affected by impurities (mostly hafnium), could not be unambiguously used to measure the degree of zircon radiation-induced disorder, the evaluation of zircon crystallinity based on EBSD mapping is still possible. The angular fit between the EBSP at each point and the theoretical index solutions, given by the mean angular deviation, was generally good and the coefficient of coincidence came up to 78%. The obtained pattern quality and phase maps show that the zircon grains are generally presented by monocrystals with sufficiently stable unit cell parameters and without zones of amorphisation (Fig.1).

Thus, the overall study of high-Hf zircon shows that crystallinity degree and secondary alteration processes hardly regulate Hf distribution in zircon. Moreover, estimation of zircon lattice disorder by the parameters of characteristic Raman bands is not suitable for zircon with high Hf content.

***Acknowledgments:*** *This work was supported by the Russian Foundation for Basic Research (project no. 16-05-00125) and the Ministry of Education and Science of Russia (basic and design parts of the state task in the scientific sphere № 5.9248.2017/BY for 2017-2019).*

## References:

Corfu F, Hanchar JM, Hoskin PWO, Kinny P (2003) Atlas of zircon textures. In: Hanchar JM, Hoskin PWO (eds) Zircon. Rev Mineral Geochem, vol 53. Mineral Soc Am, Chantilly, pp 469–500

Correia Neves JM, Lopes Nunes JE (1974) High Hafnium Members of the Zircon-Hafnon Series from the Granite Pegmatites of Zambezia, Mozambique. Contrib Mineral Petr 48:73-80

Fu B, Mernagh TP, Kita NT, Kemp AIS, Valley JW (2009) Distinguishing magmatic zircon from hydrothermal zircon: A case study from the Gidginbung high-sulphidation Au–Ag–(Cu) deposit, SE Australia. Chem Geol 259:131–142

Kempe U, Gruner T, Renno AD, René M (2004) Discussion on Wang et al. (2000) 'Chemistry of Hf-rich zircons from the Laoshan I-and A-type granites, Eastern China', Mineralogical Magazine, 64, 867-877. Mineral Mag 68:669-675

Kupriyanova II, Shpanov EP (2011). Snezhnoe field. In: Kovalenko VI (ed) Russian beryllium deposits, GEOS, Moscow, pp 186-195

Marsellos AE, Garver JI (2010) Radiation damage and uranium concentration in zircon as assessed by Raman spectroscopy and neutron irradiation. Am Mineral 95:1192–1201

Nasdala L, Wolf D, Irmer G (1995) The degree of metamictization in zircon: a Raman spectroscopic study. Eur J Mineral 7:471-478

Yin R, Wang RC, Zhang AC, Hu H, Zhu JC, Rao C, Zhang H (2013) Extreme fractionation from zircon to hafnon in the Koktokay No. 1 granitic pegmatite, Altai, northwestern China. Am Mineral 98:1714-1724

# Kiruna-type apatite-iron ore in Svalbard: the evidence from main and accessory minerals

**Maraszewska, M.[1,*], Manecki, M.[1], Majka, J.[1,2], Ziemniak, G.[1], Czerny, J.[1], Schneider, D.[3], Faehnrich, K.[1], Ofierska, W.[1], Myhre, P.I.[4], Barnes, Ch.[1], Włodek, A.[1]**

*[1]Department of Mineralogy, Petrography and Geochemistry, AGH University of Science and Technology, Kraków, Poland*
*[2] Department of Earth Sciences, Uppsala University, Villavävagen 16 SE-75266 Uppsala Sweden*
*[3]Department of Earth and Environmental Sciences, University of Ottawa, Canada*
*[4]Norwegian Polar Institute, Tromsø, Norway*
** E-Mail: marramaraszewska@gmail.com*

Apatite-iron oxide deposits (so called „Kiruna-type" iron ores) are phosphate-rich magnetite-hematite ores associated with magmatic or volcanic rocks. They are originally known from Paleoproterozoic rocks of the Baltic Shield in Sweden, and subsequently recognized in formations of various age in many other places around the world. Recent studies suggest a complex, combined magmatic and post-magmatic origin for iron oxides, and phosphates that crystallized from evolved siliceous melt, highly enriched in fluids and REE. This is reflected in the trace element chemistry of the ore as well as accessory minerals, for example enrichment in V, Mn, Cr and depletion in Ti and Ni in iron oxides, and high concentration of F and REE in phosphates. However, hydrothermal post-magmatic overprint obscures the primary geochemistry.

Small apatite-iron oxide ore lensoidal bodies were found in the northeast Prins Karls Forland, an island of the Svalbard Archipelago. They occur locally within a narrow (~1 km wide) shear zone between two distinct units: (1) the amphibole facies Pinkie Unit comprising metapelites, calc-silicate rocks and marbles to the east and (2) the greenschist facies metasediments of the Grampianfjella Formation to the west. Hydrothermally altered and slightly metamorphosed cumulate gabbro bodies, several meters in size, occur in the vicinity of the ores (Maraszewska et al. 2016). The gabbros contain relatively high amounts of ilmenite with secondary titanite rims and xenomorphic chlorapatite. Both the gabbros and the ores are hosted by tectonized metasediments of the ductile-brittle shear zone.

Iron oxides in the ores are present as magnetite and hematite. The latter is probably the product of magnetite alternation resulting from the increase of oxygen fugacity during the hydrothermal event. They are accompanied by chlorapatite and cut by quartz-chlorite veins. The structures and textures of the ore vary from augen structure to massive and even skeletal. In the augen type, strongly deformed porphyroblasts of magnetite are surrounded by hematite-dominated matrix. In the massive ore, magnetite form porphyroblasts whereas specularite hematite is developed along extension cracks and veins. In skeletal form, significantly altered type, dendritic iron oxide aggregates are overgrown by secondary titanite and iron hydroxides.

Electron microprobe chemical analysis shows that most of iron-oxides are depleted in Ti (~0.01-0.1 wt%) as well as Zn, Mn, and Ni. The content of Al and Cr is moderate, whereas V (up to 0.35 %) and Si (0.1-0.4 %) occur in relatively higher amounts. Projection of the results on Al+Mn vs. Ti+V as well as Ti vs. Ni/Cr plots indicates that these magnetites could be related to the Kiruna-type deposits (Fig. 1).

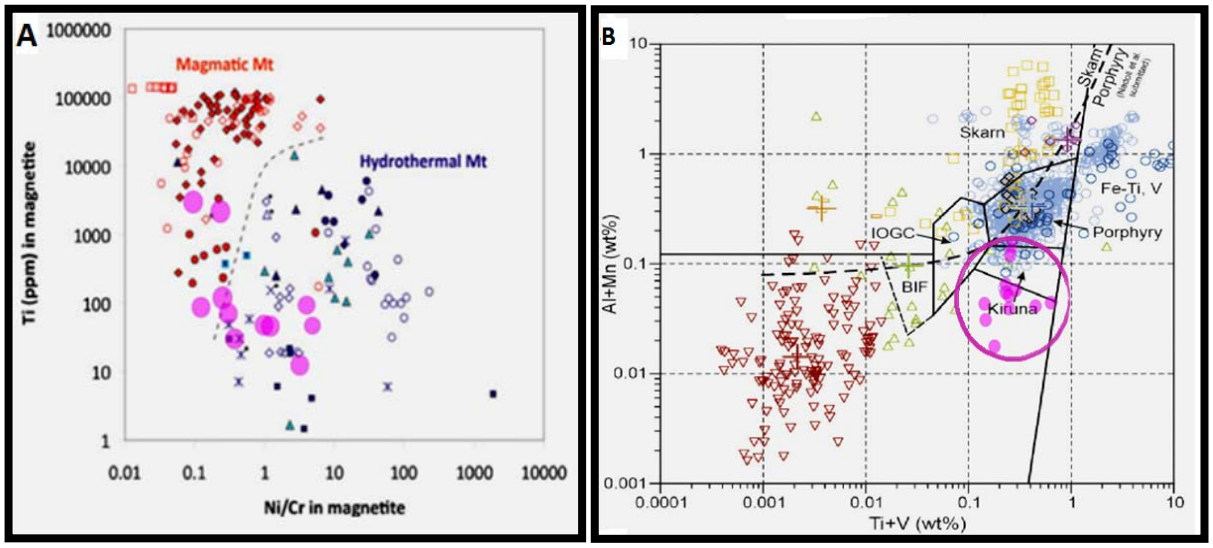


***Fig. 1.*** *A – Plot of Ti versus Ni/Cr in magnetite. B – Al+Mn versus Ti+V in magnetite discrimination diagram. Large pink dots represent magnetite samples from Prins Karls Forland on Svalbard. All other data after Dare et al. (2014) in A and after Dupuis et al. (2011) in B*

Accessory REE phosphates, such as monazite and xenotime form ahedral inclusions, several μm in size, in magnetite crystals, less commonly in silicate matrix. Monazite is Ce- and Nd-enriched (25.5-29 wt% and 10.5-13.5 wt%, respectively). Y-xenotime is generally homogenous. However, some zones show slight enrichment in LREE. Uranium and thorium content in both minerals does not exceed 0.5 wt%. Such chemistry of these phases is typical in Kiruna-type deposits (Jonsson et al. 2016).

Co-existence of iron oxides with apatite and REE-phosphates as well as geochemical signature of magnetite indicate that the Prins Karls Forland ores belong to the Kiruna-type. However, such deposits contain usually fluorapatite and are associated with intermediate or felsic magmatic rocks (e.g. Harlov et al. 2002; Jonsson et al. 2016). The Prins Karls Forland ores seem to be associated with more mafic rocks. The presence of Ti-Fe-oxides and chlorapatite in these gabbros strengthens the possible genetic link. It is the first occurrence of such ores in the High Arctic.

***Acknowledgments:*** *This work is partially funded by AGH research grant no 11.11.140.319.*

## References:

Dare SAS, Barnes SJ, Beaudoin G, Meric J, Boutroy E, Potvin-Doucet C (2014) Trace elements in magnetite as petrogenetic indicators. Miner Deposita 49:785–796

Dupuis C, Beaudoin G (2011) Discriminant diagrams for iron oxide trace element: finger-printing of mineral deposit types. Miner Deposita 46:319–335

Harlov DE, Andersson UB, Forser HJ, Nyström JO, Dulski P, Broman C (2002) Apatite-monazite relations in the Kirunavaara magnetite-apatite ore, northern Sweden. Chem Geol 191:47–72

Jonsson E, Harlov DE, Majka J, Högdahl K, Persson-Nilsson K (2016) Fluorapatite-monazite-allanite relations in the Grängesberg apatite-iron oxide ore district, Bergslagen, Sweden. Am Mineral 101:1769–1782

Maraszewska M, Manecki M, Czerny J, Schneider D, Myhre PI, Faehnrich K, Barnes Ch (2016) Metagabbro associated with the shear zone on Prins Karls Forland (Svalbard, Arctic). Geophysical Research Abstracts, EGU General Assembly 17-22 April 2016, Vienna

# The clusters of accessory minerals in Grenville marble crystallized from globules of melt

**Robert F. Martin[1,*], Dirk Schumann[2], Jeffrey de Fourestier[3]**

*[1] Earth & Planetary Sciences, McGill University, 3450 University Street, Montreal, Quebec H3A 0E8, Canada*
*[2] Fibics Incorporated, 1431 Merivale Road, Ottawa, Ontario K2E 0B9, Canada*
*[3] Mineralogical Research, 28 Broad Street, Gatineau (Aylmer), Quebec J9H 4H3, Canada*
** E-Mail: robert.martin@mcgill.ca*

We live in proximity of the Central Metasedimentary Belt (CMB) of western Quebec and eastern Ontario, part of the Grenville Province, one of the major collisional orogens of the world. Graphite-bearing white marble is a regionally important unit in the CMB; the coeval migmatitic gneissic rocks have been dated in the Otter Lake area (Quebec), 75 km northwest of Ottawa, at *ca.* 1230 Ma. Temperatures and pressures of metamorphism are estimated to have reached 700–750°C and 7–8 kilobars. We focused our attention on examples of varicoloured marble that have been transformed in some way.

We first describe the blue marble along Autoroute 5, close to Wakefield, Quebec. Polished thin sections were imaged with a Zeiss Sigma HDVP SEM using the novel large-area imaging module Atlas 5. Overview image mosaics with the BSE and CL signals were acquired at a resolution of 150 nm/pixel and 90 nm/pixel. In addition, regions of interest were imaged at 15 nm/pixel. Samples devoid of visible inclusions were found to contain numerous sets of micrometric to nanometric inclusions, locally aligned. Euhedral baryte and subhedral anhydrite crystallites ~200 nm to 540 μm across occur as single inclusions. Polymineralic inclusions, from 50 to 700 μm across, contain 1) enstatite, diopside, orthoclase, albite, titanite, and phlogopite, or 2) pyrrhotite + chalcopyrite + magnetite + galena. The minerals that coexist in such polymineralic inclusions grew together, as they fit together like pieces of a jigsaw puzzle.

Some specimens contain lemon-yellow inclusions in a matrix of blue calcite. These consist of enstatite decorated with a cathodoluminescent outer boundary that is As-rich; other crystals are green, and consist of sulphate-bearing apatite. The enstatite and apatite inclusions are roundish, possibly accumulated, and range from 234 μm to 3.6 mm in size. Some enstatite crystals contain globules of calcite that are accompanied by a small (5 to 25 μm) crystal of baryte. Rare specimens of blue calcite contain euhedral crystals of wollastonite with prominent globular inclusions of calcite, with diopside, julgoldite-($Fe^{3+}$), baryte, pyrrhotite, pyrite, and a quaternary apatite-group mineral containing phosphate, sulphate, silicate and carbonate groups.

Sinaei-Esfahami (2013) reported values of $\delta^{18}O$ of 20.8, 25.3 and 25.9‰ (SMOW) for the blue calcite, in the same range as the regionally developed white calcite. We still have not pinpointed the cause of the blue color, which fades in some samples that are kept out of direct sunlight. The textural evidence indicates that marble has melted. The baryte, anhydrite, apatite, enstatite and, lastly, calcite crystallized directly from the carbonate + sulfate + phosphate + arsenate melt. As the enstatite nucleated in this melt, it systematically rejected As until it was forced to accept it. Globules of the two melts, one silicate + "others" and one sulfide + oxide, must represent material left over after the removal of discrete minerals from the early melt.

We report results of a comparative study of orange calcite at the Otter Lake locality (Quebec). The calcite dykes there host impressive crystals of fluorapatite up to 30 cm in

length, as well as diopside, titanite, meionite, phlogopite, allanite-(Ce), orthoclase, fluorite, thorite and thorianite. All of these except the fluorite form euhedral crystals and contain globular inclusions of calcite. The fluorapatite contains a bewildering array of globular, polymineralic micro-inclusions. These range from <1 to 700 μm across, and contain some or all of the following: quartz, fluorite, calcite, hematite, julgoldite-($Fe^{3+}$), diopside, allanite-(Ce), thorite, cerite-(Ce), parisite-(Ce) and synchysite-(Ce), baryte, and anhydrite. The large globules of orange calcite themselves also contain monomineralic and polymineralic inclusions. Anhydrite primarily occurs as monomineralic inclusions in orange calcite, but was also observed together with cerite-(Ce). The polymineralic inclusions contain quartz, apatite, hematite, baryte, and xenotime-(Y).

As in the previous example, the macroscopic and microscopic inclusions, polymineralic or monomineralic in nature, formed in a fluxed silicocarbonatitic melt. Crystallization of the euhedral crystals in the low-viscosity melt likely was rapid, probably because of degassing of the melt upon its emplacement as dykes and sills. Once trapped, the domains of melt produced imbricated primary crystals. The assemblages then continued to evolve in the subsolidus realm by reacting with an oxygenated aqueous fluid. We have not encountered globules of the sulphide + oxide melt at Otter Lake.

Dykes of granitic pegmatite contains xenoliths of marble containing calcite + fluorite. Thus anatectic reactions seem to have produced coeval carbonatitic and silicate melts. The assemblage has been interpreted as a skarn, but our observations rule out a contact-metasomatic origin.

Calcite does melt in the presence of $H_2O$ and F at the ambient conditions of P and T. Such a carbonate melt is expected to react aggressively with silicate assemblages along its contacts, and to digest them efficiently. We believe that the phosphorus and fluorine needed to crystallize the prominent fluorapatite prisms were at one time constituents of the gneisses associated with the marble. Thus is born a silicocarbonatitic melt of crustal origin. The $\delta^{18}O$ value (12.4‰, SMOW) shows that the orange calcite at Otter Lake is of crustal origin, but possibly modified by rising mantle-derived fluids responsible for the addition of the rare earths, thorium and uranium.

Kennedy *et al.* (2010) have dated two crystals of titanite (U–Pb TIMS, concordia ages): 1014.8 ± 2.0 Ma (2σ) and 998.0 ± 4.5 Ma (2σ; SHRIMP data). At the time of emplacement, at roughly 1 Ga, the Grenville system was in a state of relaxation after a major collision (the Ottawan event). We believe than an asthenospheric mantle rising in response to the detachment of a slab of lower crust at the Rigolet stage provided sufficient heat and fluids to melt units of marble as well as gneiss in the lower crust.

These two case-studies show that marble can melt in granulite-grade settings. The resulting rocks satisfy the definition of a carbonatite (>50 vol. % of primary carbonate), but are of a lineage distinct from mantle-derived carbonatites. How does one prove that there was a crustal silicocarbonatitic melt? The globules of imbricated accessory minerals constitute a very important criterion. The innovative Atlas 5 imaging software has yielded incredible detail about assemblages and textures. We are now acquiring $\delta^{18}O$ data for the euhedral minerals that crystallized early in the melt. We show that anatexis can produce three coeval melts: granitic, silicocarbonatitic, and sulphidic.

**References:**

Kennedy AK, Kamo SL, Nasdala, L., Timms, NE (2010): Grenville skarn titanite: potential reference material for SIMS U–Th–Pb analysis. Can Mineral 48:1423-1443

Sinaei-Esfahani F (2013) Localized metasomatism of Grenvillian marble leading to its melting, Autoroute 5 near Old Chelsea, Quebec. M.Sc. thesis, McGill University, Montreal, Canada

# A promising tool for the investigation of alpha-particle damage in accessory minerals: $^4$He irradiation using a fabricated, Si-based energy filter

**Nasdala, L.[1,*], Akhmadaliev, S.[2], Chanmuang, C.[1], Csato, C.[3], Rosen, T.[1], Rüb, M.[3,4], Váczi, T.[5,6], Wagner, A.[1], Zowalla, A.[3]**

*[1] Institut für Mineralogie und Kristallographie, Universität Wien, 1090 Wien, Austria*
*[2] Institut für Ionenstrahlphysik und Materialforschung, Helmholtz-Zentrum Dresden-Rossendorf e.V., 01328 Dresden, Germany*
*[3] mi2-factory GmbH, 07745 Jena, Germany*
*[4] Fachbereich SciTec, Ernst-Abbe-Hochschule Jena, 07745 Jena, Germany*
*[5] Department of Mineralogy, Eötvös Loránd University, Budapest 1117, Hungary*
*[6] Wigner Research Centre for Physics, Hungarian Academy of Sciences, Budapest 1121, Hungary*
** E-Mail: lutz.nasdala@univie.ac.at*

Here we discuss a new idea for how to investigate experimentally the effects of alpha particles (i.e. $^4$He ions with energies in the range 3.9–8.8 MeV) on the structure of accessory minerals. Many accessory species (including zircon, monazite, xenotime, allanite, perovskite, and others) commonly incorporate significant amounts of the radionuclides $^{238}$U, $^{235}$U and $^{232}$Th. Alpha-decay events in their decay chains cause displacive processes that eventually may create severe structural damage in the host mineral. This is especially the case for recoils of heavy daughter nuclei (0.06–0.16 MeV) upon emission of a high-energy alpha particle: According to cautious estimates, >85 % of the bulk damage is caused by alpha recoils (Nasdala et al. 2001), which create highly localised damage clusters a few ten nanometres in size (Weber et al. 1994).

The effect of the alpha particles themselves, however, is difficult to estimate. Alpha particles transfer most of their energy to the host lattice through so-called ionisation losses. Atomic knock-ons occur predominantly near the end of the He-ion trajectories, where the alpha particles, after being slowed down significantly, may create Frenkel-type defects. The narrow penetration-depth region that suffers significant damage is commonly referred to as Bragg peak; its width lies in the micrometre range. The problem in investigating alpha particle damage by means of MeV He irradiation is that the target material will suffer strong radiation damage only within a correspondingly narrow "stripe" (Fig. 1).

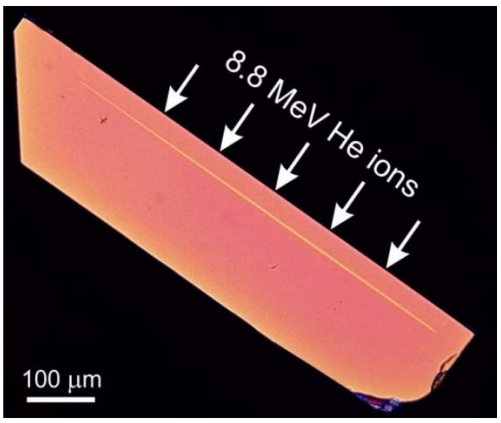


***Fig. 1.*** *Cross-polarised light image of a synthetic $ZrSiO_4$ crystal after irradiation with $1 \times 10^{16}$ He ions (8.8 MeV) per cm$^2$. The irradiation damage Bragg peak of is seen as narrow "stripe" of lowered birefringence, ca. 32–33 µm below the target surface. For details see Nasdala et al. (2011)*

The damage within the Bragg peak ("stripe") is difficult to analyse, for several reasons. Electron-beam techniques with sub-micrometre resolution are critical because the impact of a high-energy electron beam results in damage annealing (Váczi and Nasdala 2017). The application of spectroscopy is problematic also because the damaged layer is shallower than the volume resolution of modern confocal systems (Nasdala et al. 2010, 2011). In addition, the damaged (and hence expanded) "stripe" is sandwiched within less damaged regions; it hence must be affected by strong strain.

A possible way out may be the application of a micromechanically fabricated Si energy filter (Csato et al. 2015). Monte Carlo simulations with SRIM (Ziegler et al. 2010), using the displacement energies of Moreira et al. (2009), visualise the tailoring effect of the energy filter: the sharp Bragg peak is turned into a flat plateau, with a well predictable defect-concentration level in the depth range 23–31 μm (Fig. 2). We hence propose the conduction of He irradiation of thin zircon foils produced using the focused ion beam (FIB) technique (compare Nasdala et al. 2010), through an Si energy filter and a 26.5±1 μm zircon window. Concept and first results are presented and discussed.

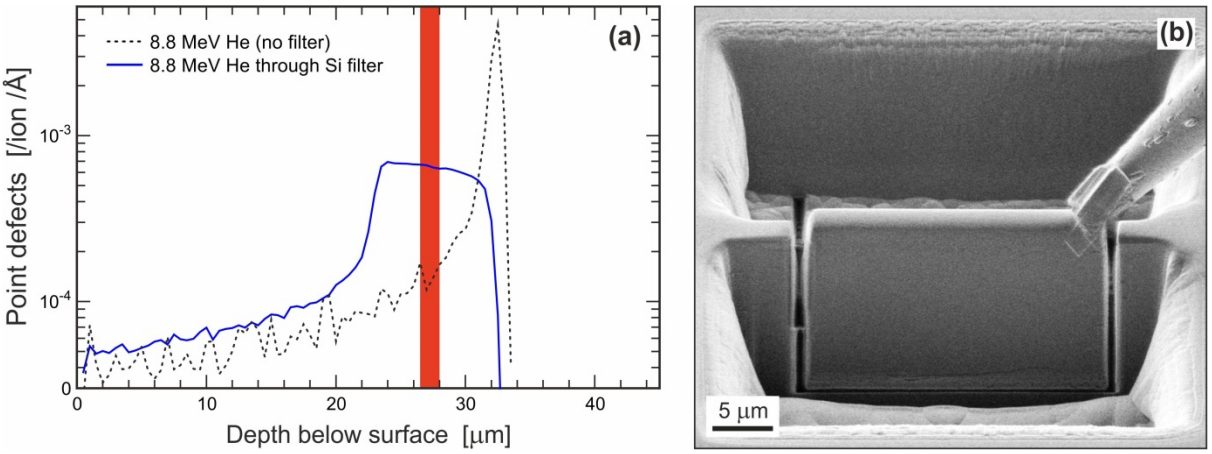


***Fig. 2. a*** *SRIM prediction of the damage distribution in He-irradiated zircon, without and with the use of an energy filter. Note that a 1.5 μm target (marked red) placed behind a 26.5 μm zircon window receives well predictable damage.* ***b*** *FIB preparation of a 1.5 μm thick target (SE image)*

***Acknowledgments:*** *We thank D. Grambole, G. Habler and C. Lenz for experimental assistance. Financial support by the Austrian Science Fund (FWF) through project P24448–N19 to L.N. is gratefully acknowledged.*

## References:

Csato C, Krippendorf F, Akhmadaliev S, von Borany J, Han W, Siefke T, Zowalla A, Rüb M (2015) Energy filter for tailoring depth profiles in semiconductor doping application. Nucl Instrum Meth B 365:182–186

Moreira PAFP, Devanathan R, Yu J, Weber WJ (2009) Molecular-dynamics simulation of threshold displacement energies in zircon. Nucl Instrum Meth B 267:3431–3436

Nasdala L, Wenzel M, Vavra G, Irmer G, Wenzel T, Kober B (2001) Metamictisation of natural zircon: accumulation versus thermal annealing of radioactivity-induced damage. Contrib Mineral Petr 141:125–144

Nasdala L, Grötzschel R, Probst S, Bleisteiner B (2010) Irradiation damage in monazite ($CePO_4$): An example to establish the limits of Raman confocality and depth resolution. Can Mineral 48:351–359

Nasdala L, Grambole D, Götze J, Kempe U, Váczi T (2011) Helium irradiation study on zircon. Contrib Mineral Petr 161:777–789

Váczi T, Nasdala L (2017) Electron-beam-induced annealing of natural zircon: A Raman spectroscopic study. Phys Chem Miner 44:389–401

Weber WJ, Ewing RC, Wang L-M (1994) The radiation-induced crystalline-to-amorphous transition in zircon. J Mater Res 9:688–698

Ziegler JF, Biersack JP, Littmark U (2010) SRIM – The stopping and range of ions in matter (2010). Nucl Instrum Meth B 268:1818–1823

# Tourmaline, an indicator of external Mg-contamination of granitic pegmatites from host serpentinite; examples from the Moldanubian Zone, Czech Republic

**Novák, M.[1], Prokop, J.[1], Losos, Z.[1,*], Macek, I.[1]**

*[1] Department of Geological Sciences, Faculty of Science, Masaryk University, Kotlářská 2, 611 37 Brno, Czech Republic*
** E-Mail: losos@sci.muni.cz*

Tourmaline is considered a perfect indicator of geochemical processes in rocks due to its refractory behaviour and compatibility with many elements. Dominant primary solidus and minor subsolidus tourmalines from a variety of granitic pegmatites enclosed in serpentinites of the Moldanubian Zone, Czech Republic were examined, mainly by electron probe micro-analyser, to reveal the degree of external Mg(Ca)-contamination from their host rocks.

The rocks include: (i) homogeneous to slightly heterogeneous nests of plagioclase-tourmaline rocks (group A) of anatectic or metasomatic origin, (ii) subhomogeneous to simply zoned barren pegmatite dikes (group B), and (iii) Li-bearing zoned pegmatite dikes of rare-element class (group C). The plagioclase-tourmaline rocks (group A) show spatial relation to pegmatites of the group B. Mostly black primary tourmalines (dravite, oxy-dravite, uvite, schorl, oxy-schorl, fluor-schorl) show extensive Mg- and Ca-contamination (group A), moderate Mg- and locally minor Ca-contamination (group B plus the locality Věžná I of the group C) and weak Mg-contamination of the tourmaline solely from outermost pegmatite units (group C); tourmalines from internal units of the pegmatites are typically Mg-free.

The substitution mechanisms include $MgR^{2+}$ ($R^{2+}$ = $Fe^{2+}$ > $Mn^{2+}$) in all groups, $NaR^{2+}$ $(\square Al)_{-1}$ and $R^{2+}$ $(OH)$ $(AlO)_{-1}$ in Ca-poor tourmalines and $CaO$ $(NaOH)_{-1}$ combined with the substitution $CaR^{2+}$ $(NaAl)_{-1}$ in Ca-enriched tourmalines (group A). Both Mg- and Ca-contamination events were very likely contemporaneous. The extent of contamination is higher in small and texturally simple plagioclase-tourmaline rocks (group A). Larger and more highly evolved Li-bearing pegmatites (group C) with zoned internal structure show a high degree of undercooling; consequently, rapid crystallization of outer zones with biotite and/or tourmaline depleted melt in almost all Mg and isolated the pegmatite body from further external contamination during solidus crystallisation. The granitic pegmatites (group B and group C) were open to the host serpentinite during early solidus crystallization immediately after emplacement of melt and then in early and/or late subsolidus crystallization (hydrothermal stage); in plagioclase-tourmaline rocks (group A) the system was likely continuously open to host serpentinite. This study affirms tourmaline as a very useful indicator of external contamination and elevated contents of Mg in tourmaline or in other Fe,Mg-minerals are the most reliable sign of external contamination in granitic rocks.

***Acknowledgments:*** *This work was supported financially by Czech Science Foundation (Grantová agentura České republiky) research project P210/14/13347S and P210/17/17276S.*

# Formation of alunite supergroup minerals and rhabdophane during supergene alteration in a highly acidic environment, the Velence Mts., Hungary

**Ondrejka, M.[1,*], Bačík, P.[1], Uher, P.[1], Sobocký, T.[1], Škoda, R.[2]**

*[1] Dept. of Mineralogy and Petrology, Faculty of Natural Sciences, Comenius University, Ilkovičova 6, 84215, Bratislava, Slovak Republic*

*[2] Dept. of Geological Sciences, Faculty of Science, Masaryk University, Kotlářská 2, 61137, Brno, Czech Republic*

** E-mail: mondrejka@fns.uniba.sk*

A unique secondary mineral assemblage of alunite supergroup minerals (ASM) together with rhabdophane group minerals (RGM), goethite and associated clay minerals (Fig. 1) were identified in the A-type porphyritic microgranite in the eastern part of the Velence Mountains, Transdanubic Unit in Hungary. The secondary sulphates/phosphates are dominated by jarosite [$KFe_3(SO_4)_2(OH)_6$] with less frequent plumbian alunite [$KAl_3(SO_4)_2(OH)_6$], Pb-rich members of the beudantite group in some areas: corkite [$PbFe_3(P_{0.5}S_{0.5}O_4)_2(OH)_6$] and hinsdalite [$PbAl_3(P_{0.5}S_{0.5}O_4)_2(OH)_6$] and all LREE-dominant rhabdophane end-members [$(Ce,La,Nd)PO_4$]·$H_2O$ rich in some places in brockite $(Ca_{0.5},Th_{0.5})PO_4·H_2O$ and tristramite $(Ca_{0.5},U_{0.5})PO_4·2H_2O$ components. Detailed EPMA study of the microgranite sample and Raman spectroscopy reveals extensive remobilization of REE, Th, U, P, S, Fe, Pb and the formation of a supergene mineral assemblage. This is most likely connected with alteration and chemical weathering of the host granite and related hypogene mineralisation in the aqueous low-temperature acidic environment near the saprolite zone. The occurrence and chemical composition of RGM suggest also distinctive fractionation of Ln (mostly LREE) during supergene processes. The source of remobilized elements (Pb, Fe, S) is most likely hypogene base-metals sulphides, while REE, Th, U and P come from weathered REE-bearing accessory minerals (allanite, monazite, xenotime).

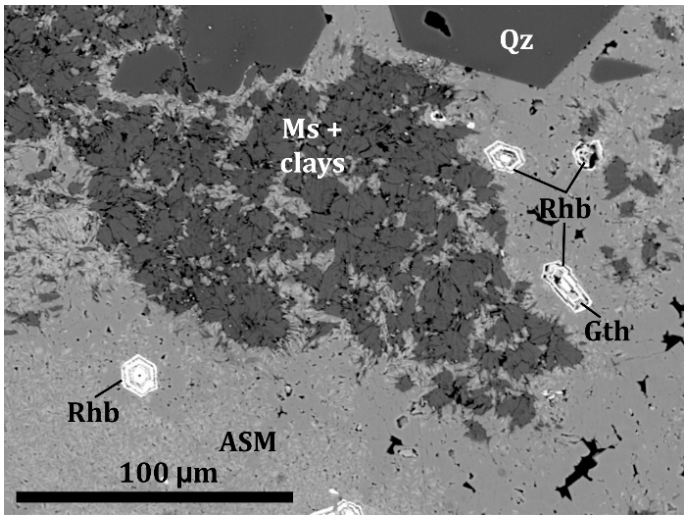


***Fig. 1.*** *Fine-grained matrix of ASM with scattered rhabdophane (Rhb) grains, partially goethitized (Gth). Rock-forming minerals are represented by quartz (Qz) and muscovite (Ms) + clays*

***Acknowledgments:*** *This work was supported by the Slovak Research and Development Agency under contract APVV-14-0278 and VEGA Agency Nos. 1/0257/13 and 1/0499/15.*

# Titanite as a tracking accessory mineral of Na-Li-Fe-rich metasomatism (La Pedriza granite massif, Iberian Variscan belt)

**Pérez-Soba, C.[1,*], Villaseca, C.[1,2]**

*[1] Departamento de Petrología y Geoquímica, Facultad de Ciencias Geológicas, Universidad Complutense de Madrid, Madrid, Spain*
*[2] Instituto de Geociencias (UCM-CSIC, Madrid, Spain*
** E-Mail: pesoa@ucm.es*

In the surroundings of the La Pedriza leucogranite pluton (Spanish Central System, Central Iberian Zone) discrete lenticular bodies of albitite (5 to 100m long) outcrop replacing peraluminous granitic wall rocks. The La Pedriza pluton is a highly fractionated Variscan I-type leucogranite. The albitite paragenesis consists of $H_2O$-poor or anhydrous minerals: albite, quartz, Li-Na-rich amphibole (ferri-ferropedrizite to sodio-ferripedrizite), Na-Fe-rich pyroxene (aegirine to ferrosylite), Li-Fe-rich micas (taneolite to siderophyllite), titanite, grossular-andradite, magnetite, fluorite, apatite and rutile. Only K-feldspar, apatite and zircon of the parental granite are variably preserved. These albitizated granites have been interpreted as resulting from Li-F-Fe-rich alkaline fluid expelled from the nearby I-type leucogranite. The albitization conditions has been estimated previously (Pérez-Soba et al. 2015) yielding temperatures of 500-630 °C and pressures about 0.2 GPa. High oxygen fugacity is deduced according to the mineral paragenesis. In situ LA-ICP-MS U–Pb titanite dating (306 ± 12 Ma) is in the range of the regional granite emplacement (305 ± 6 Ma).

Three textural domains within the albitizated granite can be identified: 1) *relic granite framework* that shows pervasive albitization of plagioclase, resulting in dirty cores with abundant growth of anhedral Ca-bearing minerals (fluorite, apatite, garnet and/or titanite), and clean rims (frequently displaying chest texture) with acicular amphibole and titanite 2) *interstitial granoblastic aggregates* of quartz or albite with amphibole, pyroxene and titanite; 3) *interstitial aggregates of mafic minerals* (pyroxene, amphibole, titanite, magnetite, micas), occasionally as inclusions within andradite and/or titanite poikiloblasts (up to 1.5 mm size). Therefore, titanite is the main accessory mineral in the three domains. The wide range of isomorphic substitutions (especially the rare-earth elements –REE– and high-field-strength elements) and sensitivity to oxygen and water fugacity make titanite a good indicator of compositional changes and conditions during magmatic and metamorphic processes. We attempt to use the titanite formation to infer evolution paths of this alkaline metasomatic process.

Three titanite generations according to their location within the albitite textural domains can be distinguished: type 1 (dirty and clean: T1d, T1c), type 2 (T2) and type3 (T3). T1 titanite crystals are usually anhedral and small (<90 μm in length); T2 are subhedral to euhedral and usually larger (<280 μm in length) and occasionally it is replacing ilmenite; and T3 are variable in shape and size (with interstitial crystals smaller than poikiloblastic ones). Most crystals are free of inclusions (occasional rutile), with the exception of the T3 poikiloblastic titanite. Backscatered electron images (BSE), coupled with microprobe analyses (about 100 spots in a total of 71 grains), show complex chemical zoning in most of the titanite generations, with predominant patchy and sector patterns, frequently combined with sectors of fine scale oscillatory zoning, which usually defines an outer rim. Occasionally, a whole crystal exhibits oscillatory or concentric

zoning. In the largest T2 crystals is possible to observe dissolution-reprecipitation textures.

Titanite shows similar compositional ranges and trends regardless of its zoning type or occurrence within any albitite body. The compositional ranges of significant non-structural cations are (in wt%): $(Fe_2O_3)_{total}$=0.38-7.79, $Al_2O_3$=0.02-6.39 (mostly <0.84), $Y_2O_3$<4.07, MnO<3.38, $Na_2O$<1.93 (average of 0.32), $Nb_2O_5$<0.75, $Ta_2O_5$<0.26, $SnO_2$<3.63, $ZrO_2$ (<1.05)and F<1.35, and (in ppm) REE=3700-22000, U=46-1270, Th=24-176. The high $Fe_2O_3$ and $Na_2O$ contents are the most outstanding data in comparison with hydrothermal or metamorphic titanite. Significant high Y, Zr (Hf), Nb (Ta), Sn and U contents are remarkable also for igneous (including granite pegmatite) titanite (e.g., Reguir et al., 1999). A limited number of trace element compositions of T3 titanite crystals (LA-ICP-MS analyses) show variable flat REE-chondrite normalized patterns (e.g., $(La/Sm)_N$= 0.22-4.43; $(La/Yb)_N$= 4.6-0.6; $(Eu/Eu^*)_N$=0.42-0.09), with a significant and systematic Ho-Lu concave pattern, opposite to REE patterns from associated amphibole and pyroxene. In BSE images the brighter sectors are systematically higher in $Fe^{3+}$ (and Al) and lower in Ti contents than the darker ones, whereas Ca, Mn, REE, Y, Na, and Nb do not show consistent correlations with brightness.

Titanite analyses show that Si tetrahedral site is not always completely full, suggesting that part of Ti may be substituting for Si. In the octahedral site, mainly $Fe^{3+}$ substitutes for $^{VI}Ti$ along 1:1 vector, whereas in the seven-fold coordinate Ca site, $(REE + Y)^{3+}$ content defines good correlation for Ca along the 1:1 substituting vector. The positive correlation between these two groups of trivalent cations suggest a charge balance substitution mechanism as: $Ca^{2+} + Ti^{4+} = (REE, Y)^{3+} + (Fe, Al)^{3+}$. Importantly, (Y + HREE) also substitutes for Ca according $2Ca^{2+} = 2(Y+HREE)^{3+} + Na^{+}$. The Na-rich fluid may explain the favourable coupled incorporation of Y+HREE into titanite and, therefore, its tendency to flat REE patterns. The variety of cations that enter in the Ca-site may explain the lack of systematic correlation between brightness and Ca contents. Cation variations in sector or oscillatory zoning are not reliable of large scale compositional evolution as depend on preferential incorporations along specific crystal faces (sector zoning) or crystal/fluid local disequilibrium along different diffusion of specific cations (Paterson and Stephens, 1992). Origin of patchy zoning is not clear, so large-scale concentric zoning would be the best record of the fluid evolution (Mclead 2007). If we consider only compositional changes of the otherwise scarce concentric zoned crystals, we found that no systematic variations in the fluid are defined.

The similar compositional range of the titanite types from the albitite bodies suggest a high ratio hot fluid/rock along the replacement channels, yielding a broad similar "co-crystallizing" paragenesis and preventing significant equilibrium between the granite minerals and the alkaline fluid. These conditions imply a compositionally and physically stable reactive flow pattern.

## References:

McLeod GW (2007) Titanite zoning and magma mixing. Ph D, University of Glasgow, 233 pp http://theses.gla.ac.uk/914/1/2007mcleodphd.pdf. Accessed 15 May 2017

Paterson BA, Stephens WE (1992) Kinetically induced compositional zoning in titanite – Implications for accessory-phase melt partitioning of trace-elements. Contrib Mineral Petr 109:373–385

Pérez-Soba C, Villaseca C, Chicharro, E (2015) Na-Li-F-metasomatism related to a highly fractionated peraluminous I-type granite (La Pedriza, Spain, Iberian Variscan belt). Book of abstracts, 8th Hutton Symposium on granite and related rocks, 40 (PT.016)

Reguir, E.P., Chakhmouradian, A.R., Evdokimov, M.D. (1999) The mineralogy of a unique baratovite- and misserite-bearing quartz-albite-aegirine rock from the Dara-i-Pioz complex, northern Tajikistan. Can Mineral 37:1369-1384

# Monazite evolution in diamond-bearing gneisses

**Petrík, I.[1,*], Janák, M.[1]**

[1] *Earth Science Institute, Slovak Academy of Sciences*
** E-Mail: igor.petrik@savba.sk*

Most of the rocks, which experienced ultrahigh-pressure metamorphism, were retrogressed *en route* to the middle/upper crust. This resulted in replacement of original eclogite facies minerals (garnet, omphacite, coesite, phengite, kyanite, rutile) by granulite facies minerals (biotite, plagioclase, quartz, muscovite, ilmenite). Relics of the original assemblage may however, be found by careful examination: phengite, omphacite, and in some rocks, also microdiamonds may occur in garnet cores. Another characteristic metamorphic mineral, monazite, is also common in high-grade gneisses, found either enclosed in by garnet or in leucocratic portions of commonly migmatized gneisses. Monazite may or may not preserve signature of ultrahigh-pressure in its chemistry. Metamorphic monazite was studied in six diamond-bearing gneisses from five localities in the Scandinavian Caledonides and one from the Rhodope massif (Janák et al 2013, Petrík et al. 2015; Klonowska et al. 2017).

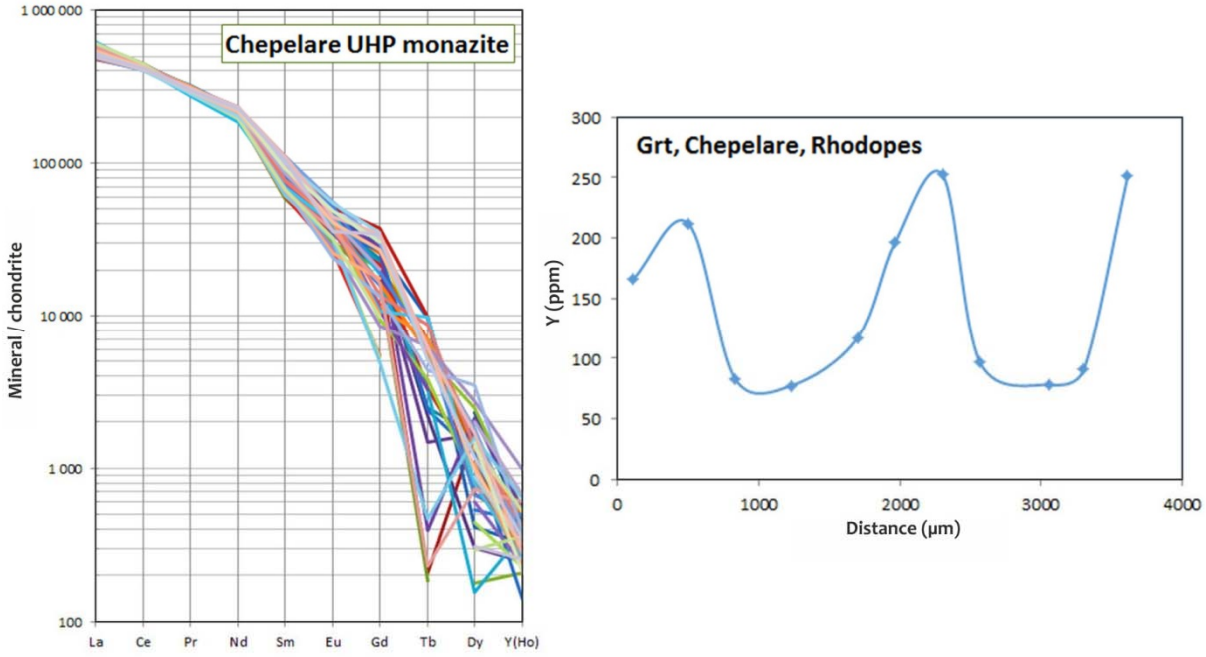


***Fig. 1.*** *Left, rare earth lemenet (REE) patterns of ultra-high pressure (UHP) monazite. Right, profile of the Y concentration across a garnet grain. All samples from Chepelare (Rhodope massif, Bulgaria)*

*Monazite* sensitively reacts to changing P-T-X conditions by changing its chemistry in relation to equilibria among silicate minerals. Two parameters appear to be most useful; i.e Eu anomaly (Eu/Eu*) and Y content. First parameter evolves depending on the presence/absence of plagioclase, whereas latter depends on the amount of coexisting garnet. The smallest Eu anomaly indicating absence of plagioclase in equilibrium with monazite is found in Chepelare gneiss (Rhodope massif, Bulgaria, Fig. 1A), followed by Tonsvika gneiss (Tromsø Nappe, Norway). Accordingly, monazite in these rocks may reflect UHP conditions. The largest negative Eu anomaly in monazite indicating

coexistence with plagioclase is seen in Åreskutan gneiss (Seve Nappe Complex, Sweden); monazite being fully equilibrated in granulite facies conditions. Passing granulite facies conditions *monazite* typically dissolves and re-precipitates on cooling, incorporating new Y from reacted garnet and losing Eu to newly forming plagioclase.

*Garnet* shows behaviour analogical to that of monazite in its HREE patterns. While major elements are typically more or less homogenized, garnet preserves prograde metamorphism indicated by decreasing Y, which enters increasing amount of garnet. The decrease is best explained by metamorphic fractionation caused by growing volume of garnet (up to 24 vol. % calculated for UHP stage of the Chepelare gneiss). Some garnets which experienced a new metamorphic phase (Chepelare), similarly to monazite, show Y-rich rims (Fig. 1B) indicating the garnet re-growth at granulite facies conditions with the same source of Y as in monazite. Both processes can be modelled using Rayleigh fractionation. Retrograde reactions of garnet to biotite resulting in the modal decrease of garnet to 15 vol.% (Chepelare) provide enough Y to form high Y rims.

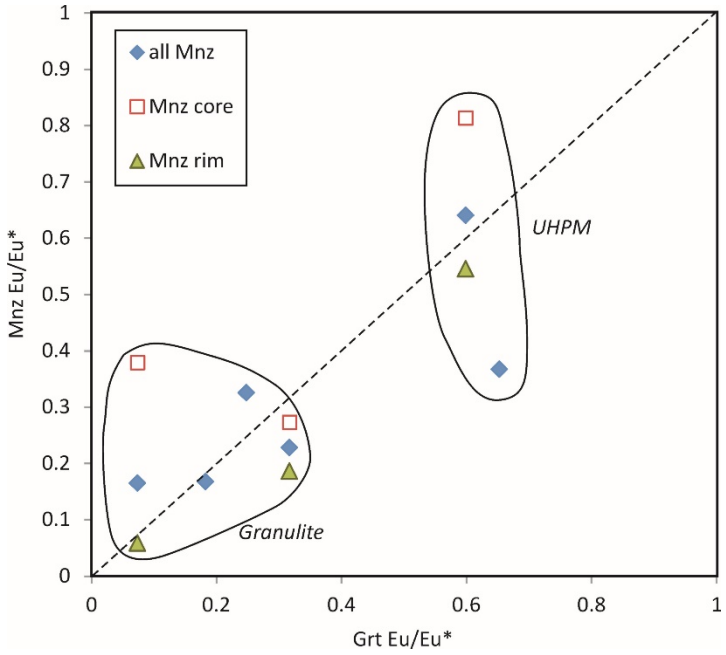


***Fig. 2.*** *Correlation of Eu anomalies in garnet and monazite from the studied rocks*

Positive correlation between Eu/Eu* in garnet and monazite, broadly following 1:1, was found in the studied localities suggesting the approach to equilibrium between garnet and monazite (Fig. 2) both in UHP and granulite stages of metamorphism.

***Acknowledgments:*** *The work was supported by grants APVV 14 0278 and Vega 0067/16, T. Vaculovič (Masaryk University Brno) is thanked for LA ICP MS analyses of garnet.*

## References:

Janák M, Ravna EJK, Kullerud K, Yoshida K, Milovský R, Hirajima T (2013) Discovery of diamond in the Tromsø Nappe, Scandinavian Caledonides (N. Norway). J metamorph Geol 31:691–703

Klonowska Y, Janák M, Majka J, Petrík I, Froitzheim N, Gee DG, Sasinková V (2017) Microdiamond on Åreskutan confirms regional UHP metamorphism in the Seve Nappe Complex of the Scandinavian Caledonides. J metamorph Geol 35:541–564

Petrík I., Janák M., Froitzheim N, Georgiev N, Yoshida, K, Sasinková V, Konečný P, Milovská S (2016) Triassic to Early Jurassic (c. 200 Ma) UHP metamorphism in the Central Rhodopes: evidence from U–Pb–Th dating of monazite in diamond-bearing gneiss from Chepelare (Bulgaria). J metamorph Geol 34:265-291

# Origin of spessartine-rich garnet in highly fractionated A-type granites of the north Arabian-Nubian Shield (Egypt): in situ EMPA and LA-ICP-MS evidences

**Sami, M.[1,2,*], Ntaflos, T.[1], Hauzenberger, C.[3]**

*[1] Department of Lithospheric Research, University of Vienna, Althanstrasse 14, Vienna, Austria*
*[2]Department of Geology, Faculty of Science, Minia University, El-Minia 61519, Egypt*
*[3] Institute of Mineralogy and Petrology, Karl-Franzens University, Graz, Austria*
** E-Mail: mabrouk.hassan@mu.edu.eg*

A combined study of EMPA and LA-ICP-MS of garnet was carried out for Gabal Abu-Diab Neoproterozoic garnet-bearing muscovite granites (GBMGs) in the CED of Egypt, in order to constrain their origin. The GBMGs are slightly peraluminous (A/CNK = 1.0–1.14) with high $SiO_2$ (>74.66 wt%) and high $K_2O$ (>4.11 wt%). Petrographic and geochemical features show that they are highly fractionated calk-alkaline A-type granites. The GBMGs have tetrad-type REE patterns ($TE_{1,3}$ >1.1) with strongly negative Eu anomalies and are extremely depleted in Ba, Sr, P and Ti. Homogenous to weakly zoned garnets occur in interstices between feldspars and muscovite with end member formulas of $Sps_{61–72}Alm_{25–35}Prp_{1–4}Adr_{0–1}$ and rare earth element (REE) patterns that are enriched in heavy REE (∑HREE= 681–2494 ppm with Y =1616–2827 ppm) and contain strong negative Eu anomalies. The occurrences, mineral assemblages, major element compositions, and REE patterns of the garnets suggest they have magmatic origin and crystallized at relatively low temperatures and pressures.

# High-precision U-Pb dating of actinide-rich accessory minerals - Using high-precision petrochronology to unravel the timing of complex magmatic and metamorphic processes

**Schaltegger, U.[1,*]**

*[1] University of Geneva, Department of Earth Sciences, rue des Maraîchers 13, CH-1205 Geneva*
** E-Mail: urs.schaltegger@unige.ch*

Accessory minerals are important containers of information about time and intrinsic parameters during the crystallisation of the mineral constituents of a rock. In addition, they may reveal the sources of melts or fluids and are also capable of recording multiple geological cycles of formation and destruction of geological materials.

Actinide-rich accessories, mainly zircon ($ZrSiO_4$) and baddeleyite ($ZrO_2$), but also the phosphates monazite ($CePO_4$) and xenotime ($YPO_4$), and titanite ($CaTiSiO_5$), play an exceptional role in reconstructing the timing of geological processes, because they are amenable to isotopic age determination. Linking time with the chemical and physical state of the system in which these minerals crystallize is called "petrochronology". The aim of petrochronology is to relate an age determination as closely as possible with elemental and isotopic composition of the dated mineral (trace element concentrations and Hf, Nd, Pb or Sr isotopes; see Fig. 1 for an example of a workflow). In an optimal case, the mineral grain has already been characterized for its textural and petrological environment (using, e.g., QEMScan on polished thin sections), and has been imaged using CL and or BSE prior to chemical and isotopic analysis. In-situ analysis using laser ablation or ion beam sputtering can yield information on chemical (trace elements, REE) and isotopic (O, Hf) composition, and is followed by high-precision, chemical abrasion, isotope-dilution TIMS U-Pb geochronology (Schaltegger et al. 2015) of carefully selected grains, possibly even followed by TIMS-TEA trace element and Hf isotopic analysis (Schoene et al. 2010). Magmatic processes last for $10^4$ to $10^5$ years and are therefore too rapid to reasonably apply low-precision LA-ICP-MS or SIMS U-Pb dating techniques for rocks that are older than 10 Ma.

Petrochronology of zircon in intermediate to felsic magmatic rocks will allow reconstruction of the temperature variations in the magma, causing successive periods of growth and resorption. It allows us to reconstruct the evolution of a magmatic plumbing system at intermediate to upper crustal levels, to model crystal fractionation paths and crystal content (see recent review by Schaltegger and Davies 2017).

The discrepancy between thermal models predicting $10^3$-$10^4$ years' durations of crystallization at emplacement level, and the $10^5$–$10^6$ years apparent duration of zircon crystallization implies that zircon is mostly crystallized at larger depth than the final intrusion level, is stored at temperatures close to the solidus in mushes and gets rejuvenated during phases of recharge by hot magma, which remobilizes crystal mushes and injects them to upper crustal levels. The resulting probability density distribution curves of zircon dates allows estimation and quantitative modeling of crystal contents of magmas, and of magma volumes and fluxes (Caricchi et al. 2014). The final solidification at upper crustal level may be approximated by ID-TIMS dating using titanite. However, due to the presence of initial Pb, titanite often cannot provide significant age information when compared to high-precision zircon dates.

High precision U-Pb geochronology in mafic rocks is limited by the abundance of zircon. Application of chemical abrasion techniques to zircon ensures that the effects of

Pb loss are removed, resulting in reliable and accurate ages. Another datable mineral in mafic systems is baddeleyite, for which there are no currently accepted techniques to remove the effect of Pb loss; therefore, baddeleyite dates are often scattered and biased to various degrees by post-crystallization Pb loss. Theoretically, in a cooling mafic melt with high Zr concentrations, baddeleyite saturation may be reached before silica saturation and zircon crystallization. Both zircon and baddeleyite will be saturated only at a late stage of evolution in a felsic residual melt, after abundant fractional crystallization of olivine, pyroxene, amphibole and plagioclase, and thus date the final eutectic solidification.

Monazite and xenotime are used for age determination in metamorphic rocks and in crustally-derived granites, where ID-TIMS zircon U-Pb dates are biased by inherited radiogenic Pb from the previous evolutionary history. Monazite shows similarly refractory behaviour even under conditions of partial melting, as long as it is not involved in chemical reactions. Complex U-Pb systematics (multiple growth periods, dissolution/reprecipitation, recrystallization) of monazite in amphibolite facies metamorphic rocks are leading to age scatter and require careful application of petrological tools prior to dating.

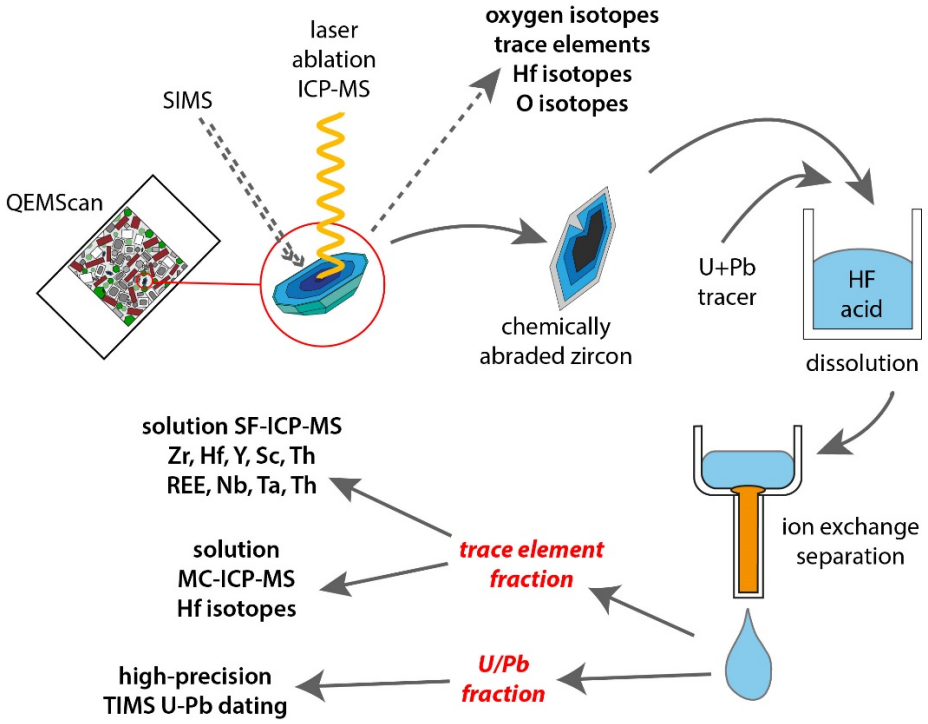


***Fig. 1.*** *Petrochronology workflow*

## References:

Caricchi L, Simpson G, Schaltegger U (2014) Zircons reveal magma fluxes in the Earth's crust. Nature 511:457–461

Schaltegger U, Davies JHFL (2017) Petrochronology of zircon and baddeleyite in igneous rocks; reconstructing magmatic processes at high temporal resolution. In: Kohn MJ, Engi M, Lanari P (eds) Petrochronology: Methods and Applications. Rev Mineral Geochem, vol 83. Mineral Soc Am, Chantilly, pp 297-328

Schaltegger U, Schmitt A, Horstwood M. (2015) U-Th-Pb zircon geochronology by ID-TIMS, SIMS and laser ablation ICP-MS: recipes, interpretations and opportunities. Chem Geol 402:89–110

Schoene B, Schaltegger U, Latkoczy C, Günther D (2010) A new method integrating high-precision U-Pb geochronology with zircon trace element analysis (U-Pb TIMS-TEA). Geochim Cosmochim Ac 74:7144–7159

# High-Y zircon from the Yastrebetskoye Zr-REE deposit (the Ukranian Shield)

**Skublov, S.[1,2,*], Levashova, E.[1], Machevariani, M.[2], Melnik, A.[2,1], Li, X.-H.[3], Müller, D.[4], Krivdik, S.[5], Lupashko, T.[5], Ilchenko, K.[5]**

*[1] Institute of Precambrian Geology and Geochronology, Russian Academy of Sciences*
*[2] Saint-Petersburg Mining University, Russia*
*[3] State Key Laboratory of Lithospheric Evolution, Institute of Geology and Geophysics, Chinese Academy of Sciences*
*[4] Ludwig-Maximilians-Universität München, Germany*
*[5] M.P. Semenenko Institute of Geochemistry, Mineralogy and Ore Formation, National Academy of Science of Ukraine*
** E-Mail: skublov@yandex.ru*

The Ukrainian shield is a unique province of Proterozoic alkaline magmatism. Alkaline rocks in this region are characterized by the presence of nepheline-free alkaline syenites, associated with Zr, REE, Y bucked ores. A previous study of zircon from Zr-REE deposits of magmatic origin (Yastrebetskoye and Azovskoye deposits, the Ukrainian Shield) showed a variety of zircons morphology and composition, and revealed that these deposits were formed under the similar geological conditions (Levashova et al., 2016). A characteristic features of zircon from the Yastrebetskoye and Azovskoye deposits are its heterogeneous structure, high content of REE and other trace elements and the uniform trend of trace elements accumulation.

Zircon from the riebeckite-aegirine-quartz rocks of the Yastrebetskiy massifs core complex (depth interval 299-300 m, sample 20) was studied by SEM, EDS, WDS, SIMS (REE, TE, O), ToF-SIMS mapping and Raman spectroscopy. The central part of the grain (point 1, fig.1) is a highly fractured and rather homogeneous zone with a ΣREE content (1943 ppm) typical of magmatic zircon, slightly increased nonstoichiometry elements (Ca, Nb) content, and also low concentration of Y and P (1659 and 69 ppm, respectively). The concentric zonal rim compared to central part of the crystal is relatively dark in BSE (point 2, fig.1), abnormally enriched in REE (up to 27667 ppm), Y (up to 61874 ppm) and nonstoichiometry elements - Ca (up to 9858 ppm), Nb (up to 7976 ppm), Be (up to 1350 ppm), B (up to 381 ppm). The enhanced values of water and F (SIMS and WDS data) in zircon rim should be also pointed out: the water content in the central part of the grain averages about 300 pmm, but not exceeding 514 ppm, whereas in the rim zone this value exceeds 4 wt%; the F content increases more than two hundred times - from 24 to 5959 ppm on an average. Rim zone is also characterized by $\delta^{18}O$ (mean value=11.52 ‰) simultaneously increasing with Y content. ToF-SIMS maps of trace elements (except B, which concentration level in the rim zone slightly exceeds the detection limit), reflect not only the enrichment of the rim zone with trace elements, but also its zonal structure. The exposed zonation resembles oscillatory one, often observed in CL images of magmatic zircon. It appears that zonation reflects fluctuations in the rare elements content in the melt/fluid during the crystallization process.

Such a high content of Y and REE was previously found in zircon from PR fluid processed zones on the Fennoscandian Shield (Y up to 84800 ppm, REE - up to 96800 ppm, Skublov et al. 2011) and zircon from the Ichetju ore occurrence in Middle Timan (Y exceeds 70000 ppm, REE - 100000 ppm, Makeyev and Skublov 2016). ToF-SIMS trace elements mapping of zircon from the Yastrebetskoye deposit confirmed the heterogeneity

of the crystals internal structure and the systematic difference in the composition of the zircons core and rim zones.

The Raman spectra profile across crystal elongation could be regarded under the aspect of zircon crystallinity: the only one relatively well-defined $v_3(SiO_4)$ band corresponds with crystal core; rim zone shows spectra with extremely broad to completely absent main peaks. The FWHM of the $v_3(SiO_4)$ band in the central zone is 11.6 $cm^{-1}$, which suggests only a partial amorphization of the crystal structure (so-called transit state) (Nasdala et al., 1995). It stands to mention that the intensity of characteristic bands is significantly reduced over the matter of the additional intense peaks, which may result from laser-induced fluorescence emission of the luminophor impurities, incorporated in zircons lattice. Significant structural radiation damage of rim zone could be a reason of the zircon reactive capacity enhancement and dramatic accumulation of REE.

The anomalous composition of the zircon rim derived from the considerable saturation of late riebeckite-aegirine-quartz syenites with fluorine-water-bearing fluids enriched with $^{18}O$, Y, REE, Nb, Be, B and other trace elements.

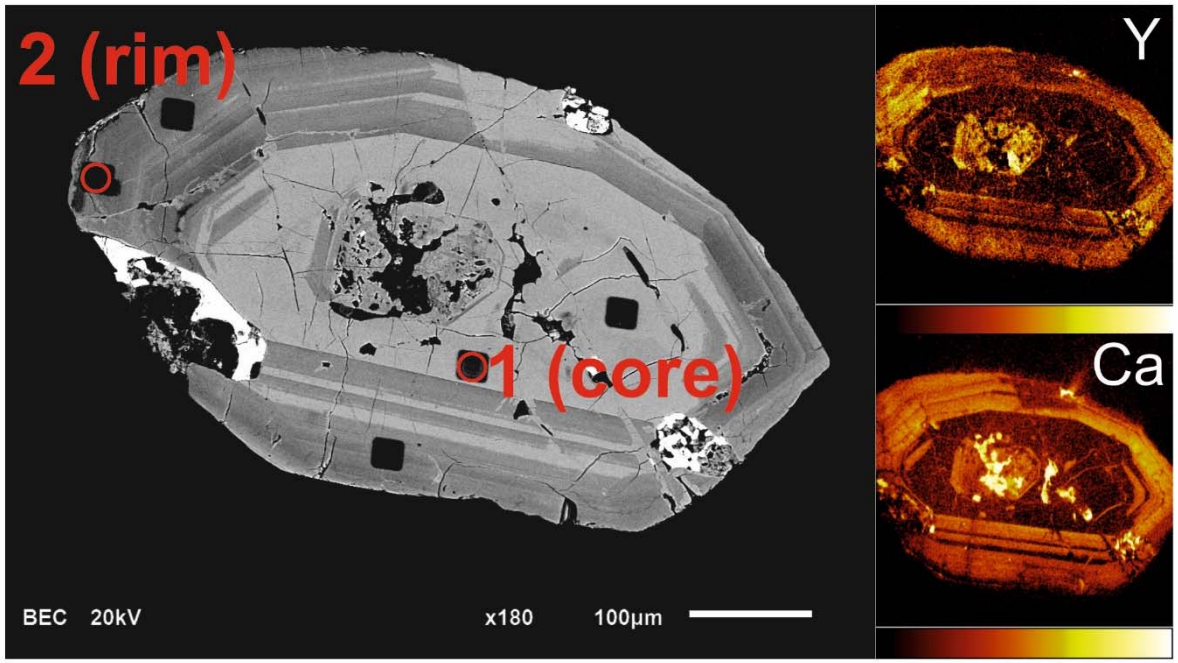


***Fig. 1.*** *BSE image and Y and Ca maps (ToF-SIMS) for zircon from the Yastrebetskoye deposit*

***Acknowledgments:*** *This work was supported by the Russian Foundation for Basic Research (project no. 16-05-00125) and the Ministry of Education and Science of Russia (basic and design parts of the state task in the scientific sphere № 5.9248.2017/BY for 2017-2019).*

## References:

Levashova EV, Skublov SG, Li X-H, Krivdik SG, Voznyak DK, Kulchitskaya AA, Alekseev VI (2016) Zircon geochemistry and U–Pb age at rare metal deposits of syenite in the Ukrainian Shield. Geol Ore Deposit 58:239–262

Makeyev AB, Skublov SG (2016) Y–REE-rich zircons of the Timan region: geochemistry and economic significance. Geochem Int 54:788–794

Nasdala L, Irmer G, Wolf D (1995) The degree of metamictization in zircon: a Raman spectroscopic study. Eur J Mineral 7:471–478

Skublov SG, Marin YuB, Galankina OL, Simakin SG, Myskova TM, Astaf'ev BYu (2011) The first discovery of abnormal (Y+REE)-enriched zircons in rocks of the Baltic Shield. Dokl Earth Sci 441:1724–1731

# Accuracy of Ti-in-zircon thermometry improved by isotope dilution determinations of Ti in zircon reference materials

**Szymanowski, D.[1,*], Fehr, M.A.[1], Guillong, M.[1], Coble, M.A.[2], Wotzlaw, J.F.[1], Nasdala, L. [3], Ellis, B.S.[1], Bachmann, O. [1], Schönbächler, M.[1]**

*[1] Institute of Geochemistry and Petrology, ETH Zürich, Switzerland*
*[2] Stanford–USGS Ion Microprobe Laboratory, Stanford University, CA, USA*
*[3] Institute of Mineralogy and Crystallography, University of Vienna, Austria*
** E-Mail: dawid.szymanowski@erdw.ethz.ch*

The temperature-dependence of Ti incorporation into zircon has been exploited as a powerful tool to estimate zircon crystallisation temperatures (Ti-in-zircon thermometer; Watson et al. 2006; Ferry and Watson 2007). The accuracy of calculated zircon temperatures derived using this method depends on assumptions made about the activity of $TiO_2$ and $SiO_2$ in the chemical environment (in particular in the absence of co-crystallising rutile or quartz) as well as, potentially, crystallisation pressure. However, given informed choices of chemical potentials and an adequate pressure correction can be made, the absolute accuracy of model Ti-in-zircon temperatures ultimately hinges on the ability to accurately determine low Ti concentrations in zircon.

Depending on the Ti content of the zircon, the analytical techniques applied to determining the Ti concentration include secondary ion mass spectrometry (SIMS), laser ablation-inductively coupled plasma-mass spectrometry (LA-ICP-MS), and electron probe microanalysis (EPMA). The applicability of EPMA is limited to only the highest-T zircons (>>10 µg/g Ti); Ti concentrations pertinent to most zircon-saturated rocks (<1 to ~50 µg/g Ti corresponding to crystallisation temperatures of ~500–900 °C) are most commonly determined by SIMS or LA-ICP-MS. However, matrix effects associated with these two analytical techniques require the use of adequate matrix-matched primary reference materials. Currently, despite the growing popularity of *in situ* trace element and isotopic analyses of zircon, there is an evident lack of zircon reference materials that are suitably homogeneous with an independently determined and fully traceable value for Ti concentration that could be used for relative trace element determinations via SIMS or LA-ICP-MS.

To improve the accuracy of future *in situ* analyses of Ti in zircon, we have identified zircon reference materials that are sufficiently homogeneous with respect to Ti to serve as primary reference materials for SIMS and LA-ICP-MS. We present traceable and independent determinations of Ti concentration in multiple aliquots of these zircon crystals using isotope dilution (ID)-ICP-MS employing a precisely calibrated $^{47}Ti$–$^{49}Ti$ double spike. We then describe a method for quantifying Ti contents in unknown zircons based on the newly-derived standard compositions and determine Ti contents of a range of other standard zircons to be used as either primary or secondary reference materials.

***Acknowledgements:*** *Co-author LN acknowledges support by the Austrian Science Fund, grant P24448–N19.*

## References:

Ferry JM, Watson EB (2007) New thermodynamic models and revised calibrations for the Ti-in-zircon and Zr-in-rutile thermometers. Contrib Mineral Petr 154:429–437

Watson EB, Wark DA, Thomas JB (2006) Crystallization thermometers for zircon and rutile. Contrib Mineral Petr 151:413–433

# Evolution of borate minerals from contact metamorphic to hydrothermal stages: Ludwigite-group minerals and szaibélyite from the Vysoká – Zlatno skarn, Slovakia

**Uher, P.[1,*], Bilohuščin, V.[1], Koděra, P.[2], Milovská, S.[3], Mikuš, T.[3], Bačík, P.[1]**

*[1] Department of Mineralogy and Petrology, Faculty of Natural Sci., Comenius University, Ilkovičova 6, 842 15 Bratislava, Slovakia*
*[2] Department of Mineral Deposits, Faculty of Natural Sci., Comenius University, Ilkovičova 6, 842 15 Bratislava, Slovakia*
*[3] Earth Science Institute, Banská Bystrica branch, Slovak Academy of Sciences, Ďumbierska 1, 975 01 Banská Bystrica, Slovakia*
** E-Mail: puher@fns.uniba.sk*

Borate minerals of the ludwigite group and szaibélyite [$MgBO_2(OH)$] in association with hydroxylclinohumite, clinochlore, a serpentine mineral, magnesian magnetite, spinel, magnesite, dolomite and sulphide minerals, occur in a magnesian exoskarn in the R-20 borehole at the depth of 1174 m, located in the Vysoká – Zlatno Cu-Au porphyry-skarn deposit, located within the Štiavnica Neogene stratovolcano, Western Carpathians, central Slovakia. The skarn is developed along the contact of Miocene (~13 Ma) granodiorite to quartz-diorite porphyry and a Middle-Upper Triassic dolomite-shale-psammite-anhydrite sedimentary sequence (Koděra et al. 2010). The boron minerals were investigated by electron probe micro-analyser (EPMA) and micro-Raman techniques. Based on textural and compositional data, the skarn minerals originated during two stages.

**Stage 1:** An early high-temperature, contact-metamorphic and metasomatic stage comprises coarse-crystalline aggregate of ludwigite-group minerals (LGM) (types 1 to 3) in association with hydroxylclinohumite, magnetite, and rarely spinel inclusions in ludwigite. The LGM form massive black aggregates (>5 cm across) of numerous acicular, euhedral to subhedral prismatic crystals (usually 0.2 to 3 mm long). In BSE images, LGM crystals show regular concentric, rarely oscillatory or irregular zoning caused by distinct compositional variations during their growth or partial alteration: the dark zones show enrichment in Mg, Al and Ti, in contrast to the pale zones which have larger amounts of Fe. Compositional variations of LGM show a crystallization sequence from early azoproite with ≤17 wt% $TiO_2$ (~0.40 apfu Ti), which correspond to ≤79 mol% of the $Mg_2(Mg_{0.5}Ti_{0.5})O_2(BO_3)$ end-member, Ti-Al-rich members of LGM, "aluminoludwigite" with ≤14 wt% $Al_2O_3$ [≤0.53 apfu Al and ≤53 mol% of $Mg_2AlO_2(BO_3)$ end-member] and Al-rich ludwigite [$Mg_2Fe^{3+}O_2(BO_3)$] in the central zone of crystals, to Ti-Al-poor ludwigite in outer parts of crystals. The contents of other constituents in LGM attain elevated concentrations in some cases: 2.5 to 3.2 wt% $SnO_2$ (0.03–0.04 apfu Sn), 0.4 to 1.0 wt% $ZrO_2$ (0.01–0.02 apfu Zr), and 0.2 to 0.5 wt% $V_2O_3$ (≤0.01 apfu V) in Ti-Al-rich LGM compositions of type 1; Sn-enriched analyses were locally documented also in ludwigite of type 3. The compositional variations indicate the following main substitution mechanisms in the studied LGM: $Fe^{2+} = Mg^{2+}$ in M1-3 sites for all compositions, $Mg^{2+} + Ti^{4+}$ ($Sn^{4+}$, $Zr^{4+}$) = 2($Fe^{3+}$, Al) in M4 site mainly for analyses including high Ti contents (type 1), and $Al^{3+}$ ($V^{3+}$) = $Fe^{3+}$ in M4 site for compositions with a small amount of Ti but moderate to high Al contents (types 2 and 3).

**Stage 2:** Minerals of the late retrograde serpentinization and hydrothermal stage of the skarn form irregular veinlets and aggregates, including partial alteration of hydroxylclinohumite to the serpentine-group mineral and clinochlore, replacement of LGM by szaibélyite, formation of the latest generation of Fe-rich, Ti-Al poor ludwigite in veinlets (type 4), and precipitation of dolomite, magnesite and sulphide minerals (valleriite, sphalerite, chalcopyrite).

The distinct compositional zoning of the LGM documents a complex evolution of the skarn beginning with a high-temperature stage 1 and ending with a low-temperature overprint, stage 2. The source of boron in the skarn could have been originated from the granodiorite/quartz diorite intrusion; however some supply of B from adjacent evaporite-bearing sediments is also possible. Conditions for the precipitation of borates and associated minerals could be estimated at ~600–700 °C and 50–70 MPa for the stage 1, and ~320 to 370 °C for the stage 2 of the Vysoká – Zlatno skarn mineralization (cf. Koděra et al. 2010).

***Acknowledgments:*** *Authors thank Ľ. Rojkovičová for mineral samples. The present work was supported by the Slovak Research and Development Agency under the projects APVV-0537-10 and APVV-15-0050, as well as the VEGA-1/0560/15 project of Ministry of Education, Slovak Republic.*

## References:

Koděra P, Lexa J, Fallick AE (2010) Formation of the Vysoká–Zlatno Cu–Au skarn–porphyry deposit, Slovakia. Mineral Depos 45:817–843

# Electron-beam annealing in radiation-damaged zircon

**Váczi, T.[1,2,*], Nasdala, L.[3]**

[1] *Wigner Research Centre for Physics, Hungarian Academy of Sciences, Budapest, Hungary*
[2] *Department of Mineralogy, Eötvös Loránd University, Budapest, Hungary*
[3] *Institut für Mineralogie und Kristallographie, Universität Wien, Vienna, Austria*
** E-Mail: vaczitamas@caesar.elte.hu*

It is known that heating to high temperatures is able to induce ordering (called thermal annealing) in damaged zircon (e.g. Geisler et al. 2001). It has been demonstrated that an electron beam is also effective in rearranging displaced atoms and increasing crystallinity (Váczi and Nasdala 2017). This contribution presents recent findings and an assessment of the real structure of minerals self-irradiated by alpha decay.

Actinide-containing minerals cause radiation damage in themselves (self-irradiation) or in their neighbouring phases (radiation haloes). Self-irradiation occurs mostly through the recoil of heavy daughter nuclei produced in alpha decay events, which gradually destroys the crystallinity of the host. Zircon, the most important accessory mineral for age determination, is notable for accumulating and preserving self-irradiation damage, the degree of which depends on crystallisation age, actinide content and thermal history.

Zircon may be heated to high temperatures inducing the recovery of damage through geological processes and in the laboratory. However, due to the importance of this mineral in geological investigations, electron-beam analysis is very commonly done. Recently, in a systematic study of a set of naturally damaged zircon samples (Váczi and Nasdala 2017) spanning a large range of radiation damage, it has been shown that an electron beam induces a dose-dependent, partial recovery of ion-irradiation damage. The recovery was observable through changes in Raman spectra recorded at electron probe analysis spots (Fig. 1).

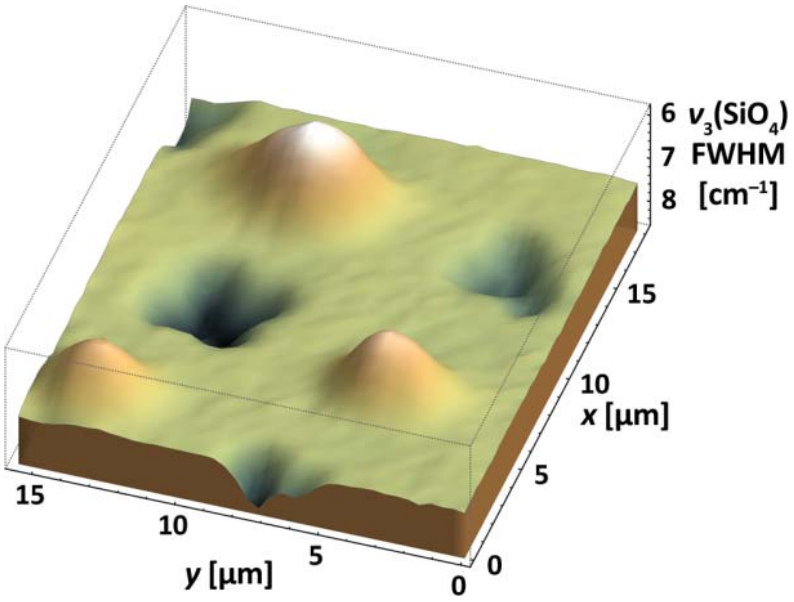


***Fig. 1.*** *Raman map from the surface of zircon sample M144 (low to moderate initial damage) after electron irradiation. The "hills" reveal increased crystalline order at electron-beam impact spots, while the crosses show the guide marks milled using a focused Ga-ion beam*

Our experimental observations and calculations revealed that electron-beam annealing is athermal. A rate change was also observed: following an initial rapid recovery of Raman band widths, the process becomes gradually slower (Fig. 2), and this pattern was recognisable in all samples. The decrease of the Raman band width is directly related to the initial damage level (in the case of small initial damage we saw little change in Raman widths). Using arguments based on a geometric model of recoil damage accumulation (Ketcham et al. 2013), we tentatively inferred that the observed recovery is actually larger in terms of phonon coherence length in the samples with less initial damage. Further study is in progress to clarify this in more detail.

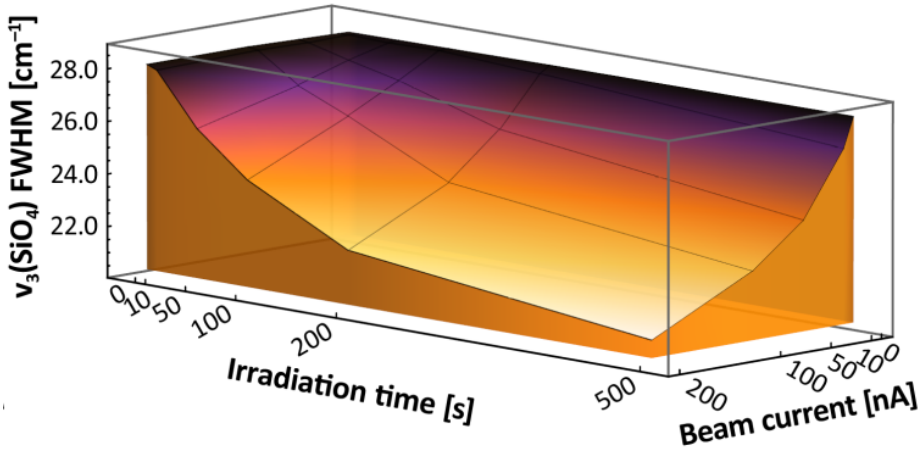


***Fig. 2.*** *Damage evolution during electron-beam bombardment in sample G4 (heavy initial damage) as a function of irradiation duration and beam current*

Based on experimental findings, the best practice during a multi-method analysis of zircon (and perhaps other accessory minerals as well) to characterise samples first by visible-light spectroscopy (Raman, photoluminescence etc.) and only subsequently turn to electron-beam methods. Our results show that short beam dwell times produce no observable spectroscopic changes (i.e., no rearrangement of ions), while prolonged exposures to the electron beam induce ion mobility in the irradiated volume. This should be kept in mind when planning the analytical agenda.

***Acknowledgments:*** *This project received support from the National Research, Development and Innovation Office of Hungary under grant no. OTKA PD116183 and from the Austrian Science Fund (FWF) grant no. P24448–N19.*

## References:

Geisler T, Pidgeon RT, Van Bronswijk W, Pleysier R (2001) Kinetics of thermal recovery and recrystallization of partially metamict zircon: a Raman spectroscopic study. Eur J Mineral 13:1163–1176.

Ketcham RA, Guenthner WR, Reiners PW (2013) Geometric analysis of radiation damage connectivity in zircon, and its implications for helium diffusion. Am Mineral 98:350–360

Váczi T, Nasdala L (2017) Electron-beam-induced annealing of natural zircon: a Raman spectroscopic study. Phys Chem Mineral 44:389–401

# Effects of chemical abrasion on zircon crystal structure, chemistry and ID-CA-TIMS U-Pb ages

**Widmann, P.[1,*], Davies, J.H.F.L.[1], Schaltegger, U.[1]**

*[1] Department of Earth Sciences, University of Geneva, rue des Maraîchers 13, CH-1205 Geneva, Switzerland*
** E-Mail: philipp.widmann@unige.ch*

Recognition and mitigation of post crystallisation loss of radiogenic lead is a still an unresolved problem in high-precision U-Pb dating. The loss of radiogenic Pb preferentially occurs along altered zones of the crystal lattice as a consequence of the structural damage produced by U decay (Nasdala et al., 2005) and results in biased ages that are too young. Reliable and meaningful U-Pb ages require a control on factors that cause Pb loss and create age dispersion. Despite state of the art procedures using chemical abrasion (CA) on single zircon grains (Mattinson, 2005) there is no guarantee to completely mitigate the loss of radiogenic Pb. Furthermore, this technique is entirely empirical and is often modified by different laboratories in terms of duration and temperature of the annealing and the partial dissolution steps. Without a proper understanding of how (1) the applied annealing temperature and (2) the temperature and duration of partial dissolution affect metamict and non- metamict zones. Therefore, data from different U-Pb geochronology laboratories following different procedures are problematic to compare quantitatively. In consequence the rejection of respectively too young zircon grains with suspected loss of radiogenic lead, while reviewing a complex data set, is often difficult to justify without a robust analytical proof. Previous studies have investigated the effect of annealing on radiation damaged zones at different time and temperature conditions (e.g. Nasadala et al., 2002), or the effect of temperature at a fixed duration during the partial dissolution step (Huyskens et al., 2016) on the reproducibility of U-Pb dates. However, no study has investigated the effect of the chemical abrasion procedure on the zircon trace element chemistry and compared this to the state of the crystal structure and the U-Pb date.

Our study intends to develop improved protocols for the chemical pre-treatment of zircon based on the state of the crystal structure and chemistry. We will present an experimental approach to quantify the effects of chemical abrasion on the zircon chemistry and crystal structure. For this purpose we have chosen the natural standard zircon Plešovice, due to its variations in trace element concentrations and domains rich in actinides (Sláma et al., 2008). Plešovice grain fragments were annealed for 48h at 900°C. Eight aliquots were separated and attacked in concentrated hydrofluoric acid at 180 °C and 210°C for 6h, 12h, 18h and 24h. We performed Raman spectroscopy, EMPA, CL imaging and LA-ICP-MS trace element analysis on each of the fractions. The zircon treated by CA are then compared to untreated and solely annealed zircons. We will show first results from the Raman and trace element analysis corresponding U-Pb dates.

Our primarily results indicate that most unannealed zircon fragments follow the radiation damage trend, exceptions are most likely the result of previous natural annealing. Successive increase in CA duration at 180°C results in more crystalline zircon fragments, indicating removal of metamict parts of zircon. However, even at 24h CA duration metamict parts are present. In contrast, Raman data from the CA at 210°C show less scatter and are more consistent. The remaining increased short range distortion of the crystal lattice (increased FWHM) is most likely the result of the trace element content.

CA does not affect the overall trace element pattern, but reduces the overall scatter, due to the removal of metamict zones. Therefore, we suspect that CA cannot fully restore the crystallinity of a pristine zircon. Based on our primarily results, we conclude that more effective removal of metamict zones at CA temperatures of 210°C already at 12h.

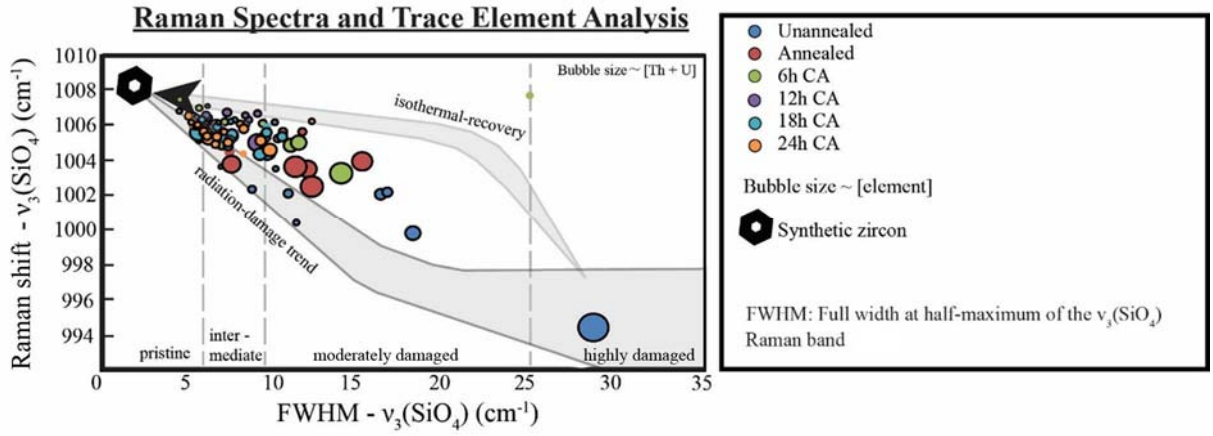


***Fig. 1.*** *Plot of Raman shift vs. FWHM of the $\nu_3(SiO_4)$ Raman band, showing a general increase in Raman shift and decrease in FWHM with increasing time of chemical abrasion*

***Acknowledgments:*** *We acknowledge financial support of the SNSF (project number 156424). We would like to thank all members of the Isotope Geochronology Group for their valuable contributions, A. Ulianov (University of Lausanne) for the LA-ICP-MS calibration and supervision during the analysis.*

## References:

Huyskens, M.H., Zink, S., Amelin, Y. (2016) Evaluation of temperature-time conditions for the chemical abrasion treatment of single zircons for U–Pb geochronology, Chem Geol 438:25–35

Mattinson, J.M. (2005) Zircon U–Pb chemical abrasion ("CA-TIMS") method: Combined annealing and multi-step partial dissolution analysis for improved precision and accuracy of zircon ages, Chem Geol 220:47–66

Nasdala, L., Lengauer, C.L., Hanchar, J.M., Kronz, A., Wirth, R., Blanc, P., Kennedy, A.K., Seydoux-Guillaume, A. (2002) Annealing radiation damage and the recovery of cathodoluminescence, Chem Geol 191:121–140

Nasdala, L.; Hanchar, J.M.; Kronz, A., Whitehouse, M.J. (2005) Long-term stability of alpha particle damage in natural zircon. Chem Geol 220:83–103

Sláma, J., Košler, J., Condon, D.J., Crowley, J.L., Gerdes, A., Hanchar, J.M. Horstwood, M.S.A., Morris, G.A., Nasdala, L.,Norberg, N., Schaltegger, U., Schoene, B., Tubrett, M.N., Whitehouse, M.J. (2008) Plešovice zircon — A new natural reference material for U–Pb and Hf isotopic microanalysis, Chem Geol 249:1–35

# Alteration and electron probe micro-analyser dating of high-U zircon from a pegmatite from the Aduiskii Massif, Middle Urals

**Zamyatin, D.A.[1,2,*], Shchapova, Yu.V.[1,2], Votyakov, S.L.[2], Nasdala, L.[3], Lenz, C. [3,4]**

*[1] Zavaritsky Institute of Geology and Geochemistry, Ural Branch of RAS (Yekaterinburg, Russia)*
*[2] Ural Federal University named after B.N. Yeltsin (Yekaterinburg, Russia)*
*[3] Institut für Mineralogie and Kristallographie, Universität Wien (Vienna, Austria)*
*[4] Australian Nuclear Science and Technology Organisation, Lucas Heights, NSW, Australia*
** E-Mail: zamyatin@igg.uran.ru*

Zircon ($ZrSiO_4$) is an accessory mineral that is used widely in U–Pb geochronology. It may incorporate significant amounts of the radioactive actinides U and Th. The U–Th–Pb isotope system may, however, be disturbed, as for instance caused by the secondary loss of radiogenic Pb. The recognition of such alteration is crucial for the sound interpretation of geochronology results.

The secondary ion mass spectrometry (SIMS) technique has various advantages, when compared with other analytical methods, for the investigation of "normal" zircon, but a number of problems may arise when using this technique for dating zircon with exceptionally high U concentrations exceeding 0.5 wt%. In such cases, chemical electron probe micro-analyser (EPMA) dating may be a more appropriate approach, in comparison to isotope dating, for determining the sample's geological age. In the present project (Zamyatin et al., 2017) we have studied partially altered, high-U zircon from a granite pegmatite from the Aduiskii Massif, Middle Urals (Russia) using analytical techniques with spatial resolutions on the micrometre range.

***Methods.*** The structural and chemical heterogeneity of samples was characterised by means of an EPMA (Cameca SX100), including joint probability distribution (JPD) analysis (Votyakov et al., 2014) of back-scattered electrons (BSE), cathodoluminescence (CL) and U $M_\beta$ images, and by Raman and photoluminescence (PL) spectroscopy (Horiba LabRAM HR Evolution). Analyses of the chemical composition including direct oxygen analysis (the O $K_\alpha$ line was measured) were carried out for a number of points. Chemical U–Th–total Pb dating based on the measured U, Th and Pb concentrations was performed according to Suzuki and Adachi (1991) and Montel et al. (1996).

***Results.*** A high-U interior region (U up to 11.4 wt%) without any obvious indication of post-growth chemical alteration was found (zone 1 in Fig. 1a). This domain has stoichiometric chemical composition, and its Raman spectrum corresponds to that of amorphous $ZrSiO_4$ (Fig. 1d). It is surrounded by two zones (zones 2 and 3 in Fig. 1a) that we interpret as high-U zircon that was formed by fluid-driven alteration reactions under the influence of aqueous fluids. Zone 2 was formed by diffusion-reaction processes whereas zone 3 is a result of coupled dissolution-reprecipitation processes. Both of these chemically altered zones are somewhat depleted in U when compared to the un-altered zone 1 (Fig. 1b) and have non-stoichiometric chemical composition; they contain non-formula elements such as Ca (Fig. 1c), Al, Fe and $H_2O$ up to several wt%. Raman spectra obtained in these regions yielded a band near 760–810 $cm^{-1}$ which is not related to any $ZrSiO_4$ vibration (Fig. 1 d); we assign it tentatively to the symmetric stretching of $(UO_2)^{2+}$ groups. This assignment is supported by the observation of a fairly intense PL phenomenon whose spectral position and vibrational-coupling structure strongly indicates a uranyl-related emission.

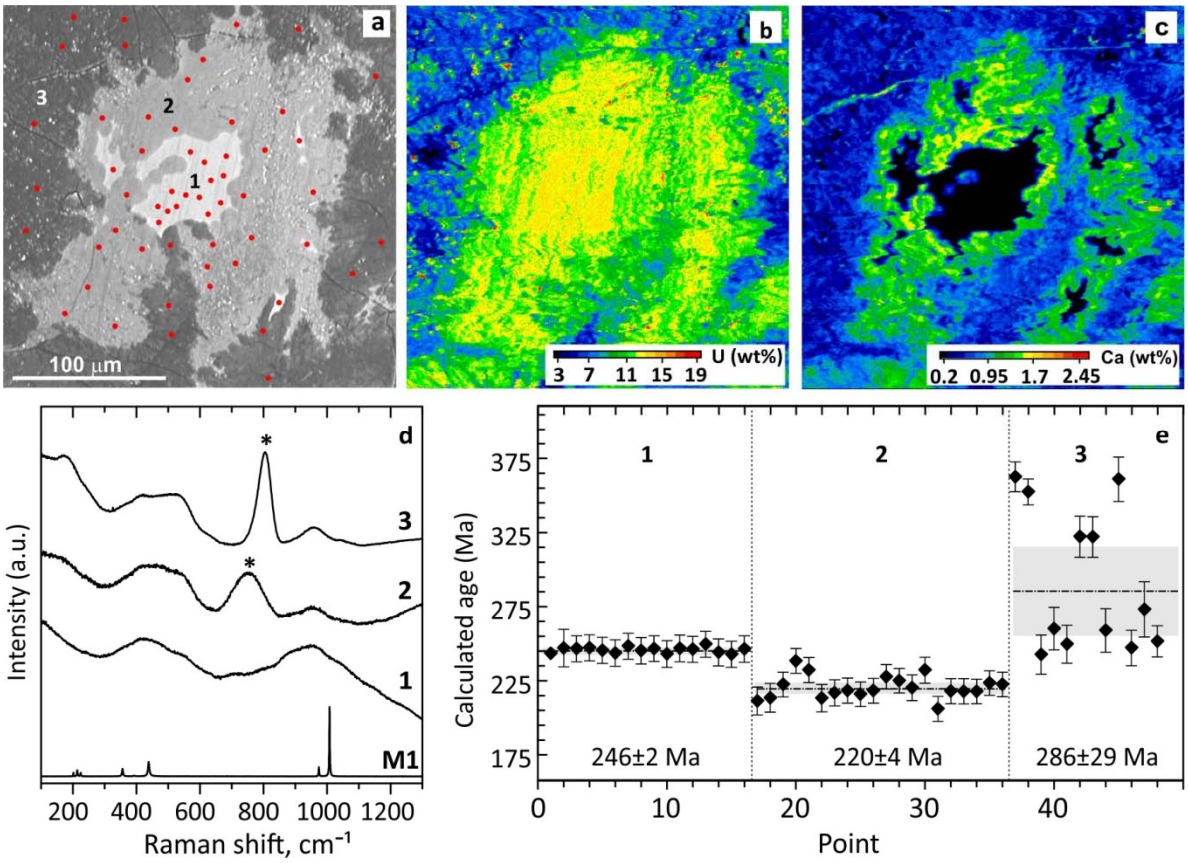


***Fig. 1.*** *Heterogeneous high-U zircon from the Aduiskii Massif (modified from Zamyatin et al., 2017). (a) BSE-image; red spots mark EPMA analysis points. (b, c) U and Ca distribution patterns. (d) Raman spectra obtained in zones 1 (high-U, stoichiometric), 2 (altered), 3(altered), and from reference zircon M1. (e) Histogram showing the variations of calculated EPMA U–Th–total Pb ages in zones 1–3. Dash-dot lines visualize the weighted mean ages and grey bars their 2σ uncertainties*

It was found that the variations of BSE and CL intensities in amorphous high-U zircon are controlled by the sample's chemical composition and the presence of $H_2O$ and $(UO_2)^{2+}$ groups. Diffusion-controlled alteration has caused preferred loss of radiogenic Pb, compared to the rather moderate losses of U and Th, which results in calculated ages that are apparently too young (Fig. 1e). Fluid-driven coupled dissolution-reprecipitation, in contrast, has caused higher losses of U, compared to Pb losses, leading to too old calculated ages (Fig. 1e). A weighted mean EPMA age of 246±2 Ma was determined for the primary, unaltered zone 1, which agrees reasonably well with previous dating results for the Aduiskii Massif.

***Acknowledgments:*** *Financial support was provided by the Russian Science Foundation through project N16–17–10283 to V.S.L. (agreement of 24.05.2016), and the Austrian Science Fund (FWF) through projects P24448–N19 to L.N. and J3662–N19 to C.L.*

## References:

Montel JM, Foret S, Veschambre M, Nicollet C, Provost A (1996) Electron microprobe dating of monazite. Chem Geol 131:37–53

Suzuki K, Adachi M (1991) Precambrian profenance and Silurian metamorphism of the Tsubonasawa paragneiss in the South Kitakami terrane, Northeast Japan, revealed by the chemical Th-U-total Pb isochron ages of monazite, zircon and xenotime. Geochem J 25:357–376

Zamyatin DA, Shchapova Yu V, Votyakov SL, Nasdala L, Lenz C (2017) Alteration and chemical U-Th-total Pb dating of heterogeneous high-uranium zircon from a pegmatite from the Aduiskii Massif, Middle Urals, Russia. Miner Petrol 111:475–497

# Abstracts author index